Funded by the European Union

Ref. Ares(2019)4119164 - 28/06/2019

Compact

XLS-Report-2019-004
27 June 2019

XLS Deliverable D5.1

Technologies for the CompactLight undulator

F. Nguyen[1)*], A. Aksoy[†], A. Bernhard[‡], M. Calvi[§], J. A. Clarke[¶], H. M. Castañeda Cortés[¶], A. W. Cross[‖], G. Dattoli[*], D. Dunning[¶], R. Geometrante[**], J. Gethmann[‡], S. Hellmann[§], M. Kokole[†††], J. Marcos[††], Z. Nergiz[*], F. Perez[††], A. Petralia[*], S. C. Richter[‡,‡‡], T. Schmidt[§], D. Schoerling[‡‡], N. Thompson[¶], K. Zhang[§], L. Zhang[‖], D. Zhu[***]

On behalf of the CompactLight Partnership

Prepared on: 27.06.2019

[*] ENEA-Frascati, Italy, [†] University of Ankara, Turkey, [‡] Karlsruhe Institute of Technology, Germany, [§] Paul Scherrer Institut, Switzerland, [¶] STFC Daresbury Laboratory, United Kingdom, [‖] University of Strathclyde, United Kingdom, [**] Kyma SRL, Italy, [††] ALBA–CELLS, Spain, [‡‡] CERN, Switzerland, [***] ANSTO, Australia, [†††] Kyma Tehnologija, Slovenia

[1] Corresponding author: federico.nguyen@enea.it

Funded by the
European Union

Compact

This project is funded by the European Union's Horizon2020 research and innovation programme under Grant Agreement No. 777431. The contents of this report reflect only the view of the CompactLight Consortium. The European Commission is not responsible for any use that may be made of the information it contains.

Abstract

The present report is a comprehensive overview of undulator technologies, which are either already exploited at fully operating free-electron laser facilities or going to be available within the forthcoming 5 years. Main emphasis is given to devices based on permanent magnets and on superconducting technologies, scrutinised in terms of status and perspectives, but also novel concepts with a different readiness level are addressed. A technology comparison based on expected performance and a cost estimate of the undulator system are drawn.

Contents

1 Introduction: XLS-CompactLight requirements on FEL and undulator parameters

In a free-electron laser (FEL), the kinetic energy of a relativistic electron bunch is transformed into an intense beam of electromagnetic radiation by wiggling the electron bunch transversely in the spatially periodic and temporally static magnetic field of an undulator. The undulator magnetic field is specified by two quantities: the undulator period λ_u and the deflection strength parameter K, defined as

$$K = \frac{eB\lambda_u}{2\pi m_e c} \tag{1}$$

where B is peak value of the on-axis magnetic field and e, m_e and c the electron charge, the electron mass and the light speed, respectively. For electrons of beam energy $E = \gamma m_e c^2$, with γ being the associated Lorentz factor, the FEL resonant wavelength λ is given by:

$$\lambda = \frac{\lambda_u}{2\gamma^2}\left(1 + a_u^2\right) \tag{2}$$

where $a_u = K/\sqrt{2}$ for planar undulators, and $a_u = K$ for helical undulators. The parameters a_u and λ_u cannot be chosen independently – each undulator technology has its own functional dependence – therefore Eq.(2) shows that in order to reach a specific FEL wavelength the electron beam energy and undulator technology must be specified together.

FELs are becoming the main source of tunable, intense and coherent photons of either ultra-short time resolution or ultra-fine energy resolution, especially in the X-ray regime. The number of both scientific applications [1] and beam time requests is rapidly growing, motivating the design of new FEL facilities. An important factor in funding new facilities is the adopted accelerator technology which is presently in rapid development. Acceleration schemes with higher gradients are under detailed test, targeting an increasingly compact accelerator infrastructure. The overall facility size can also be reduced by adopting new undulator technologies in which high on-axis fields can be obtained with short undulator periods—this reduces the total length of the undulator and from Eq.(2) it can be seen that it allows the required FEL wavelength to be obtained with a lower electron beam energy so that the accelerator length is reduced. By adopting both these techniques, of high gradient acceleration and short period undulators, a compact facility with competitive performance can be delivered. This is the primary objective of the XLS-CompactLight project.

Table 1 summarises the specification of the FEL radiation characteristics [2], as discussed at the XLS FEL Users Meeting [2]. In addition, the undulator system should allow the following requests from users to be fulfilled:

1. All FEL wavelengths within the range 0.75 Å and 5 nm accessible with at least one of the FEL beamlines;

2. Tuning across wavelengths to be performed by undulator scanning rather than electron beam energy scanning to maximize the facility efficiency, operating with only a few discrete beam energies;

3. The most compact configuration enabling two-pulse and two-wavelength experiments;

[2] https://indico.cern.ch/event/750792/

4. Variable, selectable polarization at the sample under study at all wavelengths, either via variably polarising undulators or optical elements in the photon beamline.

The main sections of this report review the current and near future – say on a timescale of about 5 years from now – undulator technologies that could be adopted in a compact FEL source that meets the specification given in Table 1. Each undulator technology will be studied assessing the strengths, weaknesses, and opportunities to advance.

In the final sections a quantitative comparison is made of the different technologies, using a parameterisation of the estimated field as a function of undulator period and gap. This comparison shows how the choice of undulator technology defines the required electron beam energy, and is used to define a baseline energy for the facility that is lower than the energy of any current hard X-ray FEL yet still allows a number of realistic options for the undulator.

Finally, a tentative cost breakdown of the whole undulator system is drawn, including fabrication and installation costs, to be compared with the other instrumental systems of the project.

Table 1: Main parameters of the CompactLight FEL.

Parameter	**Unit**	**Soft-x-ray FEL**	**Hard-x-ray FEL**
Photon energy	keV	0.25 – 2.0	2.0 – 16.0
Wavelength	nm	5.0 – 0.6	0.6 – 0.08
Repetition rate	Hz	1000	100
Pulse duration	fs	0.1 – 50	1 – 50
Polarisation		Variable, selectable	Variable, selectable
Two-pulse delay	fs	$\pm$100	$\pm$100
Two-colour separation	%	20	10
Synchronisation	fs	<10	<10

2 Permanent magnet undulators

2.1 Introduction

The use of permanent magnets for undulator construction dates back to the very first undulator described by Motz in 1953 [3]. The most straightforward realizations of undulators based on permanent magnets are the so-called pure permanent magnet [4] and hybrid [5] schemes, first introduced by Halbach in the early 1980s and shown in Fig. 1. In both cases the device consists of two magnetic arrays which generate a periodic magnetic field in the gap (g) between them; the system typically incorporates a mechanism to modify the separation between the two arrays, allowing to tune the intensity of the magnetic field. Whilst in the pure scheme the arrays are exclusively made of permanent magnet blocks, in the hybrid one the magnet blocks are combined with pieces of high permeability material in order to concentrate the magnetic flux and obtaining slightly higher peak field values. The magnetic field generated by these structures produces an undulating distortion of the electron beam's trajectory which is contained within the device's midplane; this is the reason why they are sometimes referred as *planar undulators*. The electromagnetic radiation generated by planar undulators is linearly polarized along the same plane that the electron beam is oscillating.

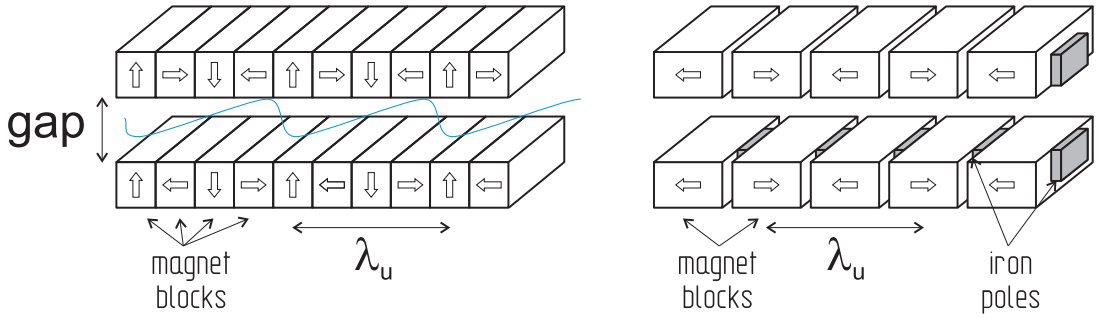

Figure 1: Pure permanent magnet (*left*) and hybrid designs (*right*) for planar undulators. The relevant parameters, undulator period λ_u and gap opening g, are indicated.

Later on more sophisticated magnetic structures were designed which opened the possibility to control the plane of oscillation of the electron beam (and hence to change the direction of polarization of the emitted light) and to induce a helical trajectory on the electron beam, allowing to generate circularly polarized light. These designs are generically referred as *elliptical undulators*. By in large, the most successful of these schemes has been the APPLE-II (for Advanced Planar Polarized Light Emitter) undulator [6], shown in Fig. 2. This device belongs to a family of designs, first proposed in [7], which is equivalent to a pure permanent magnet Halbach undulator where each array is divided into two halves that can be shifted longitudinally. The different variants of APPLE-type designs differ in the section and direction of magnetization of the magnet blocks, as illustrated in Fig. 3. In the case of the APPLE-II design, the device benefits from its relative mechanical simplicity and its ability to generate all of the desired polarization states. In addition, it does not introduce lateral restrictions inside the gap, making it well suited for the flat vacuum chambers of 3rd generation Synchrotron Light Sources. As a drawback, and due to its lack of symmetry between the horizontal and vertical directions, in order to modify the photon energy for a given polarization state with an APPLE-II undulator it is necessary to adjust simultaneously the vertical (gap) and longitudinal (phase) positioning of the magnet arrays.

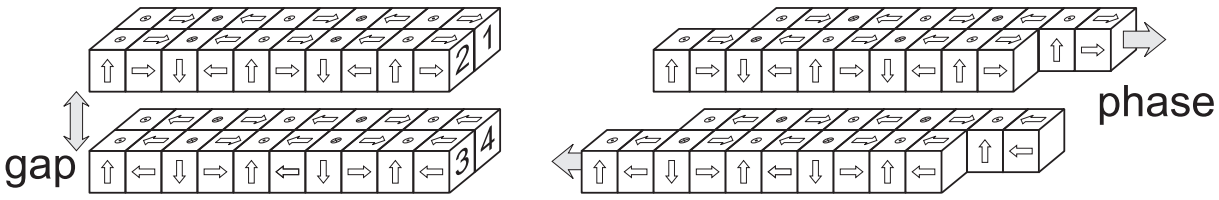

Figure 2: Sketch of an APPLE-II undulator with arrays 1 and 3 longitudinally movable, in vertical (*left*) and horizontal (*right*) field modes.

The degree of control on the polarization of the emitted radiation with an APPLE-type design depends on how many of the 4 arrays can be longitudinally shifted. In the original basic design only two of the arrays standing opposite to each other could be moved in the same direction (the so-called *parallel mode*), allowing to switch from horizontal/vertical linear polarization to circular polarization. Later on it was introduced the possibility of displacing the two movable arrays in opposite directions (*antiparallel mode*), allowing to modify the angle of linearly polarized light. The implementation of this mode requires a reinforcement of the support structure of the undulator due to the strong longitudinal forces that come into play. In order to cover all possible angles for the plane of polarization it is necessary to move all four arrays independently along the beam axis.

Once the possibility of moving the four arrays longitudinally is introduced, a gap driving mechanism to tune the amplitude of the generated magnetic field is not mandatory anymore. Such fixed-gap device was developed at the SLS [8]. Shortly afterwards a new but closely related design, called Delta due to the specific shape of its magnets, was developed at Cornell [9]. In 2016 the APPLE-X concept was developed at PSI [10], consisting of a Delta undulator where the four arrays can be independently displaced both longitudinally and radially. A similar development is ongoing at SLAC under the label Delta-II. The additional degrees of freedom of these devices allow to decouple the strength of the magnetic field from its transverse gradient [11]. The use of designs better suited to the characteristics of single-pass machines (APPLE-III, DELTA and APPLE-X) allows to increase the magnetic field with respect to APPLE-II by a factor $\sqrt{2}$ in planar mode and a factor 2 in circular mode.

As previously discussed in Eq.(1), the undulator performance is characterized by the period λ_u and the deflection parameter K. Although the magnetic field B appearing in Eq. (1) is usually approached by the peak field of the undulator, B_{peak}, the magnitude that directly correlates to the trajectory length, and hence to the resonance wavelength λ, is the so called effective field, B_{eff}, calculated from the harmonics of the magnetic field B_i through the expression:

$$B_{eff} = \sqrt{\sum_{i=1,3,5\ldots} \left(\frac{B_i}{i}\right)^2}. \tag{3}$$

In general assuming $B_{peak} \approx B_{eff}$ is a good approximation and the two parameters are used without distinction, but for hybrid undulators the difference between them increases as the ratio g/λ_u becomes smaller.

For optimization purposes, it is practical to parametrize the magnetic field amplitude B (either B_{peak} or B_{eff}) generated by a certain type of undulator as a function of the g/λ_u ratio, by means of the expression first introduced by Halbach [5]

$$B(g,\lambda_u) = a \exp\left[b\left(\frac{g}{\lambda_u}\right) + c\left(\frac{g}{\lambda_u}\right)^2\right] \tag{4}$$

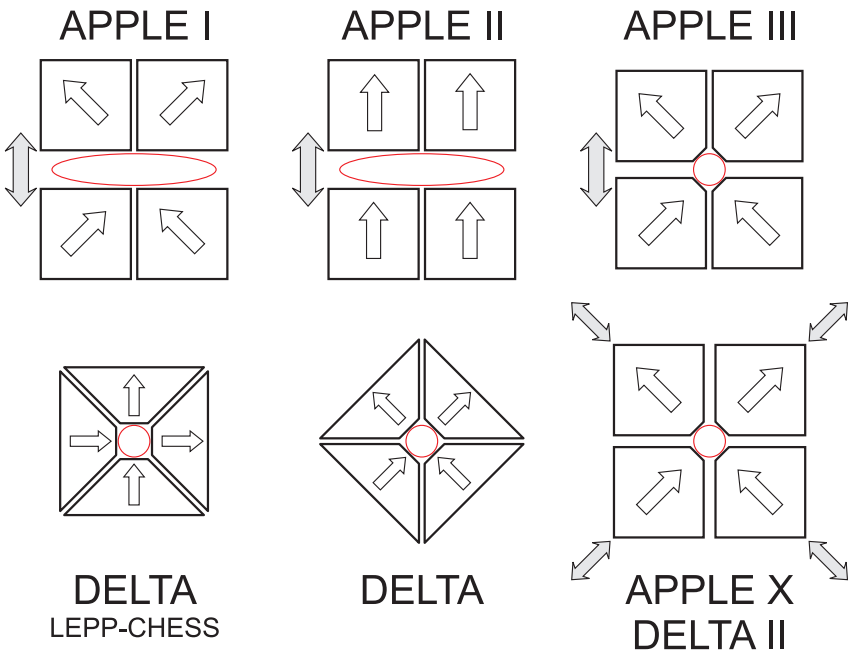

Figure 3: Different designs for elliptical undulators. Gray arrows indicate the degrees of freedom of the magnetic arrays within the transversal plane: APPLE-I [7], APPLE-II [6] and APPLE-III [12] allow to modify the vertical gap between upper and lower arrays; DELTA undulators [9, 13] are fixed-gap devices; APPLE-X [10] allow an independent adjustment of the radial position of each array. Diagram reproduced from [11].

where the parameters a, b and c are determined by means of a fit of data typically obtained from magnetic simulations.

There is a strong incentive to reduce the period length of undulators for a given value of K: it allows getting a brighter source of higher energy photons. If one reduces the linear dimensions of a coil-based undulator (either normal conducting or superconducting) the current density has to be increased accordingly in order to keep the field level constant. In contrast, permanent magnets do not suffer from this limitation, and deliver a constant peak field when scaling down its linear dimensions. On the other hand, for a given set of geometric parameters, the magnetic field delivered by a permanent magnet undulator is limited by the intrinsic magnetic properties of the material (remanence and cohercivity). In other words, permanent magnet-based undulators are limited in the (λ_u, K) parameter space by the properties of available materials. If we compare the current density j required to generate the same peak field than a planar Halbach-type pure permanent undulator of period λ_u made of a material with remanence B_r, we obtain [14]:

$$j \simeq \frac{9B_r}{\mu_0 \lambda_u}\,. \tag{5}$$

Assuming a remanence of $B_r = 1.2\,\text{Tesla}$, for a period length of $\lambda_u \sim 15\,\text{mm}$ the required current densities are close to $600\,\text{A/mm}^2$.

The main parameters defining the magnetic performance of permanent magnet materials are the remanent field, B_r, and the intrinsic coercivity, H_{cJ}, which is a measure of the magnet's resistance to demagnetization. The definition of these parameters is shown in Fig. 4. Another common figure of merit is the maximum energy product, $(BH)_{max}$, defined as the maximum product of the magnetic induction and the field strength along the second quadrant of the

hysteresis curve. This magnitude represents twice the maximum energy that can be stored in the magnetic field created in the space around a magnet of optimum shape. All these are extrinsic properties, being dependent on the processing method used to produce the magnet, and are closely linked to the size, crystallographic quality and alignment of the constituent grains. Intrinsic properties, as saturation magnetization, Curie temperature (T_C) and anisotropy field, are dictated by the crystal structure and composition of the material.

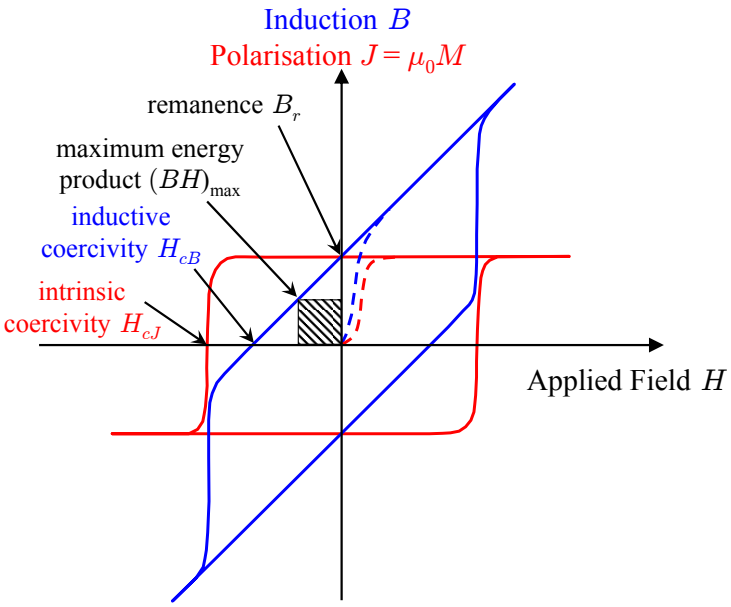

Figure 4: Typical hysteresis loop of a permanent magnetic material in terms of its magnetic induction, $B(H)$, and polarization, $J(H) = \mu_0 M$. The parameters defining the magnetic performance of the material are indicated: remanent induction, B_r, inductive coercivity, H_{cB}, intrinsic coercivity, H_{cJ} and maximum energy product, $(BH)_{max}$.

Materials for manufacturing permanent magnet blocks must provide at the same time a large remanent field and a large coercive force. There are few compounds that satisfy both conditions, the typical choice being rare-earth based compounds: samarium cobalt ($SmCo_5$ and Sm_2Co_{17}) and neodymium-iron-boron (NdFeB) [14]. The development of these materials started on the second half of the 1960s and they exhibit extraordinarily high magnetic characteristics compared to other permanent magnetic materials (ferrites, Alnico-type alloys...). Both of them are intermetallic alloys of a rare-earth (lanthanide) element with a 3d metal (Fe or Co), which rely on small grain particles with high magneto-crystalline anisotropy to produce a material with both a high magnetisation and a high coercivity. The energy product is not expected to increase much further in the future [15]. As an example, at room temperature the theoretical limit for $Nd_2Fe_{14}B$ is $509\,\mathrm{kJ/m^3}$, and $469\,\mathrm{kJ/m^3}$ has been achieved. The magnetic properties of SmCo and NdFeB magnets are summarized in Table 2.

Samarium cobalt shows a higher coercivity and a smaller variation of magnetization with temperature. Another advantage of SmCo magnets compared with NdFeB ones is that they have a smaller transverse susceptibility, which reduces the field integral fluctuations during phasing of elliptical undulators [16]. For its part, the main attractive of NdFeB is its higher remanent field. On top of this, NdFeB is mechanically more robust and less expensive than SmCo. NdFeB is available in a variety of grades whose main difference is the content of dysprosium (Dy). Dysprosium is added to increase the coercivity of the material at the cost of

Table 2: Magnetic properties of rare-earth magnets used in undulators' manufacturing [14]. $\chi_\parallel/\chi_\perp$ stand for the parallel/perpendicular components of the magnetic susceptibility, and T_C corresponds to Curie temperature.

Material	H_{cJ} [kA/m]	B_r [Tesla]	dB_r/dT [%/°C]	$\chi_\parallel/\chi_\perp$	T_C [°C]
$SmCo_5$	1500–2400	0.9–1.01	-0.05	0.01/0.04	700-750
Sm_2Co_{17}	800–2000	1.04-1.12	-0.035	0.01/0.04	800–850
NdFeB	1000–3000	1.0–1.4	-0.10	0.06/0.15	310–340

remanence, due to the inverse magnetic coupling between Fe and Dy. As a consequence, coercivity and remanence for NdFeB compounds are roughly inversely proportional. The Grain Boundary Diffusion Process (GBD) allows to incorporate dysprosium or terbium mainly in the interfaces around the grains, leading to an increase of the coercivity by 250 kA/m without sacrificing remanence [17]. This method is however limited by the thickness that can be properly diffused, of the order of a few millimeters.

Generally speaking, samarium cobalt compounds are more resistant against the loss of remanence under exposure to high energy radiation [18–20]. However, one way of taking profit of the higher remanence of NdFeB grades and to further stabilize them against demagnetizing effects (either thermal or radiation-induced) is to cool them down to cryogenic temperatures [21, 22]. In addition to the gain in coercivity, the temperature decrease also brings an increase of the remanent field of the material. In the case of NdFeB, however, below 135K the material undergoes a spin reorientation transition that reduces its magnetization [23]. In order to avoid this effect PrFeB and (Pr,Nd)FeB grades have been analyzed [24] and developed [25]. The substitution of Nd by Pr shifts the transition well below liquid nitrogen temperature. For PrFeB grades cooling from 300 K down to 77 K increases the remanence by $\sim 15\%$, whereas the coercivity is increased by a factor ~ 2.5. Therefore, the coercivity at room temperature must provide only enough stability for a safe magnet assembly; the radiation hardness is gained at low temperatures.

In Table 3 we list the characteristics of some of the magnet grades currently in use for demanding applications. As shown by the data for PrFeB taken from [26], where measurements down to 40 K were acquired, lowering the temperature below 77 K does not provide much gain in terms of magnetic performance. However, there are indeed incentives to work at temperatures below that of liquid nitrogen using cryocoolers [15]. On the one hand, the system benefits from the increase in thermal conductivity of the girder, which helps to avoid undesirable temperature gradients. On the other hand, if one wants to use sophisticated pole designs using dysprosium or holmium, temperatures below 40 K are mandatory.

Regarding the high permeability material used to concentrate the magnetic flux in hybrid designs, the typical choice are cobalt-iron alloys (vanadium permendur), which display a higher saturation magnetization (2.35 Tesla) than pure iron or low carbon steel.

Table 3: Characteristics of some of the $Re_2Fe_{14}B$ grades used in recent small period and/or cryogenic undulators.

Name	Ref	Compound	Temperature	H_{cJ} [kA/m]	B_r [Tesla]
NMX-S40UX		NdFeB (Diffused Dy)	300	>2300	1.22
NMX-S45SH	[27]	NdFeB	300	1671	1.30
			150	4000	1.50
Vacodym 131 DTP	[28]	(Pr,Nd)FeB	300	1640	1.41
			77	>3185	1.62
NMX-53CR		PrFeB	300	1680	1.35
			77	3980	1.57
NMX-68CU	[27]	PrFeB	300	1680	1.40
			77	6200	1.67
NMX-47CR	[26]	PrFeB	300	2390	1.21
			77	7620	1.396
			40	8130	1.402
NMX-50CR	[26]	PrFeB	300	1870	1.39
			77	6875	1.50
			40	7440	1.51

2.2 Out-of-vacuum

2.2.1 Status (strengths and weaknesses)

In the context of X-ray FEL facilities, out-of-vacuum PM undulators have been extensively used, as shown in Table 4. This table reveals that the out-of-vacuum solution is the adopted one when devices with $\lambda_u > 25$ mm are required, corresponding to hard X-ray sources for high energy accelerators (European XFEL with 17.5 GeV or LCLS with 13.6 Gev) or soft X-ray sources for lower energy accelerators (Athos line at SwissFEL with 2.1–3.6 GeV or FERMI@Elettra with 1.5 GeV). On top of this, essentially all the PM-based variable polarization undulators in operation in Synchrotron Light and FEL facilities are based in out-of-vacuum schemes (one exception would be the original Delta undulator developed at Cornell ERL [9]).

Out-of-vacuum undulators are the workhorses of most of currently operating FELs due to the following series of strengths:

- The high degree of maturity of the associated technology, with many active groups developing and improving the existing solutions.
- Low cost, low energy consumption and simple associated infrastructure.
- The simplicity of having the magnetic structure outside the vacuum environment, both from a mechanical and ultra-high vacuum compatibility point of view.
- In relation with the previous point, these devices usually provide a good accessibility for carrying out magnetic measurements (it is not the case for some particular designs as DELTA).
- Automated assembly and field tuning procedures exist.

Table 4: Out-of-vacuum PM devices in X-ray FEL facilities.

Facility	type	min gap [mm]	period [mm]	max K	length [m]	#	Ref
LCLS							
main line	planar hybrid	6.8 (fixed)	30.0	3.5	3.4	33	[29]
afterburner	Delta	6.6	32.0	3.37	3.2	1	[30]
LCLS II							
HXR	planar hybrid	7.2 (hor.)	26.0	>2.44	3.4	32	[31]
SXR	planar hybrid	7.2 (ver.)	39.0	>5.43	3.4	21	[31]
SXR afterburner	Delta II		44.0	>5.14	3.3	3	[32]
FLASH II	planar hybrid	9.0	31.4	2.87	2.5	12	[33]
European XFEL							
SASE 1/2	planar hybrid	10.0	40.0	3.9	5	35	[34]
SASE 3	planar hybrid	10.0	68.0	9.0	5	21	[34]
SASE 3 afterbur.	APPLE-X	10.0	90.0	7.8	2	4	[35]
FERMI@Elettra							
FEL-1	APPLE-II	10	55.2	–	2.4	6	[36]
FEL-2	APPLE-II	10	34.8	–	2.4	9	[37]
SwissFEL							
Athos	APPLE-X	6.5	38.0	3.8	2	16	[10]
PAL-XFEL							
HXU	planar hybrid	8.3	26.0	1.973	5	20	[38]
SXU	planar hybrid	9.0	35.0	3.321	5	7	[38]

- Different schemes providing full control on the polarization of the emitted light are available.

However, this technology also displays some weaknesses:

- The minimum gap between the magnetic arrays is limited by the dimensions of the vacuum chamber. Given that the generated magnetic field decreases exponentially with the ratio g/λ_u (see Eq. 4), this restriction sets a limit to the minimum value of λ_u which is practical to use in an out-of-vacuum device. This limitation is apparent in Table 4, where no devices with periods smaller than 25 mm are found.

- It exists the danger of demagnetizing the magnets at small gaps, as proven by the experience at European XFEL [39].

- The use of narrow vacuum chambers reduce the physical aperture available to the electron beam, making the operation of the accelerator more difficult, specially during the commissioning phase.

2.2.2 Opportunities and challenges

On top of being the standard choice for FELs nowadays, there is still room to improve for out-of-vacuum undulators, especially from the point of view of reducing production costs. Some steps that may be explored in this direction include:

- Research on new assembly techniques for pure permanent magnets, in addition to conventional soldering or gluing.
- Development of automated procedures for serial production and tuning.
- Incorporate as much as possible the use of cast and extruded materials, which can provide significant savings when manufacturing a series of identical devices as it is typically the case for a FEL undulator line.
- Explore alternative driving systems, as for instance hydraulic ones.
- Adoption of compact cost-saving architectures. This goal requires reducing the forces that the support structure has to withstand, and there are several complementary ways of accomplishing it:
  (i) Shifting from C-type support frames to O-type ones.
  (ii) In the case of planar devices, moving from traditional vertical-field structures to gravity neutral horizontal-field ones.
  (iii) Matching the size of the good field region of the device to the real requirements of a single-pass machine.
  (iv) Compensate as much as possible the attractive force between the two magnetic arrays by using springs, repulsive magnets, etc.

Apart from cost saving strategies, the performance of out-of-vacuum devices can benefit from the following advances:

- Adoption of aggressive designs (APPLE-X, Delta II) for elliptical undulators that will provide a better control of the magnetic field transverse gradient.
- The use of round and small diameter vacuum chambers, with wall thicknesses as small as 0.2 mm, will bring the dimensions of the air gap for out-of-vacuum devices close to the values attainable with in-vacuum ones.

The summary of SWOT analysis for out-of-vacuum PM devices is shown in Table 5.

2.2.3 Advances in science and technology to meet XLS requirements

In the case of the soft X-ray beamline at SwissFEL (Athos), in order to provide full polarization control to users and to maximize the magnetic field an APPLE-X device has been developed [10]. A drawing of the device is shown in Fig. 5. The resulting UE38 undulators made use of triangular shape magnet blocks similar to the ones used in Delta undulator, providing some saving in magnetic material and allowing an easier adaptation to PSI flexor-type keepers. The design is intended to be used with a round vacuum pipe made of copper with an inner diameter of 5 mm and a wall thickness of 0.2 mm (see Fig. 6). The lateral gap for carrying out magnetic measurements is as small as 3 mm. The magnetic structure is fully symmetric at minimum gap, which minimizes the forces on the keeper. As for the magnetic material, SmCo will be used in order to minimize non-linearities. In addition, the use of non-uniformly magnetized blocks to boost the magnetic field near the tip of the magnets is currently under investigation.

APPLE-X is also going to be used as an afterburner for SASE3 at European XFEL [35]. The device is being designed in close collaboration with PSI and will adopt the mechanical support

Table 5: Summary of SWOT analysis for out-of-vacuum PM devices.

Out-of-vacuum PM devices	
STRENGTHS	WEAKNESSES
• Technology highly mature • Many active and knowledgeable groups • Low cost • Low energy consumption • Simple associated infrastructure • Simpler mechanical and ultra-high vacuum solutions • Good accessibility for magnetic measurements • Existence of automated assembly and field tuning procedures • Availability of different schemes providing full control on the polarization of the emitted light	• Possible magnets' demagnetization • Minimum gap limited by the dimensions of the vacuum chamber • As the magnetic field decreases exponentially with g/λ_u, limitation on smaller periods • Difficult commissioning due to narrow vacuum chambers
OPPORTUNITIES	THREATS
• New assembly techniques for PPM • Application of improved permanent magnets • Development of automated procedures for serial production • Application of cast/extruded material for cost optimization on serial production • Adoption of compact cost-saving architectures • Further development of aggressive design (APPLE-X, Delta II…) for elliptical undulators • Optimum exploitation of round and small diameter vacuum chambers • Exploration of alternative driving system • Development of a technology consistent with the increasing public sensitivity to environmental issues	• Magnetic field performances not satisfying CompactLight requirements • Spare PM blocks needed in case of long term magnets' demagnetization

system of SwissFEL, with the magnetic parameters adapted to European XFEL requirements. For XFEL APPLE-X it is planned to use the same NdFeB grade with $B_r = 1.25$ Tesla that has been employed for the other XFEL undulators.

At MAX IV laboratory APPLE-X undulators are being considered as a source for the future Soft X-ray FEL [40]. The design, aiming for a period $\lambda_u = 40$ mm, a total length of 3 m and a minimum aperture of 8 mm, is based on that of the SwissFEL, but with a much more compact mechanical frame. The mechanical frame, with a cylindrical shape as shown in Fig. 7, will have an external diameter of 0.5 m, with an estimated reduction on the cost of the overall device close to 30%.

SLAC developed a 3.2 m-long version of a Delta undulator with a period length of 32 mm to add polarization control to LCLS [13, 30]. The design has a physical aperture of 6.6 mm

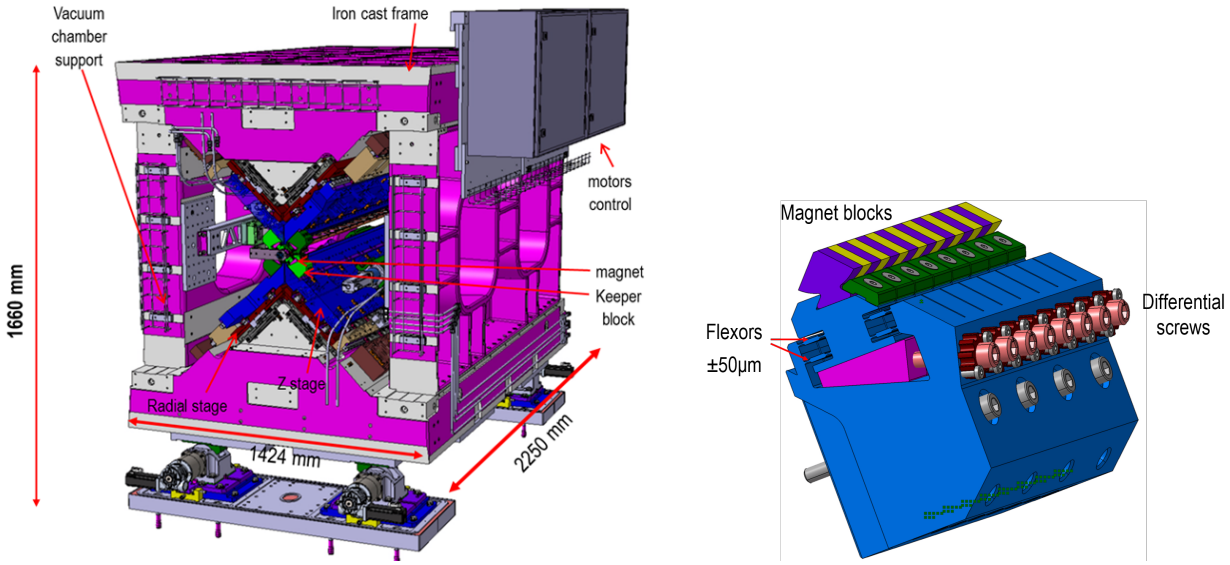

Figure 5: *Left:* Schematic view of U38 APPLE-X undulator being developed for Athos beamline at SwissFEL. *Right:* Detail of one of the magnet keepers, comprising 4 periods. Both magnets and keeper are fabricated by wire erosion.

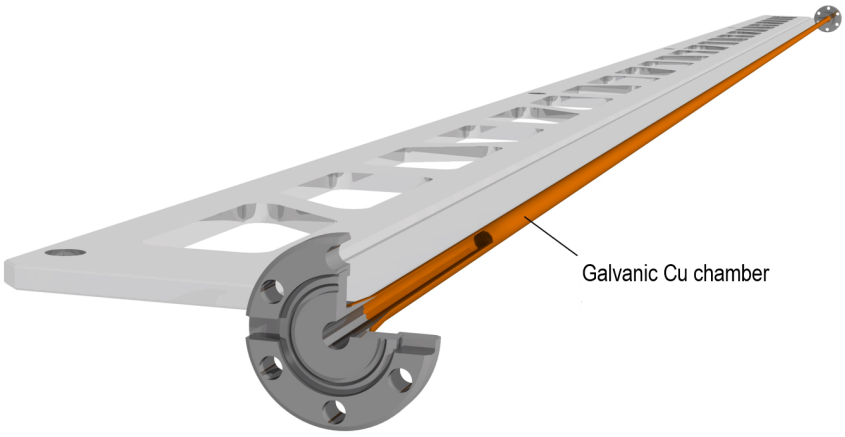

Figure 6: Drawing of the small aperture chamber that will be used with U38 APPLE X undulators at SwissFEL Athos beamline. The pipe, with a total length of 2 m and an external diameter of 5 mm, is manufactured by means of a galvanic process, yielding a wall thickness of a mere 0.2 mm. The vacuum chamber is supported through the same 3 mm lateral gap used for inserting the Hall probe during for magnetic measurements. Reproduced from [10].

in order to install a round vacuum chamber with internal/external diameters $5.08/6.4$ mm and a wall thickness of 0.66 mm. Due to access problems, each one of the 4 magnetic arrays was characterized and corrected individually, and the arrays were combined afterwards. Once assembled, a final measurement with a combination of two 3D Hall probes was carried out. The device, shown in Fig. 8, has been installed in the last (33^{rd}) segment of the LCLS undulator line as a SASE afterburner. For the upgrade to LCLS II a new type Delta II undulator is currently under development [32]. With respect to original Delta design, the Delta II incorporates radial adjustment of the magnet arrays, making it conceptually very similar to the APPLE-X design.

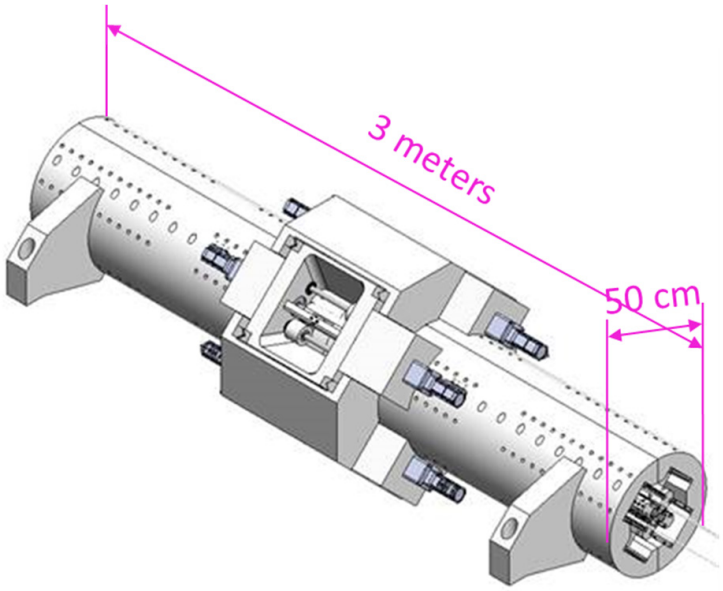

Figure 7: Schematic view of APPLE X undulator being developed at MAX IV. Reproduced from [40].

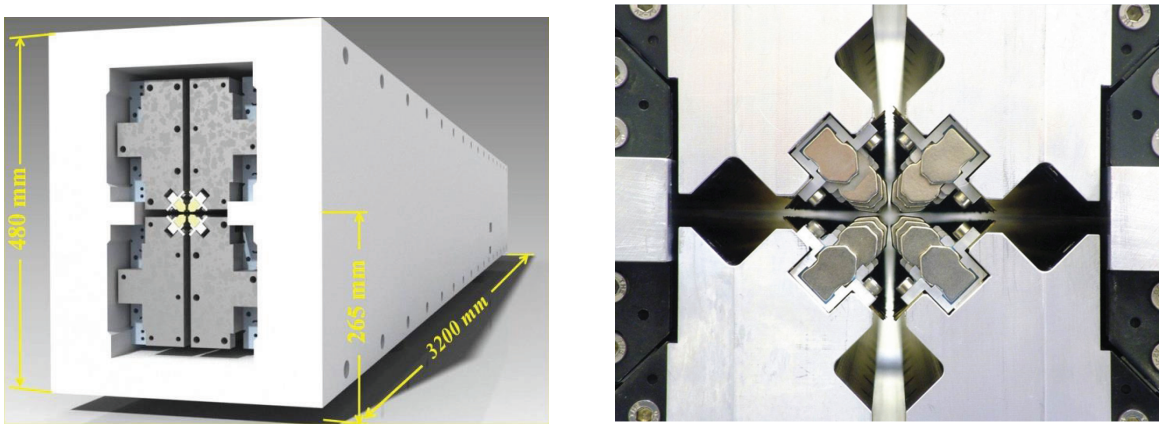

Figure 8: General drawing (*left*) and front picture of the finished device (*right*) corresponding to the Delta undulator installed at the end of the LCLS undulator line. Reproduced from [30] and [13].

An interesting new concept has been developed at APS [41] and it is planned to be used for the hard X-ray line of LCLS II [42]. It consists of a horizontal gap/vertical polarization (HGVPU) undulator, with dynamic force compensation using non-linear conical springs. This design allows to obtain much more compact support structures and gap driving mechanisms as compared with conventional vertical gap/horizontal polarization undulators, as it is shown in Fig. 9. In the case of LCLS II this compactness will allow to re-use much of the hardware and control software developed for LCLS [31]. Besides these advantages, from a general point of view vertically polarizing undulators will also allow to simplify the construction and operation of monochromators and experimental set-ups, due to the fact that they open the door to the use of gravity neutral designs.

A prototype of a NdFeB short-period planar undulator ($\lambda_u = 14\,\mathrm{mm}$), with a quatrefoil Delta-like geometry, has also been developed a few years ago by ENEA and Kyma. The undulator

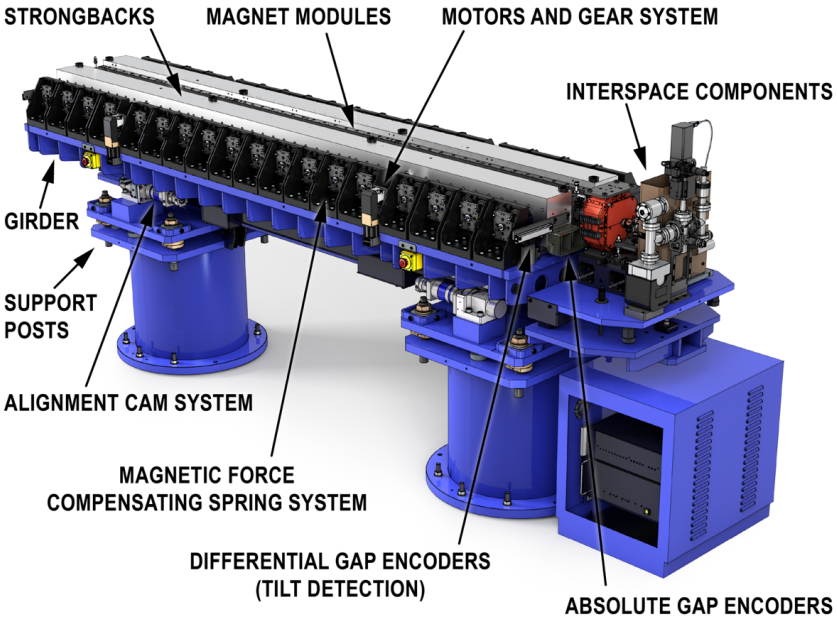

Figure 9: Horizontal gap/vertical polarization undulator (HGVPU) to be used at hard X-ray line of LCLS II. Reproduced from [31].

focuses the beam both in horizontal and vertical directions and provides a high field homogeneity. It has been tested on the SPARC-FEL (INFN-LNF and ENEA Frascati) and used as afterburner to emit radiation at 300 nm (electron beam energy of 100 MeV) [43]. It has an aperture of 5 mm, just enough to contain a round vacuum chamber with a 4 mm internal diameter. The maximum measured value for the deflection parameter is $K = 1.14$. This undulator has been considered within the context of the EuPRAXIA@SPARC_ LAB project [44], a design study for a soft X-ray FEL in the water window, where the possibility of using such a scheme for the undulator, but with $\lambda_u = 15$ mm (with expected $K < 1.2$), is currently under investigation.

2.3 In-vacuum

In the quest to reduce the period length without decreasing the K value of the undulators, the in-vacuum concept was developed. It consists in placing the magnets blocks inside the vacuum chamber in order to reach the minimum feasible gap, limited only by electron beam aperture and impedance considerations.

Leaving aside some preliminary experiences at BESSY [45], in-vacuum undulators (IVUs) as we understand them today were originally conceived at KEK in 1991 [46]. In the following years these devices were extensively developed at Spring-8 [47] and are currently used in most Synchrotron radiation facilities. Besides this, two hard X-ray FEL facilities (SACLA and Aramis line at SwissFEL) are based in in-vacuum undulators. In the particular case of FEL facilities, one additional advantage of variable-gap IVUs when compared to out-vacuum devices is that no narrow gap chambers are required, making it easier the initial commissioning and alignment.

In the typical structure of an IVU, shown in Fig. 10, the magnet arrays are supported by two backing beams: an in-vacuum and an out-vacuum one. The in-vacuum beam is usually made of aluminum and supports the magnet arrays. The out-vacuum is connected with girders to provide the gap movement. The two beams are connected by bellows shafts (also referred as link rods) that shrink and expand following the gap movement. Between the bellows shaft and out-vacuum beam are installed linear guides that allow a longitudinal movement of the bellows shaft in order to compensate the thermal expansion of the in-vacuum girder at the time of bakeout. In order to minimize the impedance of the device, two types of components are installed: a metal sheet that covers the magnet surface, and a RF transition that smoothly connects the end of the magnetic structure to the adjacent vacuum chambers, following the gap movement of the magnet arrays. In general it is made of Cu and is equipped with cooling channels to remove the heat deposited by the electron beam during operation.

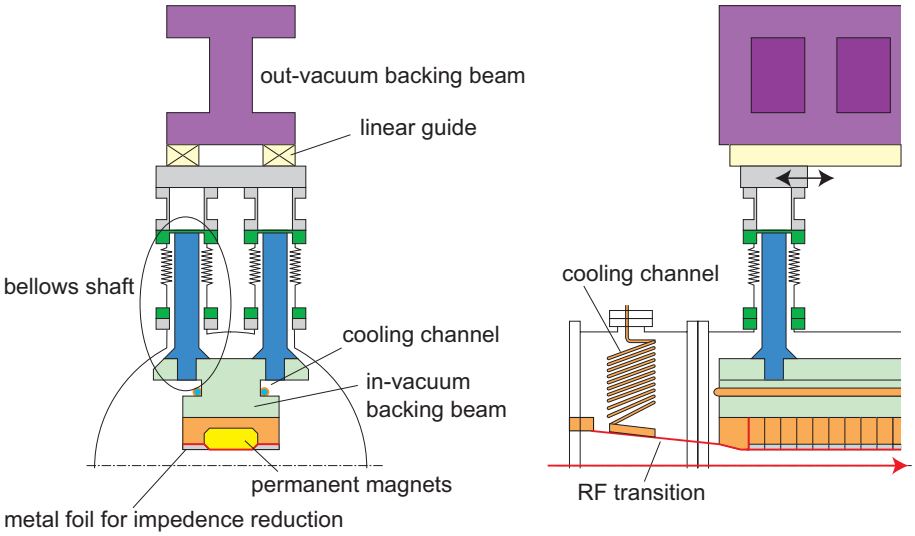

Figure 10: Diagram of a typical IVU structure. Reproduced from [47].

The magnetic gap of IVUs corresponds to the physical aperture for the electron beams except an additional 0.2 mm gap loss due to the metal sheets (generally Ni-Cu foils) covering the magnet surface. In comparison, for Superconducting Undulators (SCUs) the typical gap allowance is of at least 1.8 mm (2×0.6 mm wall thickness plus 2×0.3 mm insulation gap).

For UHV compatibility permanent magnets are customarily coated with TiN and are baked at a temperature of $\sim 125^{\circ}$C. In order to prevent demagnetization during bakeout, magnet blocks are pre-baked at a temperature slightly larger than the one used during the bakeout (e.g. 140°C). Due to these reasons, magnet grades with coercivities larger than 2000 kA/m are used [48].

One of the challenges of IVUs is the measurement of the magnetic field with a Hall probe system in order to determine the field quality and optimize the optical phase error of the assembled device. The standard method consists in characterizing and tuning the magnetic arrays with a traditional granite bench-based Hall probe system before assembling the vacuum chamber. Afterwards the magnetic arrays are disassembled from the bellow shafts, transferred inside the vacuum chamber, and re-attached again. Therefore the method relies on the accuracy and reproducibility of the assembly procedure. For most situations this method gives satisfactory results, although it does not allow to identify errors during the final assembly process, or to easily recheck the magnetic field of the device at a later stage in order to detect any radiation damage or ageing effects.

In order to overcome that difficulty and enabling the measurement of the magnetic field of IVU devices without removing the vacuum chamber, several systems have been developed. The pioneer one and by far the most successful concept has been the so-called SAFALI (for Self-Aligned Field Analyzed with Laser Instrumentation) system, conceived at SPring-8 [49]. In its original implementation, sketched in Fig. 11, it consists of a lightweight guiding system that is introduced inside the vacuum chamber and is externally supported through three flanges in the vacuum vessel. The transverse position of the measuring probe as it is displaced longitudinally is measured by means of a combination of laser beams, irises attached to the probe and position sensitive sensors (PSD), and a feedback system acting on the external supports of the guide ensures that the Hall probe is always in position. The SAFALI system has been used for the measurement of the IVU18 devices for SACLA FEL [50]. At PSI an equivalent system was built for the measurement of IVU15 devices for SwissFEL hard X-ray beamline [51].

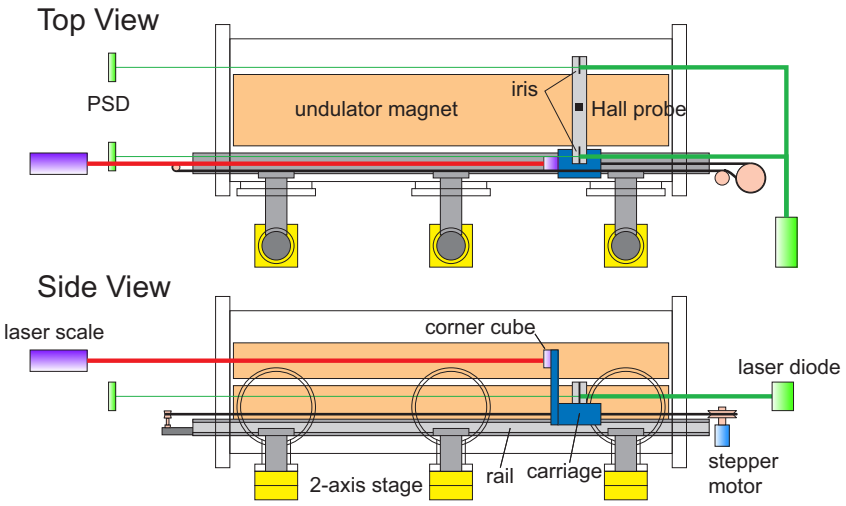

Figure 11: Schematic diagram of SAFALI system developed at SPring-8 for the in-situ measurement of IVUs. Reproduced from [49].

A different concept for an IVU measurement bench has been developed at ALBA [52]. The system, shown in Fig. 12, is based on a rigid granite bench driving a C-shape structure with

a flexible tape stretched between its ends. A light Hall probe is mounted in the middle of the tape, allowing it to be introduced inside a closed structure as an IVU.

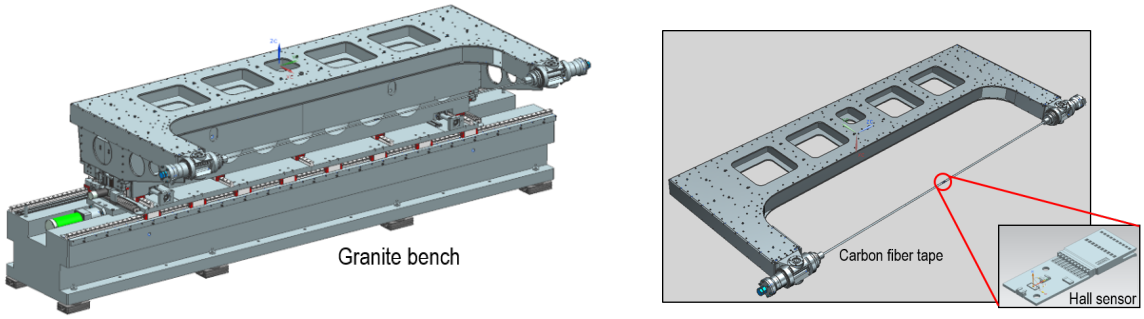

Figure 12: Drawing of magnetic measurement bench developed at ALBA for the characterization of closed magnetic structures [52].

2.3.1 Status (strengths and weaknesses)

A list of the in-vacuum undulators in operation in X-ray FEL facilities is shown in Table 6. The large experience gained with IVUs in Synchrotron Light Sources has allowed a smooth implementation of these systems in FELs.

Table 6: In-vacuum PM devices in X-ray FEL facilities.

Facility	type	min gap [mm]	period [mm]	max K	length [m]	#	Ref
SACLA	planar hybrid	3.5	18	2.2	5.0	18	[53]
SwissFEL							
Aramis	planar hybrid	3.2	15	1.8	4.0	13	[54]
SXFEL							
SASE line	planar hybrid	4.0	16	1.6	4.0	10	[55]

The strengths of this technology when compared to out-of-vacuum one include:

- Despite their higher complexity, IVUs can be considered a mature and standard technology.
- In fact, the experience at SACLA and SwissFEL has proven that the production of large batches of IVUs can be largely industrialized.
- As it has already been commented, the removal of narrow gap chambers and the large aperture that can be provided by variable-gap IVUs makes easier the initial commissioning phase of a FEL facility.

As for the weaknesses:

- The requirement of baking the magnetic structure and the closeness to the electron beam increases the risk of demagnetizing the magnet blocks. Due to this reason, grades with a high coercivity and a moderate remanent field have been traditionally used. In

more recent years the situation has improved with the introduction of grain boundary diffusion treated magnets. However, and despite these precautions, the threat of block demagnetization in room temperature IVUs remains, as proven by the experience at SACLA, where local magnetization losses of up to 20% have been reported after 4 years of operation [56].

- The in-vacuum principle has not yet been applied to a full-scale device with variable polarization.

2.3.2 Opportunities and challenges

In-vacuum undulators constitute a safe option to develop a relatively compact FEL hard X-ray source, but they are not the more aggressive solution based on permanent magnets. As in the case of out-of-vacuum devices, the main opportunities for improvement come from the side of cost savings:

- Either by reducing the dimensions and complexity of the support structure by means of force-compensating schemes.
- Or by automating the assembly and tuning of the devices in order to reduce the manufacturing time and cost.

One significant step forward will be the development of IVU versions of controllable polarization devices, which is currently undergoing.

The summary of SWOT analysis for in-vacuum PM devices is shown in Table 7.

Table 7: Summary of SWOT analysis for in-vacuum PM devices.

In-vacuum PM devices	
STRENGTHS	WEAKNESSES
• Technology mature • Well-known mechanical and ultra-high vacuum solutions • Enhanced field strength • Less limitation on smaller periods • Easier initial commissioning due the absence of the inner vacuum chambers	• Possible magnets' demagnetization • More complex mechanical and ultra-high vacuum solutions • Schemes providing full control on the polarization of the emitted light under development • Accessibility for magnetic measurements more difficult • Required the baking of the magnetic structure
OPPORTUNITIES	THREATS
• Application of improved permanent magnets • Smaller periods devices • Further development of variable polarization IVUs • Further development of magnetic measurement benches for closed gap undulators	• Spare PM blocks needed in case of long term magnets' demagnetization • Full-scale device with variable polarization not available in the short term

2.3.3 Advances in science and technology to meet XLS requirements

For SwissXFEL hard X-ray line Aramis planar IVUs with 15 mm period have been used (see Fig. 13). For this device the number of columns was reduced from 64 to 20, with a longitudinal shift between top and bottom columns [54], reducing the risk of vacuum leaks and minimizing the heat transference for a potential application of the design to a cryoundulator. The extruded aluminum keepers for the magnet blocks implement a flexible joint that, in combination with a 2°-angle wedge driven by a screw, allows to adjust vertically the pole height with micron precision [57]. Besides, the magnet and pole, with a chamfered profile, have been adapted to the characteristics of a single-pass machine, providing a significant reduction in magnetic load compared to IVU for Synchrotron Light Sources. All IVUs for Aramis were characterized using two magnetic measurement benches based on SAFALI system [51]. The first bench was designed to operate before mounting the vacuum chamber, in combination with a tuning robot unit (Yuri 2.0) for automated optimization of the magnetic array. The second bench was designed to measure the magnetic field after assembling all the vacuum components and to perform the final correction of the device by acting on the support columns. Currently PSI is developing a new version of the measurement bench that operates inside the vacuum chamber which incorporates the tuning robot unit (Yuri 3.0) [58]. This new bench will allow to perform the optimization of IVUs in a single campaign once the device is fully assembled, reducing the time required to tune the devices within specification.

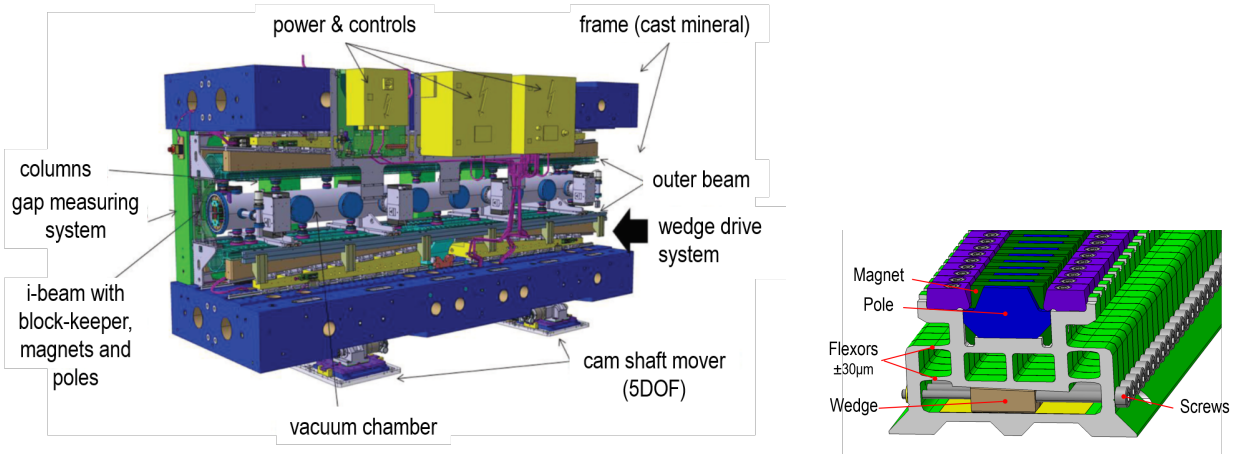

Figure 13: *Left:* Schematic view of U15 IVU for Aramis beamline at SwissFEL. *Right:* Detail of one of the magnet keepers, showing the flexor/wedge system used to adjust the vertical position of the poles.

One interesting development at SPring-8 has been the proposal to cancel out gap-dependent magnetic attractive forces in IVUs by means of periodically-magnetized monolithic magnets placed at each side of the main magnetic structure [59], a shown in Fig. 14. These monolithic magnets, also referred as MMM (Multipole Monolithic Magnets), generate a repulsive force that counteracts almost exactly the attractive one between the central arrays. The objective is to relax the rigidity requirements on the support frames and to reduce the large number of components required to distribute the mechanical load from the inner to the outer beams. The working principle has been successfully proved on a prototype, were the magnetically force has been reduced by more than a factor 30 over the whole analyzed gap range (from 20 down to 2 mm) [60]. Based on the results of that test, two different designs of IVU incorporating the

force cancellation principle have been developed, both of them providing a drastic size reduction and mechanical simplification of the device as compared to a standard IVU, as illustrated in Fig. 14.

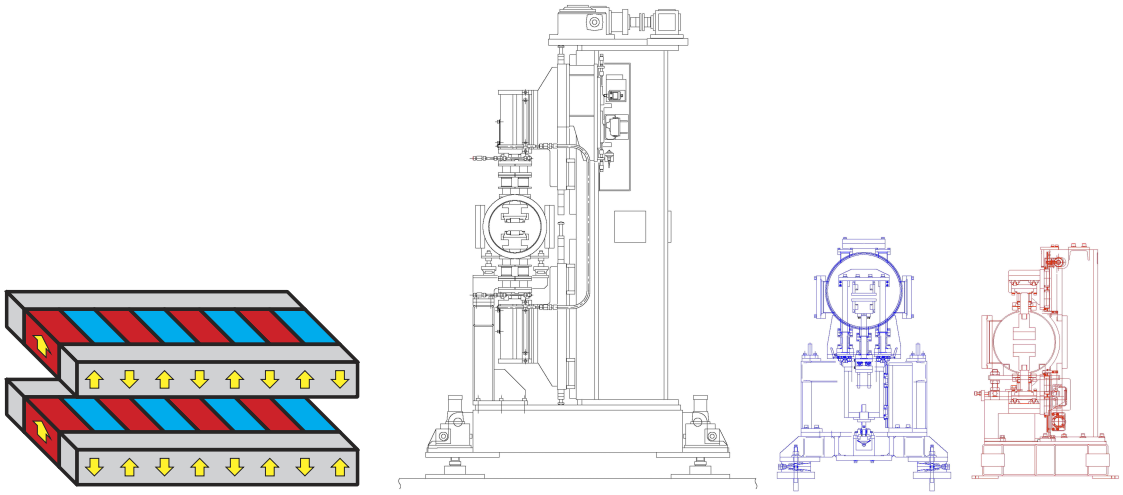

Figure 14: *Left:* Conceptual drawing of multipole monolithic magnet (MMM) force-compensated magnetic array. *Right:* Cross section drawings of the standard IVU in SPring-8 (black) and MMM compensated prototypes (blue and red). Reproduced from [60].

So far, no variable polarization IVU has been built due to engineering challenges. HZB started in 2017 an RD project for the development of a full scale planar IVU APPLE-II undulator (IVUE) [61]. The device will have a total length of 2.5m, a period length of 32mm, and a minimum gap of 7mm. The design has been carried out trying to take into account the demands and constraints of a future upgrade to a cryogenic option. The mechanical issues that have been addressed include the longitudinal bearings for the phase displacements, the implementation of the shielding foil and the flexible taper. The design also incorporates a force compensation scheme based in additional arrays of magnets in order to reduce the three dimensional forces that develop in APPLE-type undulators [62].

2.4 Cryogenic permanent magnet

Cryogenic permanent magnet undulators (CPMUs) were first proposed by Hara and collaborators in 2004 [22]. The design of in-vacuum undulators, with the magnet arrays maintained under vacuum with a good thermal insulation, can be easily adapted in order to cool the magnets down to cryogenic temperatures by means of either refrigerant channels or cryocoolers. The operation of the magnet blocks at cryogenic temperatures provides a three-fold benefit:

1. It removes the necessity of baking the magnets at high temperatures.
2. It enhances the coercive force of the magnets, making them more resistant to demagnetizing effects.
3. It increases the remanence of the magnets, with the subsequent increase of the undulator's peak field (up to $20-30\%$ higher compared to a room temperature IVU of equal design).

Compared with room temperature counterparts, CPMUs provide a field enhancement of $\sim 30\%$ for pure permanent magnet types and $\sim 50\%$ for hybrid types [22]. Compared to an IVU of equivalent spectral range (i.e. same K value), the flux is enhanced thanks to the field increase and to the additional number of periods for a given total length [63]. CPMUs are becoming the undulators of choice at medium-energy Synchrotron Light Sources. The smooth commissioning and successful operation over many years reflects the reliability of these devices. In fact, a demagnetization of CPMU magnets has not been reported yet in any facility.

In contrast with SCUs, where heat load budgets are of a few watts, CPMUs allow a very high heat load of several hundred watts. Besides, they provide a stable operation without any quench, and allow the application of standard techniques for magnetic field correction and shimming developed for room-temperature PM undulators. As an example, the second and third full-scale CPMUs constructed at SOLEIL did not require any extra shimming once finished [64].

As for the magnet cooling, there are two basic schemes available, as shown in Fig. 15. The most straightforward is using refrigerant channels with liquid nitrogen. This solution provides a cooling capacity of more than a kW, and it was the solution used at the first directly cooled CPMU to be operated at $77\,\mathrm{K}$, built at SOLEIL [65]. In the case of having to install several CPMUs, a thermosiphon system has been proposed at Diamond [66]. This system has the advantage of absorbing large amounts of heat with very small temperature gradients, and it is a particularly convenient solution when several devices are present. The other cooling concept is based on coldheads, each one of them providing a cooling capacity at $77\,\mathrm{K}$ of ~ 180–$200\,\mathrm{W}$ [67]. This principle is being used at SPring-8 [68] and TPS [69]. This technology also allows reaching temperatures below $77\,\mathrm{K}$, which is a requisite in some proposed advanced designs, as those making use of dysprosium poles [67].

The first CPMUs made use of NdFeB magnets, and hence were operated at a working temperature of $130\,\mathrm{K}$. Full scale devices were developed at ESRF [70, 71], SLS in collaboration with SPring-8 [72, 73] and Diamond [74]. However, PrFeB magnets were readily adopted, opening the door to cryoundulators cooled and operated at 77K. The first full scale realization of such a device was carried out at SOLEIL in 2011 [65, 75].

As it has been said, most of the IVU technology can be used in a CPMU, but several key components need to be adapted, in particular the cooling system, the magnet girder system,

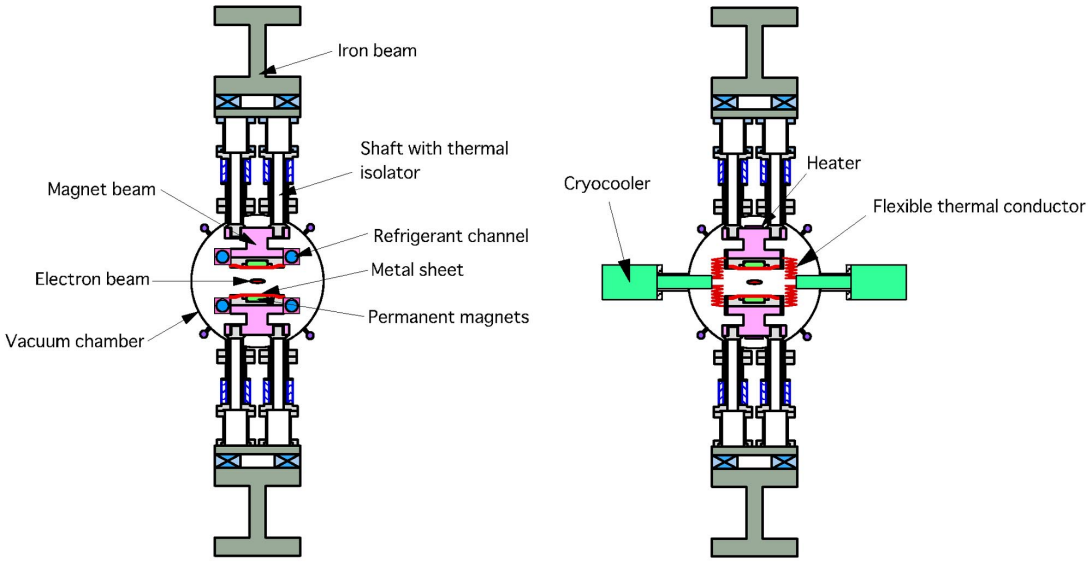

Figure 15: Diagram of a typical CPMU structure with two different cooling schemes: *Left:* refrigerant channels with liquid nitrogen. *Right:* cryocooler coldheads. Reproduced from [22].

and the gap measurement system. In addition, the magnetic field characterization of cryogenic undulators is challenging, given that magnetic measurements have to be conducted inside the vacuum chamber and at cryogenic temperature in order to optimize the undulator in the final operation conditions.

The SAFALI system developed at SPring-8 to carry out measurements inside vacuum chambers was readily adapted to the characterization of CPMUs at low temperatures [49]. The first adaptation, relying on the precision of a granite bench coupled to the Hall probes through a free standing pipe, allowed the measurement of a 0.6 m-long CPMU prototype [76]. Shortly afterwards an upgrade allowing to measure full-scale devices (typically 2.0–2.5 m) was developed and used to measure the CPMU14 for SLS [72]. In this upgraded version, which is shown in Fig. 16, the Hall probe carriage is displaced along the rail using a tensioned loop wire driven by a UHV-compatible stepper motor. In parallel, ESRF developed its own system based on a special vacuum chamber with an in-vacuum rail to guide the displacement of the Hall-probe carriage, which is moved via a magnetic coupling from an adjacent in-air granite bench system [70]. In this system two laser interferometers are used to determine the longitudinal position and the yaw angle of the Hall probe. More recently a new version of the bench has been worked out at the ESRF [77], with the advantage that it can be operated inside the final vacuum chamber of the device. The mechanics of the driving system are incorporated inside the vacuum system, and the transverse position and roll angle of the Hall probe are determined by means of a laser setup using PSDs.

At SOLEIL a first measurement system [64] was developed sharing some of the characteristics of the ESRF original one (Hall probe carriage actuated through an external stepper motor via a magnetic coupling), but with some differences (the in-vacuum rail was independent from the vacuum chamber, and was fixed from the outside with seven fixed rods). The deformations of the guiding system were measured using an optical system and corrected using shims. All three CPMU18 devices manufactured at SOLEIL were characterized using this bench, but an upgrade incorporating a SAFALI-style active feedback system based on piezo actuators is

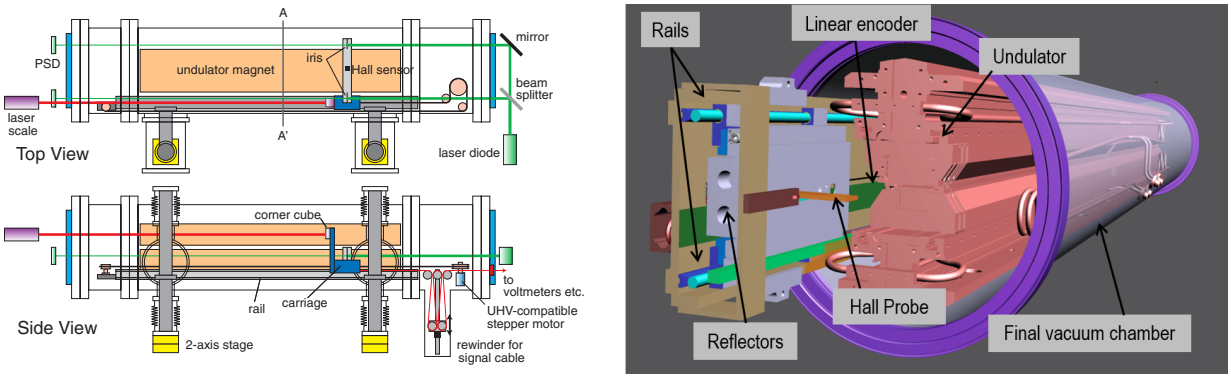

Figure 16: Schematic diagram of some of the available measurement systems for the in-situ measurement of full-scale CPMUs. *Left:* SAFALI system developed at SPring-8 (reproduced from [72]) *Right:* system developed at ESRF (reproduced from [77]).

undergoing, and will be used to characterize the CPMU15 device which is being built in the framework of a SOLEIL/MAX-IV collaboration [78].

Finally, HZB is developing a sophisticated SAFALI-type bench with active correction of all 6 degress of freedom (position and orientation) of the Hall sensor [67, 79].

2.4.1 Status (strengths and weaknesses)

In Table 8 we summarize the characteristics of some CPMUs devices currently under operation, most of them in Synchrotron Light Sources.

Table 8: Non-exhaustive list of full-scale cryogenic PM devices in operation or being manufactured.

Facility	material	min gap [mm]	period [mm]	B_{peak} [Tesla]	K_{max}	length [m]	Temperature [K]	Year	Ref.
ESRF	NdFeB	6.0	18.0	0.88	1.48	2.0	150-175	2008	[70]
SLS	NdFeB	3.0	14.0	1.186	1.551	1.7	135	2009	[72]
Diamond	NdFeB	5.0	17.7	1.04	1.72	2.0	155	2010	[80]
SOLEIL	PrFeB	5.5	18.0	1.152	1.94	2.0	77	2011	[24]
SOLEIL	PrFeB	5.5	18.0	1.152	1.94	2.0	77	2015	[78]
SOLEIL	PrFeB	5.5	18.0	1.152	1.94	2.0	77	2017	[78]
ESRF	(Pr,Nd)FeB	5.0	14.4	1.0	1.35	2.0	80	2016	[81]
SSRF	NdFeB	6.0	20.0	1.03	1.92	1.6	140	2016	[82]
SSRF	PrFeB	6.0	18.0	0.91	1.53	2.6	80	2017	[82]
BESSY-II	(Pr,Nd)FeB	5.5	17.0	1.17	1.85	1.6	80	2018	[83]
SOLEIL	PrFeB	3.0	15.0	1.735	2.34	3.0	77	—	[78]
TPS	PrFeB	3.0	15.0	1.77	2.48	2.0	77	—	[69]
Diamond	(Pr,Nd)FeB	5.0	17.6	1.20	1.97	2.0	77	—	[84]

The strengths of this technology include the following features:

- This technology allows to push the period of undulators down to the limit of the possibilities of PM materials.
- CPMUs expand the advantages of conventional IVUs (enhanced field strength and improved radiation resistance) at the extra cost of implementing a cryogenic system. This

system, however, is much simpler and relaxed than the one required by SCUs.

- Due to the large cooling capacity of the magnet structure, the problem of electron beam and synchrotron radiation induced heating is much alleviated when compared to conventional IVUs. As a result these devices have a more stable operation than SCUs.
- Despite the fact that CPMUs have not been yet used in a FEL facility, the experience gained at Synchrotron Light Sources allows to foresee a straightforward transfer of this technology to a future FEL.
- In fact, it is to be expected that CPMUs will become the workhorses for Storage Ring-based and FEL light sources for the next 5–10 years, until they are eventually superseded by the development of superconducting technology.

As for the weaknesses:

- The main weakness of CPMU technology is that it is limited by the properties of PM materials, which are not expected to improve in the future. In contrast, the materials properties in the case of SCUs keep on improving steadily.
- In a way similar to IVUs, no cryogenic versions of variable polarization undulators have been developed yet. However, the R&D efforts directed to build an APPLE-II in-vacuum undulator are including the demands and constraints of a future cryogenic option wherever possible.

2.4.2 Opportunities and challenges

Unlike in the case of IVUs, no experience is yet available for the series production of a batch of 10–20 identical CPMUs for a FEL. However, many of the lessons learned with IVUs for SACLA and SwissFEL (Aramis) will help to undertake such an effort. In fact, most of the tools required to characterize and tune IVUs have been developed taking CPMUs already in mind, and they are readily available. On top of this, a series of several CPMUs as the one required for a FEL will benefit from cooling schemes based on a thermosiphon as the one developed at Diamond, with the associated reduction of costs.

It is worth noting that the limits posed by the properties of available PM materials on CPMU technology have not been reached yet. In this sense there is still room for improvement, specially shrinking the period length of the devices down to the limit of what is mechanically feasible: full-scale operating devices have periods larger than 14 mm, whilst short prototypes with periods as small as 7–9 mm have already been developed. Another direction for improvement involves adopting more sophisticated pole geometries (wedged poles, compound poles with side magnets, etc) or pole materials with higher saturation magnetization (dysprosium or holmium). This latter option, however, will require a significant R&D program before becoming feasible on a full-scale device.

The summary of SWOT analysis for cryogenic PM devices is shown in Table 9.

2.4.3 Advances in science and technology to meet XLS requirements

For single pass light sources the transverse good field region is solely defined by the electron beam size and alignment tolerances, allowing the use of transversally narrow and shaped poles to further enhance the magnetic field. As an example, in their prototype for a 9 mm

Table 9: Summary of SWOT analysis for cryogenic PM devices.

Cryogenic PM devices	
STRENGTHS	WEAKNESSES
• Lowest period achievable • Enhanced field strength • Improved radiation resistance • No baking of the magnetic structure needed • Higher coercive force of the magnets • More resistant to demagnetization effects • Higher magnets' remanence • Increased undulators' peak field	• Technology not mature • Few active and knowledgeable groups • Minimum industrial involvement • More expensive • Challenging magnetic field characterization • Complex mechanical, ultra-high vacuum and cryo solutions • No schemes providing full control on the polarization of the emitted light
OPPORTUNITIES	THREATS
• Application of improved permanent magnets • Smaller period devices • Longer durability of magnetic structures • Higher performance achievable • Further developments of magnetic measurement benches for closed gap undulators • More stable operation due to large cooling capacity • Possible application for future FEL	• Serial productions are far to being feasible • Full-scale device with variable polarization not available yet

period and 2.5 mm fixed-gap CPMU the team at Helmholtz-Zentrum Berlin proposed to use a compound pole [85] (see Fig. 17). The compound pole provides an enhancement of the peak field by a 15% with respect to a conventional design. The achieved effective field at 20 K was 1.28 Tesla, for a g/λ_u ratio of 0.28.

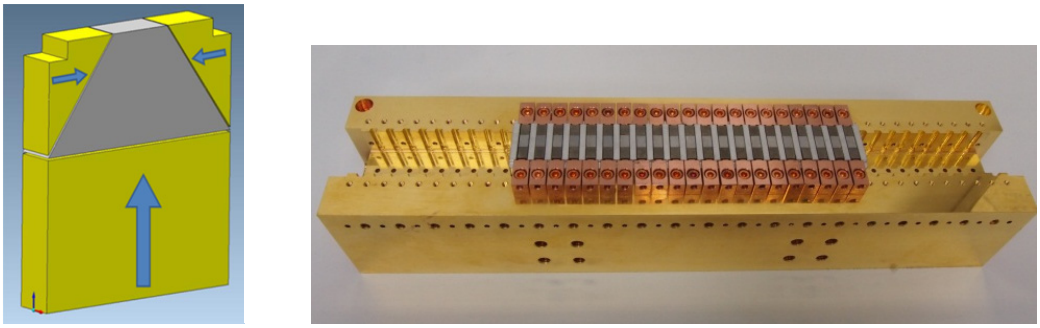

Figure 17: Single compound pole (*left*) and single girder with magnets and poles (*right*) corresponding to the short period ($\lambda_u = 9$ mm) fixed gap ($g = 2.5$ mm) undulator prototype developed at HZB. Reproduced from [85].

Another way of pushing the peak field to its limit is replacing the pole tips by textured Dy or Ho, that in principle would allow to increase the field by a $\sim 20\%$ for $g/\lambda_u = 0.1$ [15]. This requires cooling the system below liquid nitrogen temperature and no experience is available yet.

Operating devices have period lengths comprised in the range 14–20 mm, but efforts to

reduce further are being carried out at HZB [86]. Within this R&D effort a couple of 2.5 mm fixed gap prototypes with a period of 9 mm have been constructed. The first prototype used conventional rectangular CoFe poles, whereas the second prototype, as it has been mentioned at the beginning of this section, used compound poles which combined a trapezoidal CoFe piece with side magnets, all elements being soldered together [85]. Both prototypes made use of a new concept without magnet keepers; instead, permanent magnets are directly mounted inside the slots defined by two comb-like gauges located at both sides of the girder, and the poles are introduced into the spaces between the magnets. The girder was made of Cu for a better thermal conductivity. Some of these principles have been applied to the construction of a full scale device with a period length of 17 mm and a gap of 5 mm [83].

The company RadiaBeam Technologies launched some years ago an R&D program aimed to build short-period CPMU [87]. One of the goals of the project was developing textured dysprosium (TxDy) as a material suitable for manufacturing undulator poles. Eventually the development of textured dysprosium was discontinued, and the first prototype, with a period of $\lambda_u = 7$/,mm and a fixed gap $g = 2$ mm, made us of conventional vanadium permendur poles combined with (Pr,Nd)FeB magnets. The magnetic field generated by the prototype has only been characterized at room temperature, with the peak field turning out to be $B_{peak} = 1.11$ Tesla, corresponding to a deflection parameter $K = 0.72$.

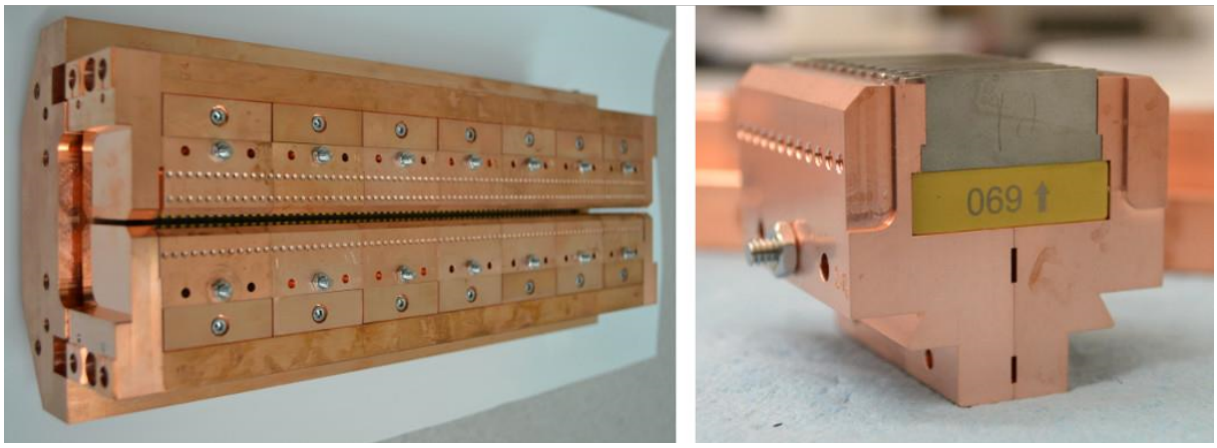

Figure 18: Images of the fixed-gap short-period cryogenic undulator prototype developed by RadiaBeam Technologies. Reproduced from [87].

2.5 Field scaling for PM undulators

In Table 10 we provide a list of the parameters a, b, c in the scaling expression Eq. (4) determined for different types of PM undulators. In each case we indicate if the fit was carried out for the peak (B_{peak}) or the effective (B_{eff}) magnetic field. Those entries in Table 10 with the reference [D5_1] have been obtained as a result of a dedicated study in the framework of the present project, by means of magnetostatic simulations carried out using RADIA [88, 89].

Table 10: Scaling law parameters for the magnetic field (either peak or effective value) as a function of the gap over period ratio for different types of PM undulators.

Type	Material	Field	a	b	c	Range ($x = g/\lambda_u$)	Ref
planar PM ver. field	SmCo ($B_r = 1.1$ T)	B_{peak}	1.87	-3.01	-0.14	$0.3 < x < 3$	[D5_1]
planar PM ver. field	NdFeB ($B_r = 1.25$ T)	B_{peak}	2.13	-3.01	-0.14	$0.3 < x < 3$	[D5_1]
planar PM ver. field	NdFeB ($B_r = 1.42$ T)	B_{peak}	2.42	-3.01	-0.14	$0.3 < x < 3$	[D5_1]
CPMU planar PM ver. field	PrNdFeB ($B_r = 1.7$ T)	B_{peak}	2.89	-3.01	-0.14	$0.3 < x < 3$	[D5_1]
Hybrid	SmCo ($B_r = 1.1$ T)	B_{peak}	3.50	-4.75	0.89	$0.3 < x < 3$	[D5_1]
Hybrid	NdFeB ($B_r = 1.25$ T)	B_{peak}	3.60	-4.45	0.67	$0.3 < x < 3$	[D5_1]
Hybrid	NdFeB ($B_r = 1.42$ T)	B_{peak}	3.70	-4.18	0.49	$0.3 < x < 3$	[D5_1]
CPMU Hybrid	PrNdFeB ($B_r = 1.7$ T)	B_{peak}	3.88	-3.87	0.26	$0.3 < x < 3$	[D5_1]
APPLE-II ver. field	NdFeB ($B_r = 1.42$ T)	B_{peak}	1.76	-2.62	-0.55	$0.3 < x < 3$	[D5_1]
APPLE-II circular	NdFeB ($B_r = 1.42$ T)	B_{peak}	1.36	-2.98	-0.28	$0.3 < x < 3$	[D5_1]
APPLE-X ver. field	NdFeB ($B_r = 1.42$ T)	B_{peak}	3.25	-4.11	0.35	$0.3 < x < 3$	[D5_1]
APPLE-X circular	NdFeB ($B_r = 1.42$ T)	B_{peak}	2.41	-4.27	0.40	$0.3 < x < 3$	[D5_1]
planar PM ver. field	NdFeB	B_{peak}	2.076	-3.24	0	$0.1 < x < 1$	[90]
planar PM hor. field	NdFeB	B_{peak}	2.400	-5.69	1.46	$0.1 < x < 1$	[90]
planar PM circular	NdFeB	B_{peak}	1.614	-4.67	0.62	$0.1 < x < 1$	[90]
APPLE-II ver. field	NdFeB	B_{peak}	1.76	-2.77	-0.37	n/a	[91]
APPLE-II hor. field	NdFeB	B_{peak}	2.22	-5.19	0.88	n/a	[91]
APPLE-II circular	NdFeB	B_{peak}	1.54	-4.46	0.43	n/a	[91]
Delta ver./hor. field	NdFeB ($B_r = 1.26$ T)	B_{peak}	1.96	-0.82	-3.31	$0.2 < x < 0.32$	[9]
Delta circular field	NdFeB ($B_r = 1.26$ T)	B_{peak}	1.45	-1.28	-2.24	$0.2 < x < 0.32$	[9]
Hybrid	SmCo	B_{peak}	3.33	-5.47	1.8	$0.07 < x < 0.7$	[5]
Hybrid	NdFeB/permendur	B_{peak}	3.694	-5.068	1.520	$0.1 < x < 1$	[90]
Hybrid	NdFeB ($B_r = 1.1$ T)	B_{peak}	3.44	-5.08	1.54	$0.07 < x < 0.7$	[92]
Hybrid	NdFeB ($B_r = 1.3$ T)	B_{peak}	4.3	-6.45	1.00	$0.04 < x < 0.2$	[92]
Hybrid	SmCo ($B_r = 1.12$ T)	B_{eff}	2.94	-4.62	1.37	$0.1 < x < 0.6$	[93]
Hybrid	NdFeB ($B_r = 1.22$ T)	B_{eff}	3.276	-4.51	1.20	$0.1 < x < 0.6$	[93]
CPMU hybrid	NdFeB ($B_r = 1.5$ T @150K)	B_{peak}	3.121	-3.204	-0.193	$0.2 < x < 0.6$	[27]
CPMU hybrid	PrFeB ($B_r = 1.67$ T @77K)	B_{peak}	3.198	-3.062	-0.332	$0.2 < x < 0.6$	[27]
CPMU hybrid	(Nd,Pr)FeB ($B_r = 1.62$ T @77K)	B_{eff}	3.177	-3.111	-0.495	$0.14 < x < 0.8$	[67]

3 Superconducting undulators

3.1 Basic conceptual design

The history of superconducting undulators (SCUs) and their application to free-electron lasers (FELs) goes back to the first experimental demonstration of FEL amplification in the 1970's [94, 95]. Elias, Madey and co-workers used a helical SCU consisting of a double helix winding around the beam tube. The first planar SCUs for storage rings and potential use in FELs were developed and applied shortly after that [96–99]. The development of SCUs, however, did not keep up with the tremendous progress of permenant magnet undulator technology, except for the niche of high-field multipole wigglers [100, 101]. In their frequently cited review article "Design considerations for a 1 Å SASE undulator" of the year 2000, Elleaume, Chavanne and Faatz came to the conclusion: "It clearly appears that while superconducting technology appears very attractive for producing high field at low magnetic gap, due to the inexistence of any prototype of such high-field superconducting undulator, it is not yet a real option for the undulator designer." [90].

This situation has changed. SCU development programmes started in the 1990's at several laboratories around the world, leading to the successful demonstration and routine operation of planar SCUs in storage ring light sources [102–105], and to a re-consideration of their application particularly to hard-X-ray FELs [106]. In spite of the progress made on permanent magnet undulators, SCUs still offer higher magnetic flux density amplitudes and/or shorter period lengths. The development of low-emittance, medium energy storage rings and the tendency towards compact short-wavelength FELs create an increasing demand for narrow-gap, short-period undulators, which SCUs can serve very well. On the other hand, SCU technology today can take benefit from many years of superconducting accelerator magnet technology and cryogenics development. The trade-off between magnetic performance on the one hand and technological challenges on the other is not any more to the disadvantage of SCUs.

The basic design of an SCU magnet consists of an array of superconducting coils, typically wound on a soft iron former or around soft iron poles, or of a (high-temperature) superconducting bulk structure including soft iron poles. As for permanent magnet devices, several different field configurations are possible, including planar and helical periodic fields, configurations for electrically variable polarization or periodic fields with a transverse gradient. Depending on those on the one hand, and on the choice of conductor on the other hand, different winding schemes and winding procedures, splicing techniques, possibly after-winding processing steps, cooling and powering configurations apply, as will be described in more detail in the following subsections of this report.

All SCU species have in common that their magnet assembly forms a cold mass for which typical operation temperatures of 2–4.5 K need to be maintained with the high-energy particle beam and potentially a high-power photon beam passing through the (narrow) undulator gap. For almost all types of SCU magnet assemblies, indirect cooling schemes are favoured. An exception are coil assemblies directly wound on the beam vacuum tube (or a tube concentric with it), which more conveniently are immersed in a liquid Helium bath. Prominent examples for such structures are double-helix helical SCUs.

Indirect cooling schemes either employ liquid Helium flow through the coil former or a heat exchanger thermally connected to it, driven e.g. by the thermosiphon effect [108], or contact cooling by cryocoolers. Both schemes have been shown to work reliably in storage ring light

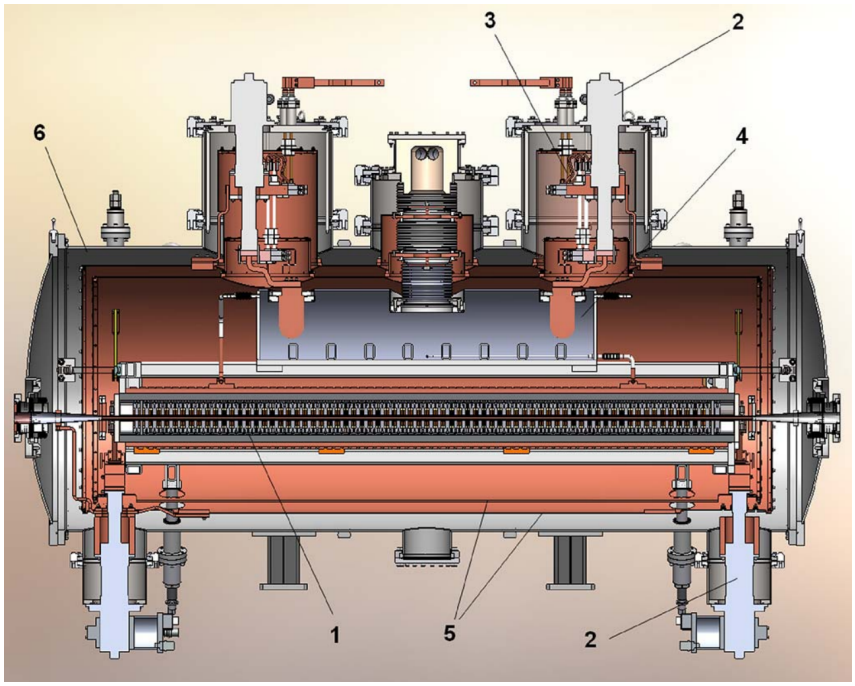

Figure 19: Exemplary sectional view of a cryostat for superconducting insertion devices using a thermosiphon-based conduction cooling scheme. The example shows the CLIC damping wiggler prototype manufactured by the Budker Institute of Nuclear Physics and installed in the Karlsruhe Research Accelerator (KARA). A similar cryostat design is used for the APS superconducting undulators. 1: wiggler magnet, 2: cryocoolers, 3: current leads, 4: internal liquid Helium reservoir, 5: radiation shields, 6: vacuum vessel. Graphics reproduced from [107]

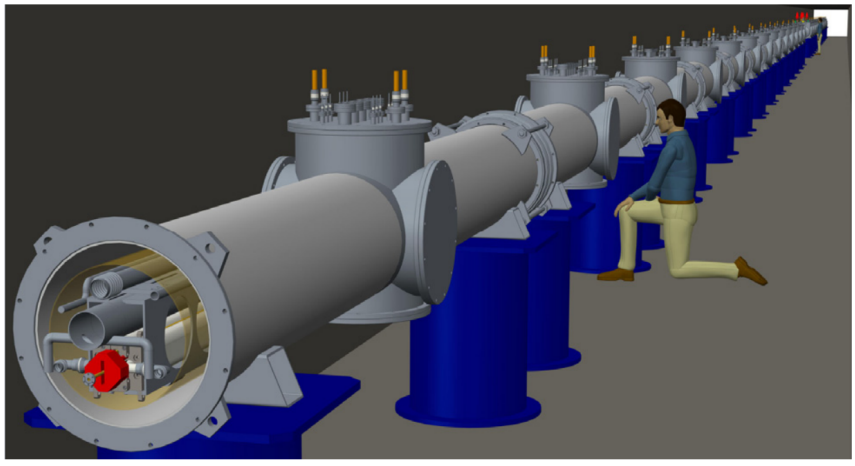

Figure 20: Conceptual view of a minimally segmented line of SCU cryostats as proposed for the LCLS-II. Graphics reproduced from [106]

sources [104, 109–112]. Schemes using liquid Helium as a cooling medium can be designed as closed cycle, zero boil-off systems with Helium recondensers [107, 113], either with a liquid Helium reservoir incorporated in the SCU cryostat (exemplarily shown in Fig. 19), or – an option more applicable for FELs – with a set of SCU cryostats forming a line supplied by a central cryoplant [114].

For storage ring applications, the cryostat's insulation vacuum (typically in the order of 10^{-5} mbar in warm, 10^{-8} mbar in cold conditions) and the beam vacuum ($\leq 10^{-9}$ mbar) are separated. In order to sustain the beam-induced heat load, the beam vacuum chamber is thermally isolated from the coils and may be kept at a somewhat higher temperature level (order of 10–20 K) where higher cooling power is available [107, 115]. The wall thickness of the beam vacuum chamber and the mechanical separation of the superconducting coils from the beam chamber result in a difference between the magnetic gap and the beam-stay clear, which for the most advanced designs is in the order of 1 to 2.3 mm [116, 117].

As pointed out by J. Clarke [118], for a single-pass application like an FEL, it might be a feasible option to omit the beam vacuum chamber, i.e. to operate SCUs as in-vacuum devices. That would enable much lower differences between beam-stay-clear and magnetic gap height (0.2 mm) and thereby significantly higher field amplitudes for a given period length and beam-stay-clear. We shall consider this option in more detail below.

Rather independent from the particular choice of superconducting magnet technology, a complete SCU-FEL beam line will typically consist of a line of cryo modules as shown in Fig. 20, each containing one or two SCU modules, at least two focusing magnets (possibly but not necessarily also superconducting) as part of the magnetic lattice, steerers, phase matchers and beam diagnostic elements, all operated at cryogenic temperatures in order to avoid space-consuming cold-warm transitions as far as possible.

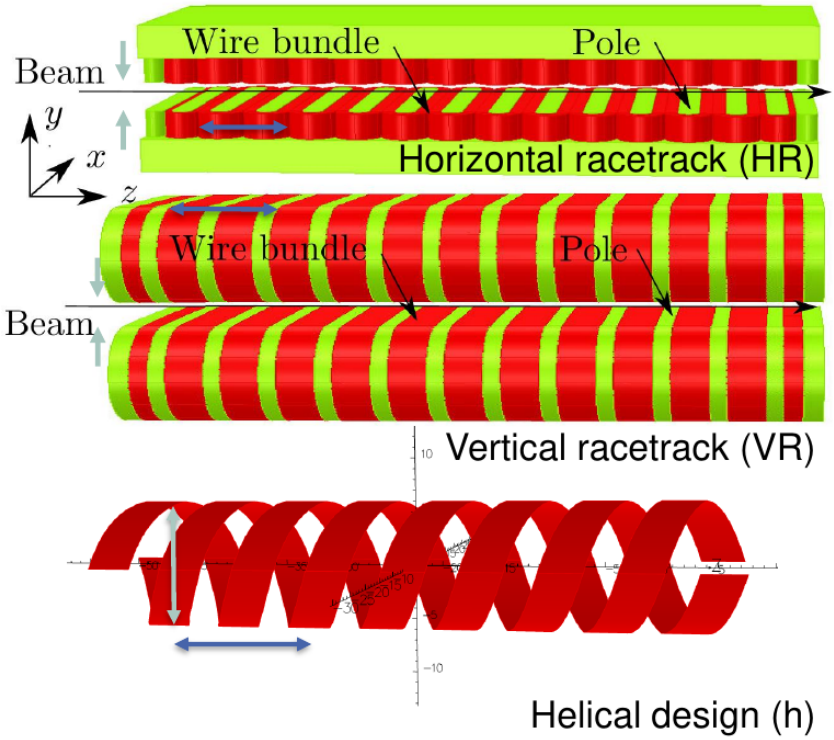

Figure 21: Winding geometries for superconducting insertion devices. Graphics partly reproduced from [119]

3.2 Low temperature

Superconducting planar undulators Superconducting planar undulators typically consist of two opposing periodic arrays of superconducting coils as depicted in Figure 21 (top) and (middle). In most cases, the coils are wound on a soft magnetic former which leads to an increase of the on-axis magnetic flux density as compared to a purely coil-generated undulator field. Each period consists of two poles and two superconducting coils carrying a current of equal magnitude but opposite direction. The most common design is the vertical-racetrack (VR) arrangement shown in Fig. 21 (middle). The horizontal-racetrack (HR) design shown in Fig. 21 (top) is typically applied for superconducting wigglers with period lengths down to 20 mm. Since the bending radius of the superconducting wire is a limiting factor, it seems rather clear that ultimately short period lengths of planar SCUs can only be achieved in a vertical coil arrangement. It is worth noting, however, that superconducting wigglers with ever shorter period lengths have been developed and implemented over the years and a design for a HR-SCU with 15.6 mm period length has been designed and experimentally tested [120], which is not necessarily the limit in terms of short period lengths. Since the HR option can have advantages over the VR option in terms of mass production, mechanical alignment, maintenance and repair, it should, although uncommon, not be excluded.

In general the gap of low-temperature superconducting undulators is fixed and the undulator is tuned by varying the current in the superconducting coils. In that respect the mechanical design of superconducting undulators is much more simple than that of variable-gap permanent magnet devices.

The applicable current is limited by the critical current density on the load line, i.e. intersection of the maximum magnetic flux density felt by the conductor as a function of applied current

Table 11: SCUs in storage rings and FELs.

Name	mag. gap (mm)	stay clear (mm)	period (mm)	B (T)	K	length (m)	year	Ref.
ANL APS								
SCU0	9.5	7.2	16.0	0.7	1.1	0.3	2015	[27, 102]
SCU18-1	9.5	7.2	18.0	1.0	1.6	1.1	2016	[27, 123]
SCU18-2	9.5	7.2	18.0	1.0	1.6	1.1	2016	[27, 123]
Helical SCU	31	29	31.5	0.4	1.2	1.2	2018	[27, 124, 125]
SLAC LCLS								
FEL SCU[3]	8.0	5.7	21	1.7	3.3	1.5	2018	[123] [125]
Daresbury & Rutherford Appleton Laboratory								
Helical ILC test[4]	6.4	5.9	11.5	0.9	0.9	2×1.74	2011	[122]
KIT KARA								
SCU14	8.0	7.0	14.0	0.4	0.6	1.4	2010	[126]
SCU15	8.0	7.0	15.0	0.7	1.0	1.5	2016	[105]
SCU20	8.0	7.0	20.0	1.2	2.2	1.6	2018	[104]
Stanford University/first FEL								
Helical		10.2	32	0.2	0.7	5.2	1976	[94, 127]
BNL ATF/FEL								
Planar	4.4		8.8	0.5	3.9	0.6	1992	[127, 128]

with the critical surface of the phase transition to the normal conducting state. The load line depends on the actual coil geometry. The critical surface in terms of engineering current density depends on the properties of the superconducting strand, the packing density of the coils and the operating temperature. In the parametric studies discussed below, typical properties of presently commercially available strands are assumed.

Superconducting helical undulators Superconducting helical undulators (SCHU) are in many ways more straightforward to manufacture than superconducting planar devices. They are not a new idea, in fact the original FEL employed an SCHU [95] and they have been used in particle physics experiments [121] and developed to drive high intensity positron sources for future linear colliders [122]. The most common design, since it is efficient and relatively easy to wind, is the bifilar helix [92], which is depicted in Fig. 21 (bottom). This essentially consists of two interlocking helical windings with currents flowing in opposite directions. To increase the field, the space separating the windings can be filled with a helical iron former. The fields generated by such a magnet are very strong since the beam axis is fully surrounded by superconducting windings and iron poles. Recently an SCHU has also been built and installed into a third generation light source [117].

3.2.1 Status (strengths and weaknesses)

Superconducting planar undulators Thanks to the SCU development programmes in several labs, particularly driven by the Argonne and Lawrence Berkeley National Labs (ANL/LBNL)

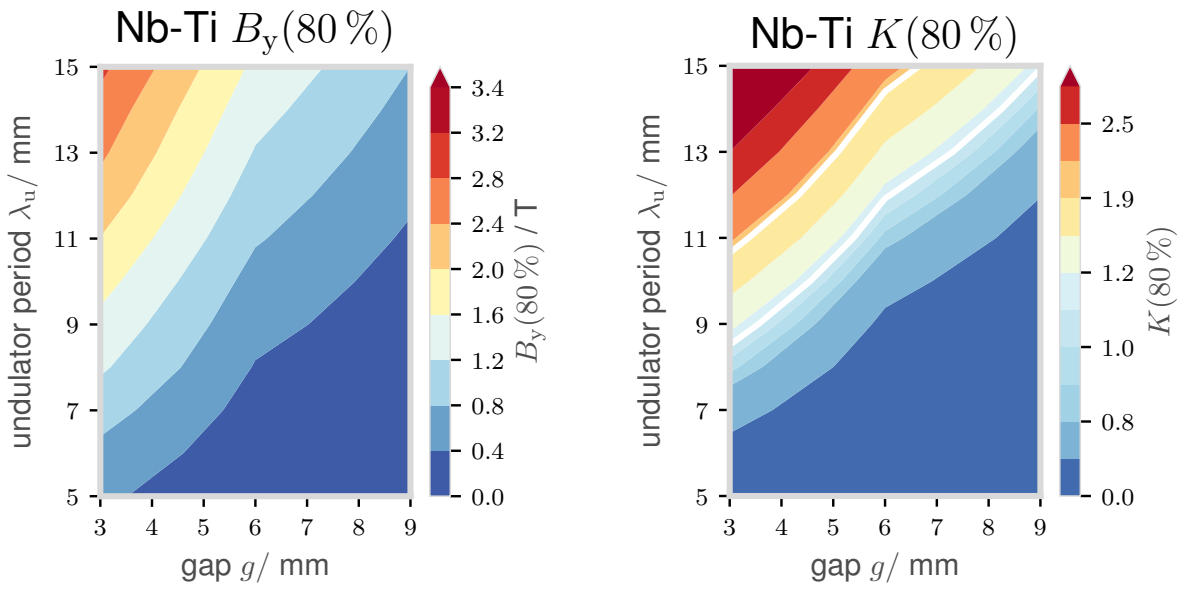

(a) Magnetic strength B

(b) Undulator parameter K

Figure 22: Magnetic strength B_y ((a)) and undulator parameter K ((b)) depending on the magnetic gap g and the undulator period length λ_u. Nb-Ti at 80% of its maximum field strength

in the US, the cooperation of the Karlsruhe Institute of Technology (KIT) and Bilfinger Noell GmbH in Germany and the Daresbury and Rutherford Appleton Laboratories within the UK Science & Technology Facilities Council (STFC), Nb-Ti-based superconducting planar undulators have become a mature technology. Several devices have been installed and tested in storage ring light sources, and several are being successfully and reliably operated at the Advanced Photon Source (APS) at the ANL and at the KIT synchrotron light source. Moreover, Nb-Ti-based superconducting planar undulators are being offered as a customized commercial product by Bilfinger Noell [116, 129, 130]. Table 11 summarizes the full-scale Nb-Ti-based devices successfully tested and/or currently in operation in storage ring light sources.

Nb_3Sn-based SCU technology, while promising a significantly higher performance in terms of magnetic flux density amplitude for given gap width and period length, is much less advanced due to the much more severe technical challenges [131], which we shall address below. However, examples of successful manufacturing, processing and cold testing of Nb_3Sn-SCU short models [132, 133] and full-scale coils [134] exist, suggesting that Nb_3Sn-based SCUs will probably become feasible in the future.

Not only has the SCU technology (including the associated cryo-technology) been strongly advanced over the last two decades, but also the required laboratory infrastructures for testing, characterizing and conditioning the SCU coils [135, 136].

The main reason for considering SCUs as for FEL driver for XLS is clearly the achievable magnetic performance in terms of e.g. the ratio of flux density amplitude to period length for a given gap width. In these terms, already the least advanced SCU technology (Nb-Ti) outperforms permanent magnet technologies over a wide range of period lengths. Figure 22 shows a contour map of FEM calculated magnetic flux density amplitudes (a) and corresponding undulator parameters (b) at 80% of the critical current density on the load line as a function of gap width and undulator period length, showing that K values above one are well feasible at

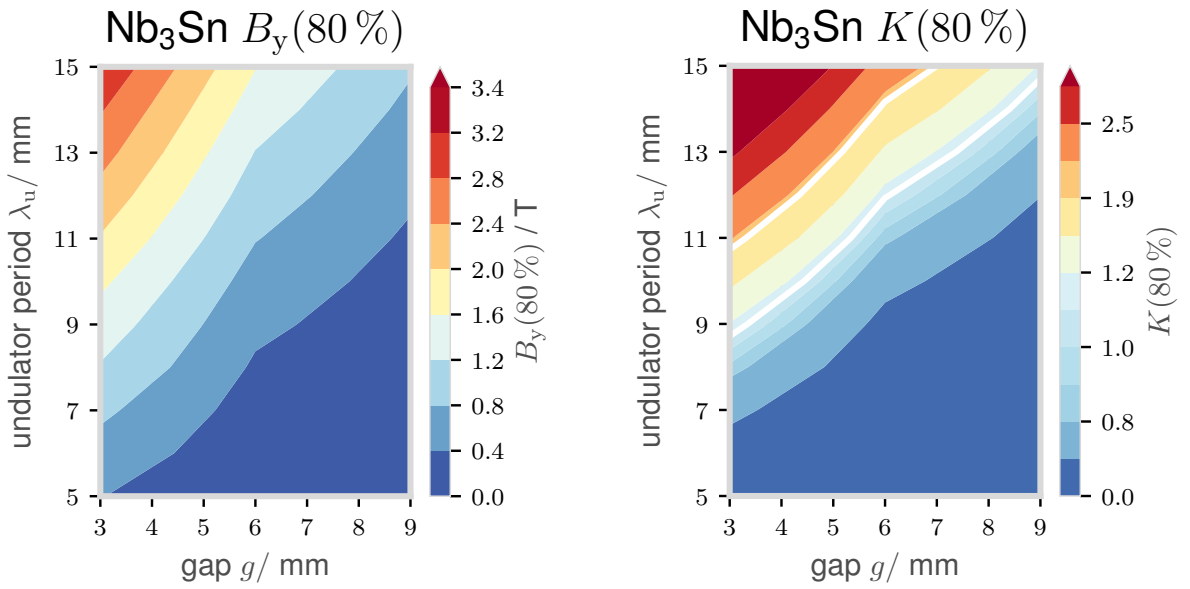

(a) Magnetic strength B

(b) Undulator parameter K

Figure 23: Magnetic strength B_y ((a)) and undulator parameter K ((b)) depending on the magnetic gap g and the undulator period length λ_u. Nb_3Sn at 80% of its maximum field strength

period lengths down to 9 mm for a magnetic gap of 4 mm. Note that this model calculation was made under rather conservative assumptions.

Further strengths of Nb-Ti-based planar undulators are their already described technical maturity and their proven operational stability under the comparably harsh operation conditions in a highly reliable storage ring light source. As far as the cryogenic part of this technical maturity and operational performance is concerned (which is in fact a major part of the SCU technology in general), this statement also applies to Nb_3Sn and even high temperature superconductor-based SCUs.

Nb_3Sn-based SCUs could offer an even higher magnetic performance. A similar contour plot as shown for Nb-Ti in Fig. 22 is shown for Nb_3Sn in Fig. 23. The gain in performance shown by this calculation is not as high as one might have expected. The reason for that lies in the assumptions made on achievable quench currents, which are based on data of Nb_3Sn strands commercially available today. Since the development of Nb_3Sn strands is mainly driven by the development of high-field accelerator magnets [137–139], these strands are not well suited for the application in SCUs particularly when pushing for short periods. The comparably low flux density at the conductor in short-period SCUs leads to low pinning forces and in turn to unstable operation conditions for the Nb_3Sn strand. This effect currently puts a limit to the performance of short-period Nb_3Sn SCUs, which might be overcome or at least shifted by future developments in the part of the conductor.

A strength common to all low-temperature superconducting undulator technolgies and important to note particularly in the context of XLS is the radiation hardness of superconducting magnets (as stated e.g. in [106, 140]). In fact, the superconducting properties of low temperature superconductors are hardly affected at all by irradiation with electrons and photons [141]. The limiting factor for the lifetime of SCUs in an FEL environment is therefore the radiation-induced degradation of the insulating material, which is also mechanically stabilizing

the superconducting coils. Polyimid-based insulation materials commmonly used in accelerator magnets are typically able to withstand doses 1–30 MGy.

What may be regarded as a weakness common to all types of superconducting undulators, is the indispensable cooling to cryogenic temperatures, which is reflected in technical complexity of the device itself as well as of the appropriate test and characterization facilities, investment and running cost and effort required for implementing, optimizing and maintaining a beam line of several tens to hundreds of metres of SCUs. Along with that, field measurement and particularly field correction schemes, as far as available, are technically complex and much less elaborated than the established shimming techniques for permanent magnet undulators [142, 143].

Today's state of the art planar SCUs designed for storage rings are, as mentioned in the introduction to this section, out-of-vacuum devices. Thus, they share with the out-of-vacuum PMUs the weakness that their magnetic gap is significantly larger than the beam-stay-clear, which puts a limit to the achievable magnetic flux density amplitude particularly at short period lengths. In-vacuum SCUs would considerably push this limit.

Employing Nb_3Sn technology for SCUs comes with additional challenges, one of which we already addressed, the fact of available strands not being optimized for the application in undulators. The further challenges mainly arise from the material properties of Nb_3Sn, which is a brittle intermetallic compound with strain-sensitive superconducting properties. Unlike Nb-Ti, Nb_3Sn can only be reacted after winding, which requires a thermal treatment which is very challenging to apply to SCU coil compounds and makes it very difficult to maintain mechanical tolerances required for a good field quality. Due to the sensitivity of the material to strain, among other reasons, a Nb_3Sn undulator coil is much more likely irreversibly damaged than a Nb-Ti coil in case of a quench.

Superconducting helical undulators The challenge with using an SCHU for CompactLight will be the combination of very short period and narrow beam aperture whilst maintaining suitable field strength and quality for the FEL. The bifilar helix is not intrinsically a rigid device since in some ways it resembles a spring. The engineering challenge then is likely to be mechanically achieving and maintaining the periodicity and straightness along its length. The SCHU already demonstrated with parameters nearest to those required by CompactLight is that developed for positron production [122], using Nb-Ti wire, which had a period of 11.5 mm, an aperture for the electron beam of 5.35 mm, a length of 1.74 m per unit (two units in one cryostat), and a design field of 0.86 T on axis. Two units were built and tested successfully, each achieving ~ 1.15 T on axis, far more than the design value. The same group later investigated the application of Nb_3Sn superconductor to this type of undulator in the framework of the EuCARD project. They identified extra challenges related to the superconductor not being optimised for low field (< 4 T) operation which led to instabilities, to the insulation between the iron former and the wire having to cope with the high temperature reaction process of the superconductor, and also with the brittleness of the activated wire itself. Two short prototype SCHUs were built with similar parameters to those of the Nb-Ti version but both gave disappointing performance and were not followed up. It is clear that were CompactLight to pursue the use of Nb_3Sn in this type of device there would be an extra layer of challenges to overcome beyond those already present with the established NbTi technology.

3.2.2 Opportunities and challenges

From the data on magnetic performance discussed in the previous section it can be concluded that already the most conservative superconductor technology (Nb-Ti) enables a rather aggressive design of a modern X-ray FEL facility in terms of compactness. With the exception of the early history of FELs, Nb-Ti superconducting undulators have not been employed in FEL facilities so far. However, they have become a state-of-the-art technology for storage ring light sources and are being further developed and validated for their application to free electron lasers in an active R&D programme for the upgrade of the Linac Coherent Light Source (LCLS-II) [106, 117].

This programme has lead to promising results also with regard to the intrinsic SCU field quality and SCU field correction techniques [143] and has significantly advanced the Nb_3Sn superconducting undulator technology.

Obviously, if fully utilisable, Nb_3Sn technology has great promise for high-performance short-period undulators and in turn for compact FELs. Recent achievements on short models [134, 144] suggest that the fabrication of stable, high-quality Nb_3Sn SCU magnets, though demanding, is in fact feasible, and that by advances of the Nb_3Sn strand technology also the issue of instabilities at high current densities and low fields could be resolved. It is well possible that an increasing demand for Nb_3Sn strands optimized for “low field” applications like SCUs will stimulate an according R&D and bring this technology into reach for a future CompactLight facility.

The cryogenics realized for SCUs so far are adapted to their use as single devices in storage rings. Conceptual cryostat designs for many superconducting insertion devices in a row have been proposed for damping rings [145] as well as for FELs [114]. As suggested in [114], it is relatively straightforward to employ multiple independent SCUs, especially helical, in parallel within a single cryostat, enabling an extremely close packing of undulator lines virtually unachievable with permanent magnet undulators.

3.2.3 Advances in science and technology to meet XLS requirements

With the background of the advances in low-temperature SCU technology for storage rings over the last decade, it seems relatively straightforward to develop a baseline conceptual design for a superconducting undulator beam line serving the XLS requirements in terms of FEL performance and compactness, based on the established out-of-vacuum Nb-Ti technology.

There is a high potential for further improvements and developments. We already addressed in-vacuum SCUs and Nb_3Sn SCUs which are actively being investigated and will likely become available in the near future.

Above that, there is a potential for advancing the magnetic design of SCUs with respect to optimal FEL performance and enhancements such as tapering schemes, two-colour, broad band radiation and variable polarization schemes.

3.3 Field scaling for low temperature superconducting undulators

Table 12 summarizes the scaling parameters for Nb-Ti and Nb_3Sn planar and helical undulators applied to the scaling expression

$$B(\lambda_\mathrm{u}[\mathrm{mm}], g[\mathrm{mm}]) = c_1 \cdot (c_2 + c_3\lambda_\mathrm{u} - c_4\lambda_\mathrm{u}^2 + c_5\lambda_\mathrm{u}^3) \exp\left(-\pi\left(c_6\frac{g}{\lambda_\mathrm{u}} - 0.5\right)\right). \quad (6)$$

Based on the scaling laws described in [146] and put into practical formulae by [27], we updated the equation by a factor of 1.17 for Nb-Ti to match simulations and measurements done at the Rutherford Appleton Laboratories for planar Nb-Ti undulators. The equation for Nb_3Sn which fits to our simulations is also taken from the aforementioned papers. To get scaling laws for helical superconducing undulators we fitted the parameters in Eq. 6 to Opera 3d [147] simulations done in the period range of 3–15 mm for the magnetic gap heights of 3 mm, 6 mm and 9 mm.

Table 12: Scaling law parameters for the magnetic field as a function of the gap over period ratio for different types of SC undulators. The planar fits are based on [27, 146, 148], but for Nb-Ti multiplied with a factor $c_1 = 1.17$, because of new fit-data. For helical undulators completely fitted to simulated data.

	Nb-Ti		Nb_3Sn	
	Planar	Helical	Planar	Helical
c_1	1.17	1.70 ± 0.15	1.3	1.25 ± 0.12
c_2	0.28052	0.055 ± 0.013	0.28052	0.04 ± 0.05
c_3	0.05798	0.063 ± 0.005	0.05798	0.056 ± 0.018
$c_4/10^{-4}$	9	25 ± 3	9	-10 ± 20
$c_5/10^{-6}$	5	51 ± 12	5	-30 ± 80
c_6	1	0.8333 ± 0.0015	1	0.940 ± 0.006
λ_u/g	0.5	0.5	0.5	0.5

3.4 Coils from high temperature superconducting tapes

This section focuses on high-temperature superconductors (HTS) in the form of tapes and their application to superconducting undulator magnets. The investigated conductor material is from the group of Rare-earth Barium Copper Oxides (REBCO), such as Yttrium Barium Copper Oxide (YBCO) or Gadolinium Barium Copper Oxide. REBCO based conductors become superconductive above the boiling temperature of liquid nitrogen. For instance the critical temperature of YBCO was found at 93 K, corresponding to $-180.15\,^{\circ}\mathrm{C}$ [149].
Besides REBCO there is another type of HTS conductor available on today's market which exists in the shape of a round wire: Bismuth Strontium Calcium Copper Oxide (BSCCO). However BSCCO has two notable disadvantages: First, since BSCCO wires are heavily depending on the use of silver for forming a filament matrix, the lower limit of the cost will always be driven by silver. Second, an extensive and complicated manufacturing process is needed (worse than for Nb_3Sn) undergoing high temperatures and pressures [150]. Contrary, REBCO is promising a more inexpensive and more economical way of production in the future. REBCO material is deposited as a thin layer (1 to 5 µm) on a carrier substrate, like stainless steel or Hastelloy and usually surrounded by layers of copper, optionally silver, and thin buffer layers. A schematic sketch of the different layers can be seen in Figure 24. The tape shape gives the coated conductor easy and hard bending directions, which must be taken into account during the process of coil design.

Undulator magnet structures wound from HTS tape can follow the same geometrical designs as low-temperature superconductor (LTS) devices, presented in a previous section (see Figure 21). In this work we investigated horizontal and vertical racetrack geometries as well as helical designs.

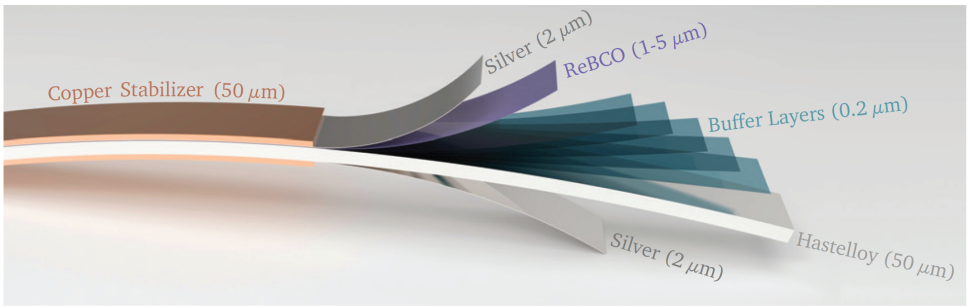

Figure 24: Schematic sketch cross-section of coated REBCO conductor tape structure [151].

3.4.1 Status (strengths and weaknesses)

At present the main application for HTS conductors are electric power applications such as power cables. In the field of magnet technology, high-temperature superconductors are still undergoing the process of research and development.
Due to their upper critical field of (168 ± 26) T [152] HTS conductors have been successfully used for solenoidal insert coils in LTS coil generated background fields over the past years, generating fields beyond 30 T [153].

Recently, steps have been made in designing, building and testing dipole magnets from HTS tape conductor within the European funded FP7-EUCARD2 collaboration [151],[154]. Built as

insert, the Feather-M2.1-2 magnet reached $3.1\,\mathrm{T}$ stand-alone at $5.7\,\mathrm{K}$ and was tested between $5\,\mathrm{K}$ and $85\,\mathrm{K}$. Basically the same field is expected to be reached in the background field of the Fresca-2 magnet, which is approximately $13\,\mathrm{T}$ [155],[156].

In addition first undulator coil concepts have been proposed for planar windings [157] as well as for modified REBCO tape by means of lithography [158], laser-scribing [159] or tape cutting [160]. First short models using vertical racetrack geometry have been built from HTS tape conductors and successfully tested with one reaching current densities of more than $2.1\,\mathrm{kA/mm^2}$ in the coil cross-section [161], showing the conductor's potential and the proof of concept. Simulations and measured data agreed in terms of magnetic field values for these experiments.
Currently there are different options of insulation under investigation when using HTS tapes for coil winding: Partially insulated coils show better field settling times and less eddy currents [161],[162]. In contrast, non-insulated or even fully soldered coils may be self-protective in case of a quench due to better current sharing [163],[164].

Besides planar geometries, helical designs are a possible option as well. Here, at present, the limiting factor is the minimum bending radius of coated REBCO conductor tapes which is not smaller than $5\,\mathrm{mm}$ [165], making smaller gaps than $10\,\mathrm{mm}$ impossible without some breakage in the REBCO layer. Taking this and the resulting lower magnetic fields into account, helical designs from REBCO tape are currently inferior to vertical and horizontal racetrack geometries.

All superconducting magnets, whether based on LTS or HTS conductors, require cryogenic cooling technology. Cryogenic technology is readily available, as for example shown by CERN's Large Hadron Collider (LHC) magnet system which is operated at $1.9\,\mathrm{K}$. Another example is the superconducting undulator SCU15 at the Karlsruhe Research Accelerator (KARA), which is ran as synchrotron research facility. SCU15 is operated at $4.2\,\mathrm{K}$ having a period length of $15\,\mathrm{mm}$ and a total length of $1.5\,\mathrm{m}$ [112].
Whereas for CERN's high-field magnet system no other technological solution exists, superconducting undulator technology competes with permanent magnet undulator (PMU) technology which does not necessarily require cooling. Therefore, the cost and complexity of a cryogenic system is an important factor for the decision whether or not to procure and install superconducting undulator magnets in an FEL. HTS has the advantage compared to LTS that it can be operated at higher temperatures allowing to use a more cost-efficient and simplified cryogenic system. This becomes as well useful in terms of compensating heat loads, e.g. caused by joint connections of superconductors.

Some of the mentioned experiments [160],[161] investigated methods of reducing resistive joints, connecting the superconductive undulator coils, which have typical values of 40 $\mathrm{n\Omega \cdot cm^2}$ [166] at $4.2\,\mathrm{K}$. This implies a significant heat load to the cryogenic system when aiming for high magnetic fields driven by operating currents in the order of $1\,\mathrm{kA}$. Especially in the FEL scenario where undulator section lengths with multiples of $10\,\mathrm{m}$ are needed having a period length in the order of tens of millimeters, reducing the number of joints is essential to minimize the total heat load of the undulator. Typically few $\mathrm{W/m}$ can be sustained by the cryogenic cooling system at $4.2\,\mathrm{K}$. The joint resistance scales reciprocal with the joint area: The bigger the area, the smaller the resistance. Considering an undulator with a period length of $15\,\mathrm{mm}$, a heat load of approximately $1.8\,\mathrm{W/m}$ is expected.

However having no joints in the superconductive undulator, implying to wind the coils from one piece of conductor, comes with a limitation: Designs without joints are losing their modular structure. Here the advantage is an easy way to replace defect conductors or regions, that may have been damaged due to e.g. quenches. Hence, the number of joints has to be well balanced because their influence on the heat load must be reasonably small.

A significant difference between LTS cables and HTS tape conductors is the angular dependence of HTS tapes regarding applied magnetic fields. The critical current of an HTS tape in a magnetic field strongly depends on the angle of the field lines relative to the REBCO plane within the tape. Typically larger currents are reached when magnetic field lines are aligned in parallel to the tape plane, thus perpendicular to the plane's normal vector. The critical current drops rapidly for other configurations coming to a minimum for the perpendicular arrangement. This behavior becomes more distinct when higher magnetic fields are applied. Here the discrepancy in critical current, between parallel and perpendicular magnetic field directions, may drop by more than $50\,\%$ [151]. So the critical current density is a function depending on the temperature T, the applied magnetic field B and the angle of the magnetic field β: $J_c(T, B, \beta)$. This has to be taken into account when designing an HTS magnet.

For this study the critical current was assumed to be a function of temperature, applied magnetic field and field angle, as discussed above. The planer undulator models feature iron poles, whereas the helical model was designed iron free. No geometric optimization regarding the field angular dependency was performed. Planar simulations were performed in Opera 2D, whereas the helical geometry was studied in Opera 3D [147].
The angular dependency can be seen when comparing magnetic field values B_y and undulator parameter K for horizontal racetrack (HR) to vertical racetrack (VR) geometries (Figures 25 and 26). When comparing HR to VR concerning the magnetic field component B_y (Figures 25(a) and 26(a)), higher values can be found for the horizontal geometries. Because the magnetic field lines follow the iron pole, they are more parallel aligned to the tape planes in the HR geometry. As already discussed this implies a higher $\mathrm{J_c}$ thus higher magnetic peak fields.

For a compact FEL, undulator periods λ_u of $15\,\mathrm{mm}$ or smaller are of general interest. Studies have already shown that critical current values up to $8000\,\mathrm{A}$ are technically achievable [167], supporting the conductor's potential and the here presented field values.
Table 13 compares the LTS Nb-Ti to HTS REBCO tape in terms of magnetic peak fields for such small periods. The helical geometry performs similar or inferior to Nb-Ti, although it is presented with a $10\,\mathrm{mm}$ gap since the bending radius of coated REBCO conductor does not tolerate smaller gaps, at present. A significant improvement of the magnetic peak field B_y by up to factor 2 compared to Nb-Ti can be seen for the HR geometry. VR may increase the peak field by up to factor 1.5. Compared to the optimized Nb-Ti case, we can therefore state that HTS is able to outperform Nb-Ti for the $\mathrm{B}/\lambda_\mathrm{u}$ ratio.

3.4.2 Opportunities and challenges

Compared to low-temperature superconductor technologies, HTS is still evolving in all terms of characteristics. Techniques like flux pinning [168],[169] as well as reducing the thickness of stabilizer and substrate [170] further increases today's possible critical current density values. The presented values in Figures 25 and 26 changed significantly over the last three years.

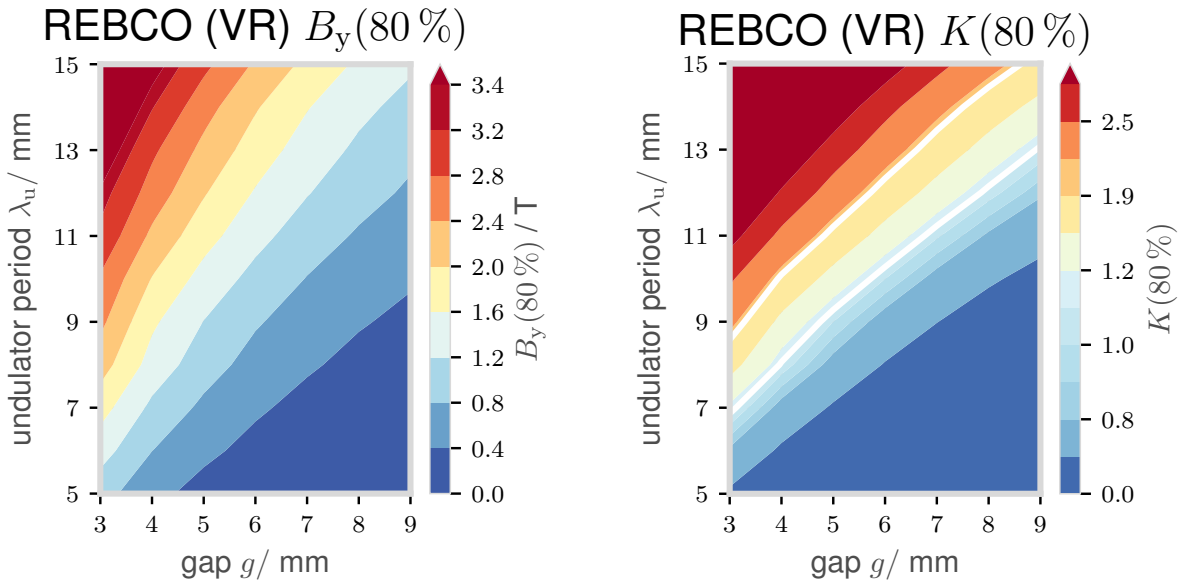

(a) Magnetic field B_y (b) Undulator parameter K

Figure 25: Magnetic field B_y (a) and undulator parameter K (b) depending on the magnetic gap g and the undulator period length λ_u. REBCO tape vertically wound at 80% of its maximum field strength at 4.2 K.

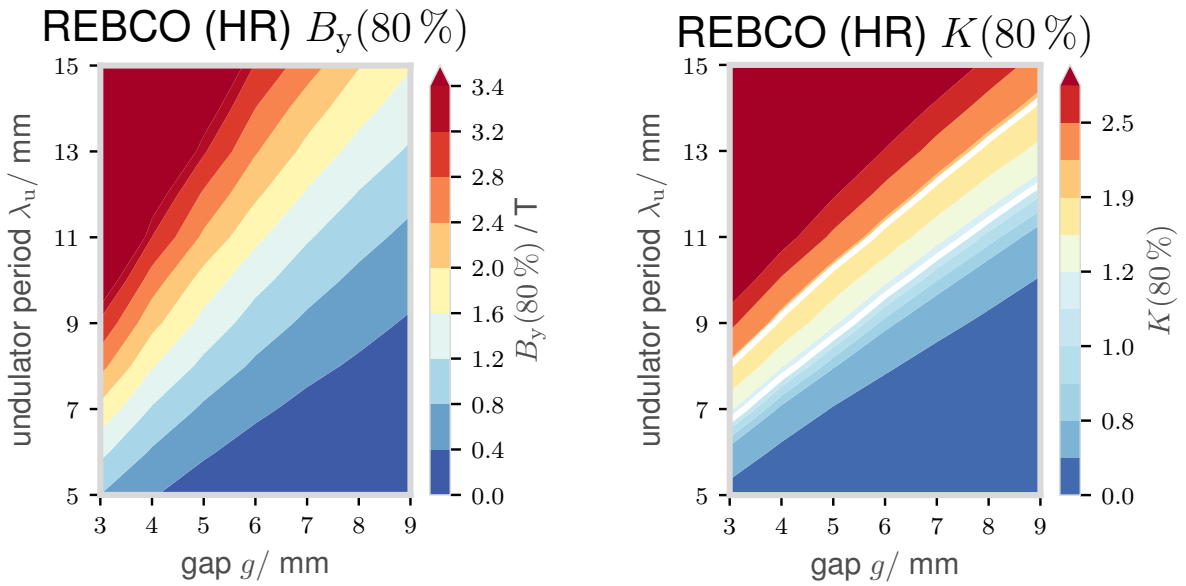

(a) Magnetic field B_y (b) Undulator parameter K

Figure 26: Magnetic field B_y (a) and undulator parameter K (b) depending on the magnetic gap g and the undulator period length λ_u. REBCO tape horizontally wound at 80% of its maximum field strength at 4.2 K.

Table 13: Optimum magnetic peak field values for 6 mm gap and operation at 80 % of J_c, respectively. *Helical data is given for a 10 mm gap. An average peak field increase of up to 77 % may be possible by using coated REBCO conductor. HR and VR data is based on 2D simulations whereas Nb-Ti and the helical design were investigated in 3D.

period length λ_u / mm	HTS(VR) B / T	HTS(HR) B / T	HTS(hel*) B / T	Nb-Ti B / T	Ratio HTS(VR+HR) / 2×Nb-Ti
13	1.7	2.3	1.0	1.2	1.67
14	2.0	2.7	1.2	1.4	1.67
15	2.3	3.0	1.5	1.5	1.77

Table 14: Optimum magnetic peak field values for 6 mm gap and operation at 80 % of J_c, respectively. From the year 2016 to 2019 the performance with regard to theoretical undulator performance, a peak field increase between 64 % and 80 % was found for VR and HR geometry, respectively.

	2016		2019		2019 / 2016	
period length λ_u / mm	HTS (VR) B / T	HTS (HR) B / T	HTS (VR) B / T	HTS (HR) B / T	HTS (VR) ratio	HTS (HR) ratio
13	1.1	1.3	1.7	2.3	1.55	1.77
14	1.3	1.5	2.0	2.7	1.54	1.80
15	1.4	1.7	2.3	3.0	1.64	1.76

This rapid development can be seen in Table 14, where 2D simulations with different REBCO conductor parameters from the year 2016 are compared to today's, in 2019. A performance increase by up to factor 1.8 and 1.6 for HR and VR geometry can be seen, respectively.

Another opportunity is given by the broad range of operation temperatures, up to almost 90 K which may lead to machines cooled to 10 K, 20 K or even by liquid nitrogen implying a significant reduction of cooling costs. Operating a magnet in temperatures higher than 4.2 K not only affects the costs but also entails more control over compensating heat loads, as already mentioned.

Certainly one must take the geometric properties of the tape shaped conductors into account, especially the easy and hard bending directions, which will lead to alternative winding schemes. For periods λ_u of 15 mm or less, tape widths of 5 mm or smaller are essential. At present the most common produced tape width is 12 mm. As an economic consequence, smaller tapes are cut from wider ones. Even though not finally demonstrated, mechanical cutting processes (mainly used by all manufactures at present) might lead to degradation owing to micro-cracks and oxygenation at edges of the superconducting REBCO layer. This may be improved by using laser cutting and is currently under investigation.

An essential issue for superconducting magnets is quench detection and protection. The normal zone propagation velocity is roughly three orders of magnitude smaller in HTS ($\sim$1 mm/s) compared to LTS ($\sim$1 m/s) [171]. In comparison to the well known procedures when working

with LTS, working solutions must be found. Since quench detection is essential to trigger any protection mechanism, a wide range of concepts have been investigated varying from optical techniques [172] to acoustic [173] and acoustic thermometry approaches [174].
This is supplemented by many studies on quench protection. Here a possible solution might be non-insulated undulator coils. As already mentioned, they show a self-protecting reaction in a quench scenario [163]. Furthermore techniques using protection heaters [175] or coupling loss induced quenching (CLIQ) [176] were investigated for coils from HTS conductors. Although there is no general solution for quench detection and protection systems yet, in summary HTS magnets have shown to be stable and there are many promising concepts under investigation.

3.4.3 Advances in science and technology to meet XLS requirements

Summing up, HTS coated REBCO tape conductors are able to provide magnetic fields of around $2\,\mathrm{T}$ for small periods like $\lambda_\mathrm{u} = 15\,\mathrm{mm}$ already today. For both SCU technologies, HTS and LTS, the magnetic field is proportional to the operating current. Therefore, an FEL performance optimization and regulation is possible by controlling the magnetic field amplitude. HTS outperforms LTS, therefore PMU technology as well, in terms of magnetic peak field values. Though one should notice that not all the presented field values may be feasible with today's commercial available REBCO tape technology, yet. Additionally, and as already mentioned in the beginning, by using the superconducting material REBCO there is no need for any special treatment like the high-temperature superconductor BSCCO or the low-temperature superconductor Nb_3Sn, which makes the handling more simple and straight forward.

As shown, development of coated REBCO conductors for HTS coils has made progress in the last years. Critical current densities have been increased and conductors perform more uniform over greater length and can withstand higher magnetic fields. This positive trend is expected to be continued.
Nevertheless, for making HTS undulators with period lengths of $15\,\mathrm{mm}$ and smaller available for the use in FELs, a technical solution in terms of quench detection and protection has to be established. Mechanical properties like the bending radius should be further improved as well as reducing and improving the joint resistance for coated REBCO conductors. Further the production of high quality HTS tapes with widths smaller than $12\,\mathrm{mm}$ must be enhanced, for instance, by producing thinner widths independently or using laser cutting techniques. Finally, the manufacturing costs of HTS tape conductor in general has to be optimized as well as available conductor lengths and performance of commercial available coated REBCO conductor tapes.

3.5 Field scaling for undulators wound from high temperature superconducting tape

Tables 15 and 16 summarize the scaling parameters for coated REBCO conductor tape in 2016 and 2019, respectively. The parameters of the investigated planar (HR and VR) and helical geometries applied to the scaling expression

$$B(\lambda_\mathrm{u}[\mathrm{mm}], g[\mathrm{mm}]) = c_1 \cdot (c_2 + c_3\lambda_\mathrm{u} - c_4\lambda_\mathrm{u}^2 + c_5\lambda_\mathrm{u}^3) \exp\left(-\pi\left(c_7\frac{g}{\lambda_\mathrm{u}} - c_6\right)\right). \quad (7)$$

This scaling is based on the scaling laws described in [146] and put into practical formulas by [27]. Equation 7 was fitted to the data obtained by Opera 2D (HR and VR) or Opera 3D (helical) simulations done in the undulator period range of 3–15 mm for magnetic gap heights of 3 mm, 6 mm and 9 mm [147].

Table 15: Scaling law parameters for the magnetic field of coils from high temperature superconducing tapes as a function of the gap over period ratio for different types of HTSC undulators. Here presented values are based on properties from coated REBCO conductor in 2016.

	REBCO 2016		
	Horizontal	Vertical	Helical
c_1	1.32 ± 0.08	1.28 ± 0.04	1.29 ± 0.02
c_2	0.12 ± 0.06	0.51 ± 0.07	0.071 ± 0.008
c_3	0.07 ± 0.02	0.017 ± 0.003	0.058 ± 0.003
$c_4/10^{-4}$	9 ± 5	0.4 ± 1.4	18.3 ± 0.8
$c_5/10^{-6}$	11 ± 16	28 ± 5	38.2 ± 1.7
c_6	0.55 ± 0.16	0.49 ± 0.03	0.565 ± 0.019
c_7	1	1	0.8520 ± 0.0003

Table 16: Scaling law parameters for the magnetic field of coils from high temperature superconducing tapes as a function of the gap over period ratio for different types of HTSC undulators. Here presented values are based on properties from coated REBCO conductor in 2019.

	REBCO 2019		
	Horizontal	Vertical	Helical
c_1	1.47 ± 0.04	1.73 ± 0.06	1.46 ± 0.02
c_2	0.27 ± 0.07	0.07 ± 0.02	0.063 ± 0.007
c_3	0.102 ± 0.019	0.0115 ± 0.0005	0.054 ± 0.003
$c_4/10^{-4}$	16 ± 6	10.8 ± 0.3	19.0 ± 0.4
$c_5/10^{-6}$	3 ± 10	39.98 ± 0.14	39.92 ± 0.11
c_6	0.63 ± 0.06	1.15 ± 0.05	0.738 ± 0.018
c_7	1.187 ± 0.010	0.9859 ± 0.0020	0.8449 ± 0.0003

3.6 High temperature superconducting bulk structures

The option of using bulks HTS is intimate related to the geometry of the staggered array undulator proposed in the early 90 [177]. In its original version it consists of a superconducting solenoid surrounding two rows, an upper and a lower row, of iron poles staggered half the desired undulator period to shape the homogeneous on axis field into an undulator field. This geometry has inspired Kinjo and co-workers [178] and led to the implementation of ReBCO bulks [179] in place of iron to enhance its performance. The first test at the Kyoto university demonstrated 0.85T undulation field for the compact geometry of 10mm period and 4mm magnetic gap magnetised with a 2 T solenoidal field [179].

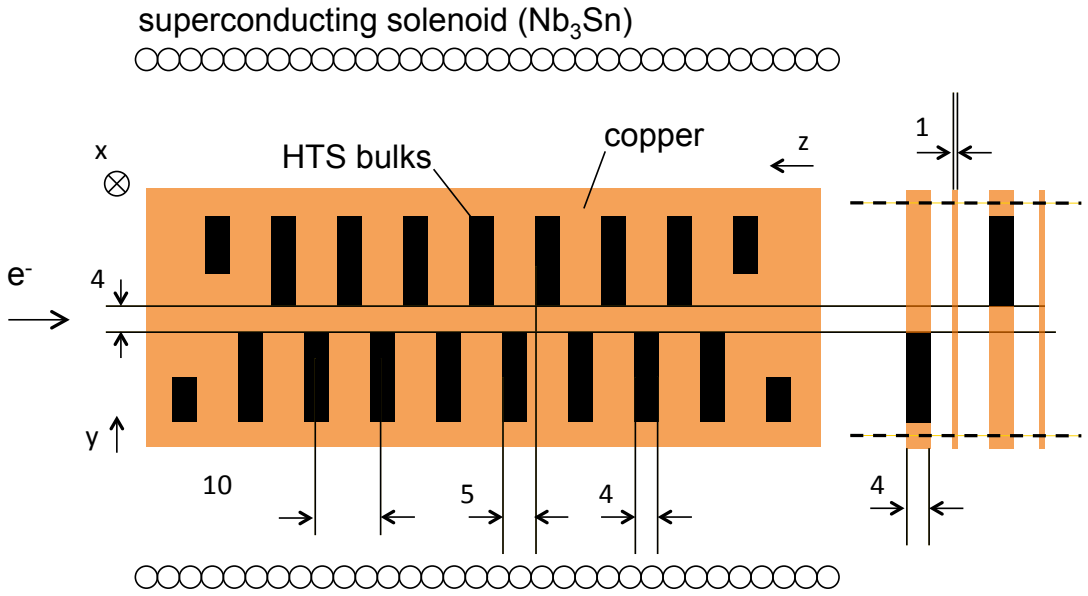

Figure 27: The simplified 2D view of a staggered array undulator with matched end fields. The black rectangles represent the HTS bulks and the remaining structural material is copper to improve the temperature homogeneity. In this example additional thin disks of copper are positioned in between the superconducting ones, their thickness can be varied from pole to pole to compensate the inhomogeneity and thus improving the field quality.

3.6.1 Status (strengths and weaknesses)

The scaling of the first experimental results by mean of numerical simulations indicates the potential of fields above 2 T for the previous mentioned compact geometry (10mm period, 4mm gap). The absence of a complex winding, as it is the case already for permanent magnet undulator, simplifies the protection and allows a simple scaling to shorter periods. At the same time the absence of the direct control of the trapped current creates challenges on the operation and suggests to develop online measuring system to directly control the undulator field. A superconducting solenoid of about 10 T is required to magnetise the bulks at the desired performance. This device is today available for NMR magnets (Nb3Sn) and can be procured in industry. A dedicated solenoidal design is highly recommended to match the challenges of this new application. The best performing ReBCO material today is $GdB_{a2}Cu_3O_{7-\delta}$ where

trapped field as high as 17.6T has been demonstrated by Durrell and co-workers [180]. Nevertheless the material available today still shows measurable field decay after the magnetisation, referred as flux creeping. Techniques to reduce this effect are investigated and they are referred as flux freezing technique. PSI is starting the experimental activities this July 2019 at the University of Cambridge and it will measure the first 10 period device to investigate all these effects. Two samples are planned for the first experimental section, one made of bulk material and the second of stack tapes of GdBCO (see Figure 28) to make a first assessment of the most promising technological approach. Today the bulks have the highest engineering current density (Je) while they are brittle and requires additional mechanical support and prestress to withstand high mechanical load. Their poor homogeneity in Jc is also a concern for this application which requires ideally identical pole strength to achieve phase error as low as few degrees. The tapes on the contrary does not have yet the performance required (factor of two with respect to bulks) but they are well mechanical stabilised and the inhomogeneity, also present in this technology, can be mitigated randomly (or with a pre-sorting criterion) because hundreds of them are requited to build up a pole in the stack configuration. A detail computational description can be conveniently done today using the so-called H formulation of the Maxwell equations and commercial softwares are available. For this project both COMSOL (see Figure 29 for an example) and ANSYS have been used to give an estimation of the undulator parameters and to optimise its geometry.

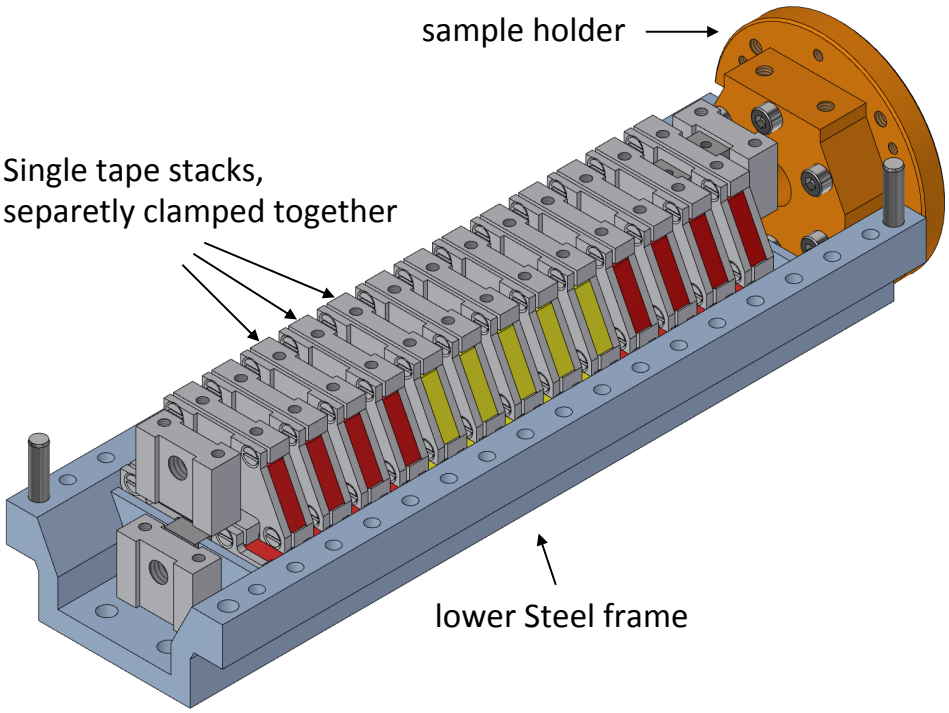

Figure 28: The staggered array undulator sample number 2 to be tested in Cambridge this year. The upper steel support (symmetric to the lower grey one) is removed to show the inner core of the undulator, in this sample made of stack of GdBCO tapes.

3.6.2 Opportunities and challenges

This technology allows today the best performance among the family of superconducting undulator presented in this review and it opens new opportunities for compact X-ray facilities, both FEL as well as storage rings. The undulator field can be tune changing the solenoidal field, this avoid complex gap drive but at the same time requires an accelerator optics and alignment techniques which can cope with high solenoidal field, in first estimation as high as 4T. This new ingredient has to be considered starting from the early design of the accelerator lattice and additional optical elements has to be allocated to smoothly operate this device without compromising the performance. A comprehensive beam dynamic study is still missing and shall be triggered after the feasibility of this technology is demonstrated.

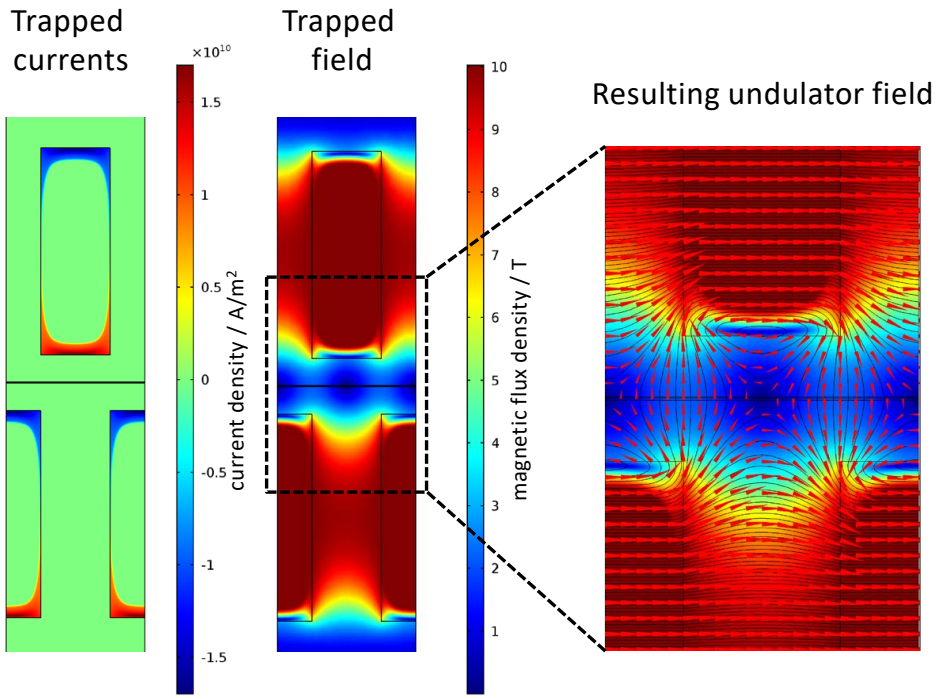

Figure 29: the details of an undulator period (10mm), on the left the currents, in the middle the field and on the right the magnetic vector plot where the negative and positive poles of the undulator are visible.

3.6.3 Advances in science and technology to meet XLS requirements

The staggered array undulator design with HTS bulks, either actual bulks or bulks made with tape stacks, does not present particular technical problems to be manufactured and a full beamline could be assembled out of those modules in the next few years. It is too early to give a cost estimation but it should be in the same ballpark of the permanent magnets undulators but with higher operation costs due to the cryogenics installation. Nevertheless there are still many open questions which have been previously introduced and one potential showstopper: the lack of reproducibility of the magnetisation process. An online monitoring system of the magnetic field helps only if the magnetic profile and consequently the phased error does not change after repeating the magnetisation process. The possible degradation of individual pole performance due to local defects triggered by the large magnetic forces or a high sensitivity

to temperature homogeneity during the magnetisation process could make this approach not adequate for the high quality required by an FEL undulator. The answers to those question will be address during the short sample campaign at the Cambridge University and a preliminary assessment is expected for the end of this year (2019).

3.7 Field scaling for undulators based on high temperature superconducting bulk structures

For GdBCO structures, the analytical scaling expression describing the magnetic field behaviour as a function of the undulator g/λ_u ratio is the following:

$$B\left(\frac{g}{\lambda_u}\right) = B_0 \exp\left[-a\left(\frac{g}{\lambda_u}\right) + b\left(\frac{g}{\lambda_u}\right)^2\right]. \tag{8}$$

This parameterisation is the result of the fit to simulation studies assuming $\lambda_u = 10\,\text{mm}$ and covering an undulator gap range of $g \in [3, 10]\,\text{mm}$. The parameters for the considered undulator structures are summarised on Table 17.

Table 17: Scaling law parameters for the magnetic field as a function of the g/λ_u ratio for different types of GdBCO undulators.

parameter	bulks	tapes
B_0 [T]	7.757	5.266
a	3.165	3.237
b	−0.0012	0.0961

4 Exotic undulators

4.1 Introduction

Undulators are one of the most important components in the CompactLight X-ray FEL. Electrons with relativistic energies passed through undulator results in the generation of radiation. The undulator, which is the backbone of such a light source, is conventionally a series of permanent magnets with a strong magnetic field, constant in time but alternating in space. These undulators, however, provide limited control over the properties of the generated radiation. Moreover, it is very challenging to scale the magnetic undulators down to smaller undulating periods which would result in the generation of shorter wavelength radiation by spending less energy in the acceleration of the electrons, making the machine more compact. Such scaling will also require strict limits on the maximum electron beam aperture, field strength, and consequently the radiation brightness. To overcome these shortcomings of the magnetic undulator technology, a few new ideas such as microwave undulators and laser-wave undulators have been proposed and studied in recent years.

4.2 Microwave undulators

4.2.1 Cavity-type undulators

In FEL radiation, the fundamental radiation wavelength is directly proportional to the undulator period while it is inversely proportional to the square of the electron beam energy. Thus, to get short wavelength radiation, like hard-X-rays, one prefers to have shorter undulator periods instead of spending energy in the acceleration of the beam whose cost increases prohibitively with increasing electron beam energy. Permanent magnets are challenging to obtain the much sought after feature of shorter undulator period, which enables economically lower energy systems, while maintaining adequate aperture for the electron beam and without compromising on the field strength. Also, with the undulators based on permanent magnets, dynamic control is slow and limited. Fast dynamic control of the radiation can offer exciting scientic opportunities. For example, in the study of magnetic materials and chiral molecules, increased sensitivity to small magnetic effects which underlie modern magnetic materials has been obtained only through pump-probe experiments [181]. Similar sensitivity is required for cases where pump-probe techniques cannot be used.

These limitations could be overcome baanvy the use of high-power guided microwaves to produce a periodical transverse wiggling field. Microwave undulators (MU) [182, 183] that also have a periodic magnetic field can be potential undulators and have the following advantages compared with conventional permanent magnet undulators (PMUs). (1) Fast dynamic control of the polarization. (2) Easy control of the field strength, which can be adjusted through the input microwave power, while in a PMU mechanical methods are required to adjust the magnet gap, or the magnet period has to be mechanically adjusted which can be complicated. (3) It is challenging for a PMU to achieve short periods as the magnetic field strength would be significantly reduced. In contrast in a MU, the equivalent period is mainly determined by the wavelength of the electromagnetic wave, therefore a short period can be achieved if the MU operates at a higher frequency. (4) The MU is essentially a metallic cavity and hence it is robust against damage by ionising radiation near the electron beam dump regions, as compared with the PMUs that are made of rare earth materials, which may be more susceptible to damage in harsh ionising radiation environments.

However, since the concept of the microwave undulator was proposed in 1982 [182], progress has taken longer than expected, mainly due to the limited availability of high power microwave sources. In 1983, the first MU experiment was carried out and an equivalent magnetic field B_u of 0.045 T with an undulator parameter K of 0.24 was achieved when driven by a 300 kW, 2.856 GHz microwave source. A ridged rectangular cavity was used and a quality factor Q of 7100 was measured. To achieve a similar performance to a state-of-the-art PMU, for example, 1.29 T for a 15 mm period PMU used in the Swiss-FEL at the Paul Scherrer Institute, the required driving power would need to be more than 20 MW at 10.5 GHz (assuming the same Q factor of 7100 can be achieved for a similar structure scaled for operation at 10.5 GHz). However, the electric field at the wall of the ridged rectangular cavity would be too high and susceptible to microwave breakdown. A significant improvement on the MU was made with the use of a low loss HE_{11} mode in a corrugated waveguide. A cavity made of a corrugated waveguide operating at X-band was measured and it was able to achieve a Q-factor as high as 91000. When it was driven by a 50 MW SLAC klystron at 11.424 GHz [184], such an MU was able to achieve an equivalent B_u of 0.65 T with a period of 13.9 mm.

The principle of the MU can be found in [185]. The relativistic electrons in an MU cavity will interact with both the electric field $E_x = E_0 \sin(2\pi z/\lambda_g)\sin(\omega t)$ and magnetic field $B_y = B_0 \cos(2\pi z/\lambda_g)\cos(\omega t)$. Compared with a PMU, the Lorentz force in a MU can be rewritten in the form:

$$F_x = \frac{eE_0}{2}(\frac{\varsigma}{Z_w}+1)\cos(2\pi z(\frac{1}{\lambda_0}+\frac{1}{\lambda_g})) + \frac{eE_0}{2}(\frac{\varsigma}{Z_w}-1)\cos(2\pi z(\frac{1}{\lambda_0}-\frac{1}{\lambda_g})) \tag{9}$$

where e is the charge of electron, λ_0 is the free space wavelength, and λ_g is the wavelength of electromagnetic wave in the undulator cavity. E_0 and B_0 are the peak electric and magnetic field strength in the microwave undulator cavity, respectively. Z_w is the wave impedance in the cavity and ς is the wave impedance in free space. The second term leads to a long wavelength and is undesirable in the undulator of a short wavelength FEL. The second term can be ignored if the wave impedance is close to the free space impedance, which means the operating frequency is far away from the cut-off frequency of the waveguide. In this case, the equivalent magnetic field B_u and wavelength λ_u of the microwave undulator are given by

$$\begin{gathered} B_u = \frac{E_0}{2c}(\frac{\varsigma}{Z_w}+1) \\ \frac{1}{\lambda_u} = \frac{1}{\lambda_0}+\frac{1}{\lambda_g} \end{gathered} \tag{10}$$

If the microwave source starts to fill the cavity at time zero, the stored energy at time t in the cavity can be expressed as [186]

$$W(t) = P_0\tau_0\frac{4\beta}{(1+\beta)^2}(1-e^{-\frac{1+\beta}{2}\frac{t}{\tau_0}})^2 \tag{11}$$

where P_0 is the input power, $\tau_0 = Q_0/\omega$, $\beta = Q_0/Q_e$. Q_0 and Q_e represent the intrinsic and external quality factor of the cavity. In the steady state, where $t \gg \tau_0$, the stored energy reaches its maximum value of $P_0\tau_0$ if the coupling aperture is specifically designed to achieve $\beta = 1$. The input power in this case will be equal to the Ohmic loss in the cavity. In the cases of an under coupled ($\beta < 1$) and over coupled ($\beta > 1$) regime, the stored energy in the steady state is smaller. The filling time of the cavity t_{tf} can be calculated if a charging factor η, defined as the ratio of the charged energy and its maximum value, is known.

$$t_{tf} = 2Q_0/(\omega(1+\beta))\ln(\frac{1+\sqrt{\eta}}{1-\eta}) \tag{12}$$

From Eq. 11 and 12, to achieve maximum storage at a given input power, a higher Q factor of the cavity is preferred. However, the filling time increases at the same time. In applications of MUs, high power microwave sources with output powers of MWs, or more, are needed to achieve a high equivalent magnetic field. Such high power microwave sources normally operate in pulsed mode to reduce the power supply requirements and associated thermal stress. The filling time of the MU cavity should match the pulse length of the microwave source. The coupler can be slightly over-coupled to reduce the filling time while maintaining a high Q factor. If the input microwave frequency is 36 GHz, with a 2 μs pulse length, the Q factor of the cavity should be under 150,000 if $\beta = 1$ and $\eta = 0.9$.

The electric field strength inside the cavity along the electron beam path can be calculated by careful selection of the operating mode of the cavity. Knowing the input power and the Q factor, the parameters of the MU can be determined.

A high Q, low loss cavity is of great importance when it is used as an MU. In a circular waveguide, the mode with the lowest loss is the TE_{01} mode. However, the field strength at the waveguide center for this mode is small and hence is not a good option for an MU as the electrons are to propagate down the center of the structure. The corrugated waveguide, as shown in Fig. 30, can be used in other applications such as a feed horn for a transmission line system due to its advantages of low cross polarization field, low loss and wide bandwidth. Its low attenuation feature is attractive for transmission of high power microwaves. The fundamental mode HE_{11} was found to have lower loss compared with the TE_{01} mode in the circular waveguide. It has been used to transport MW-level millimeter wave radiation generated by gyrotron oscillators for fusion experiments such as ITER. In recent years, the corrugated waveguide has been proposed to be used as an MU [187–189].

The corrugated waveguide contains circular waveguide steps and smooth sections. The properties of a corrugated waveguide with arbitrary radial corrugation depth can be accurately solved using a mode-matching method [190, 191]. For the periodically corrugated waveguide used for transmitting the microwave power, analytical equations can be derived based on the fact that the waveguide radius is larger than the wavelength. The propagation characteristics of the periodically corrugated waveguide were studied using the simplified surface-impedance approach or the rigid equations taking into account the spatial harmonics in the corrugation gaps.

The surface-impedance approach assumes only the lowest TM standing wave exists in the slot and ignores its spatial harmonics. It gives a good approximation when the period per wavelength, defined by λ_0/p, is a reasonably large value and the corrugation slot length, defined by $w = p - b$ in Fig. 30, is a small value. At low frequency, for example in the application of the microwave undulator, these assumptions would be normally satisfied. If only the lowest TM standing wave were present in the corrugation slot, its surface admittance at $r = r_1$ can be written as

$$\frac{H_\psi}{E_z} = -jY_0 \frac{J_m^{'}(x_1^{'})Y_m(x_0^{'}) - J_m(x_0^{'})Y_m^{'}(x_1^{'})}{J_m(x_1^{'})Y_m(x_0^{'}) - J_m(x_0^{'})Y_m(x_1^{'})} \tag{13}$$

where m indicates the azimuthal mode number, $x_1^{'} = kr_1, x_0^{'} = kr_0$. J_m and Y_m are the first and second kind of Bessel functions of order m respectively. Y_m is the free-space wave admittance.

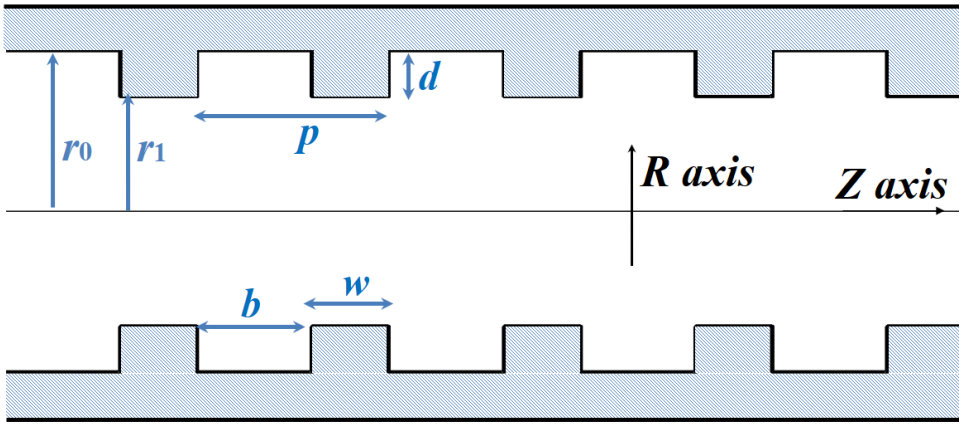

Figure 30: Schematic drawing of the corrugated waveguide.

The surface admittance becomes 0 when

$$J_m^{'}(x_1^{'})Y_m^{'}(x_0^{'}) - J_m^{'}(x_0^{'})Y_m^{'}(x_1^{'}) = 0 \tag{14}$$

This is known as the balanced hybrid condition. If the operating frequency (f) and the waveguide radius (either r_0 or r_1) are given, the corrugation depth $d = r_0 - r_1$ can be determined from the equation. At $m = 1$ and $x_1^{'} \gg 1$, the surface admittance can be further simplified as $H_\psi / E_z = jY_0 \cot(kd)$. The corrugation depth d would be equal to $\lambda_0/4$ to ensure $H_\psi = 0$.

Under the balanced hybrid condition and $x_1^{'} \gg 1$, the dispersion curve between k and k_z is determined by

$$Kr_1 \frac{J_m^{'}(Kr_1)}{J_m(Kr_1)} = \mp m \frac{k_z}{k} \tag{15}$$

where $K^2 = k^2 - k_z^2$, the '-' in '$\mp$' denotes the HE modes, and the '+' denotes the EH modes. At large radius which leads to $k_z \approx k$ and $m = 1$, Eq. 15 can be further simplified as $J_0(Kr_1) = 0$ for HE_{1n} modes, and $J_2(Kr_1) = 0$ for EH_{1n} modes.

To describe the field distribution inside the corrugated waveguide, different eigenmode sets using TE/TM and HE/EH combinations had been derived [192]. The field inside the corrugated waveguide with the linearly polarized mode sets can be simplified as

$$\begin{cases} E_z = a_m J_m(Kr)\cos(m\phi) \\ E_r = -ja_m \frac{k}{K} J_{m\mp1}(Kr)\cos(m\phi) \\ E_\phi = \mp(-j)a_m \frac{k}{K} J_{m\mp1}(Kr)\sin(m\phi) \end{cases} \tag{16}$$

Usually, a higher order HE or EH mode is not linearly polarized. The suitable operating modes in the corrugated waveguide for the microwave undulator application are the HE_{11} and HE_{12} modes because they are low loss and linearly polarized and have the peak electric field at the waveguide center. The electric field patterns of the HE_{11} and HE_{12} modes are shown in Fig. 31. The HE_{12} mode has larger field density at the waveguide center. It can have a bigger electric field compared with the HE_{11} mode at the same input power.

The attenuation coefficient defined by the ratio between the lost power and the transported power per meter for the HE_{1n} modes, under the balanced hybrid condition, can be written as [193]

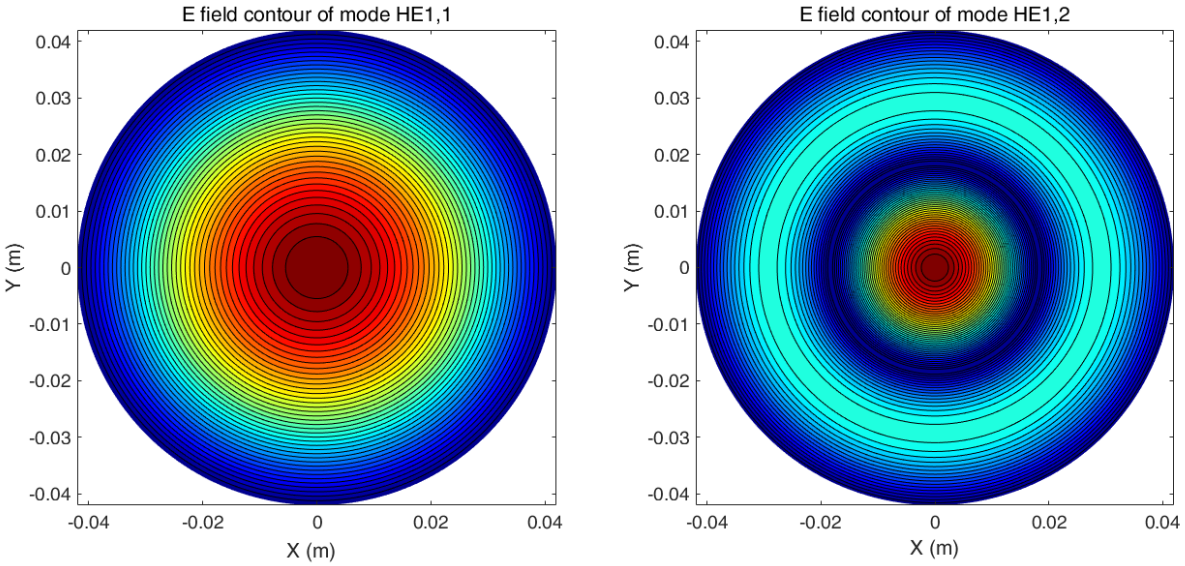

Figure 31: Contour plot of the electric field patterns of (a) the HE_{11} and (b) the HE_{12} modes.

$$\alpha = \frac{1}{2}(\frac{R_s}{Z_0})\frac{x_1^2 k}{x_1^{'4}}[\frac{1}{kb}(1+\frac{x_1^{'}\pi}{2})+x_1^{'}] \tag{17}$$

where $Z_0 = 1/Y_0$ is the free space wave impedance. $R_s = \sqrt{\pi f \mu_0 \sigma}$ is the resistivity of the corrugated metal waveguide, and σ is the conductivity of the metal. In this paper, oxygen-free high conductivity copper was chosen and $\sigma = 5.8 \times 10^7$ S/m was used in the simulation. Eq. 17 implies that the attenuation coefficient is proportional to r_1^{-3} and f^{-2} in the case of $x_1^{'} \gg 1$.

The corrugated waveguide can be shorted at both ends to form a cavity. The resonance frequency of the corrugated waveguide can be estimated as

$$f = \frac{c}{\lambda_0} = \frac{c}{2\pi}\sqrt{K^2 + (\frac{N\pi}{\lambda_g})^2} \tag{18}$$

where c is the speed of light, N is an integer, λ_g the wavelength of the resonance mode in the cavity. Because the corrugated waveguide is normally overmoded, $\lambda_0 \approx \lambda_g$ when $N = 2$. As mentioned earlier, the surface-impedance approach gives good approximation when λ_0/p is a reasonably large value. Therefore when designing the corrugated waveguide, the period p can be chosen to be smaller than $\lambda_0/2$. It is of course the case that "the smaller the period the better", however, as the operating frequency increases, the wavelength becomes smaller resulting in a small corrugation period and a thin corrugation slot $w \approx 0$ which significantly increases the machining difficulty. The final choice of the geometry should also therefore consider the machining tolerance.

Since $x_1^{'} = kr_1 = 2\pi r_1/\lambda_0 \gg 1$ has to be satisfied. The corrugated waveguide radius r_1 is a large value. As the attenuation coefficient is proportional to r_1^{-3}, it is preferable to have a large r_1 at a given operating frequency. From eq. 16, the waveguide radius affects the field strength if the input power is a fixed value. In a microwave undulator, a high field at the electron beam path, in this case the waveguide center, is desired. Therefore r_1 should be as small as possible under the constraint of $kr_1 \gg 1$. On the other hand, it is preferred for the electron

beam that travels through the microwave undulator to see a uniform field in the radial direction. The minimum waveguide radius can be solved from the field pattern of the operating mode if an electron beam aperture R_b and a threshold, for example 90% of the maximum field at the beam edge, are defined. For HE_{1n} modes, it follows that $J_1(KR_b) = 0.9$. Taking the first two solutions of $J_0(Kr_1) = 0$, K is approximately equal to $2.4/r_1$ or $5.5/r_1$ for the HE_{11} or the HE_{12} mode, respectively. Therefore the parameters below were chosen

$$r_1 = \begin{cases} 3.8R_b, & for\ the\ HE_{11}\ mode \\ 8.6R_b, & for\ the\ HE_{12}\ mode \end{cases}$$

resulting in a reasonable value of r_1. Meanwhile the value of r_1 should satisfy $x_1^{'} = 2\pi r_1/\lambda_0 \gg 1$. If $x_1^{'} = 5$ is used, then $r_1 \geq 0.8\lambda_0$ and the results become

$$r_1 = \begin{cases} \max(3.8R_b,\ 0.8\lambda_0), & for\ the\ HE_{11}\ mode \\ \max(8.6R_b,\ 0.8\lambda_0), & for\ the\ HE_{12}\ mode \end{cases}$$

A corrugated waveguide cavity, operating at 36 GHz, was designed as a potential microwave undulator for the CompactLight [194]. The initial geometry parameters were calculated from the equations described in the previous sections. Both of the HE_{11} and HE_{12} modes are considered. A summary of the geometry parameters as well as the undulator deflection parameter $K_u = 0.09336 B_u \lambda_u [T \cdot mm]$ are listed in Table 18.

Operating mode	**HE_{11}**	**HE_{12}**
Operating frequency (GHz)	36	36
λ_0 (mm)	8.33	8.33
r_1 (mm)	$4R_b$=8.0	$9R_b$=18.0
$d = \lambda_0/4$ (mm)	2.1	2.1
λ_g (mm)	9.06	9.12
$p = \lambda_g/3$ (mm)	3.00	3.02
w (mm)	0.5	0.5
$b = p - w$ (mm)	2.50	2.52
w (mm)	0.5	0.5
Q factor	94344	187073
Input power (MW)	50	50
B_u (T)	1.27	1.23
λ_u (mm)	4.34	4.35
K_u	0.52	0.50

Table 18: Parameters of the MU composed of a corrugated waveguide.

4.2.2 Flying undulators

An ideal undulator should have a shorter period to generate shorter wavelength radiation from the FEL. Further improvements on the MU including higher field and longer cavity section are dependent on access to microwave sources capable of both high power (tens of megawatts) and long duration (a few microseconds) at a higher frequency (Ka-band).

However, generation of short pulse duration (nanosecond range), GW level microwave radiation is feasible and such a source can even be compact because of the low average power

when operating in pulsed mode. For example, at X band, a peak output power of 3 GW can be achieved with a relativistic backward wave oscillator [195]. At Ka-band, the GW-level output power can be achieved by a Cherenkov maser, or a superradiant Cherenkov source [196, 197].

A "flying" MU, which uses a waveguide structure that supports a traveling wave instead of a standing electromagnetic wave, was proposed by Kuzikov et al [198]. The "flying" undulator is a high-power short rf pulse co-propagating together with a relativistic electron bunch in a helically corrugated waveguide. The electrons wiggle in the rf field of the first spatial harmonic with the phase velocity directed in the opposite direction in respect to the bunch velocity, so that particles can irradiate high-frequency Compton photons. A high group velocity (close to the speed of light) ensures long cooperative motion of the particles and the copropagating rf pulse. It can potentially make use of the high-power, short-pulse microwave sources to drive the MUs.

In a PMU that only has the magnetic field, the motion of the electron is given by

$$dp_x/dt = eB_u \cos(2\pi z/\lambda_u) \tag{19}$$

Comparing with Eq. 9 and 19, the force in an MU contains two terms. The first term denotes the force from a backward traveling (counter propagating) wave and the second term is the force of a forward traveling (co-propagating) wave. It indicates the electrons are modulated by the standing wave in the cavity composed of the forward and backward waves.

The transverse motion of the electron bunch in the backward traveling wave was analytically studied in reference [198], under the assumption of a paraxial wave condition. The ratio between the transverse and axial velocities was found to be on the order of K/γ, which is also a small value.

The co-propagating wave will also modulate the electron bunch to generate low-frequency motion. From Eq. 9, its impact can be minimized if the impedance of the MU is close to the impedance of free space. Recent study on the electron motion showed the effect of the co-propagating wave could not be ignored and it could cause spectrum degradation at larger K values.

It is possible that the electron beam interacts with the backward traveling wave in a waveguide instead of a cavity structure, as shown in Fig. 32(a). In this counter-propagation mode, the effective interaction time is $\tau = L/(v_e + v_g)$, where L is the waveguide length, and v_e, v_g are the velocity and group velocity of the electron beam and the microwaves, respectively. However the effective ineraction length is only $L^{'} = v_g\tau$. In a FEL, the relativistic electron has $v_e \approx c$, therefore $L^{'}$ will be less than $L/2$. On the other hand, as shown in Fig. 32(b), if the EM wave co-propagates with the electron bunch, and generates a proportion of backward traveling wave, or reflected wave, at the same time, the effective interaction time can be much longer and becomes $\tau = L/(v_e - v_g)$. The effective interaction length in this case is

$$L^{'} = v_g L/(v_e - v_g) \tag{20}$$

To achieve the same interaction length, the waveguide length in the counter-propagation mode will need to be 3 times longer compared with the co-propagation mode when $v_g = 0.5v_e$. The ratio will be even greater as the value of v_g increases.

Following the appropriate choice of the suitable modes, a waveguide-type microwave undulator by using a helically corrugated waveguide (HCW) operating at 30.3 GHz was designed [199]. When driven by a high power microwave source with an output power of 1 GW and pulse

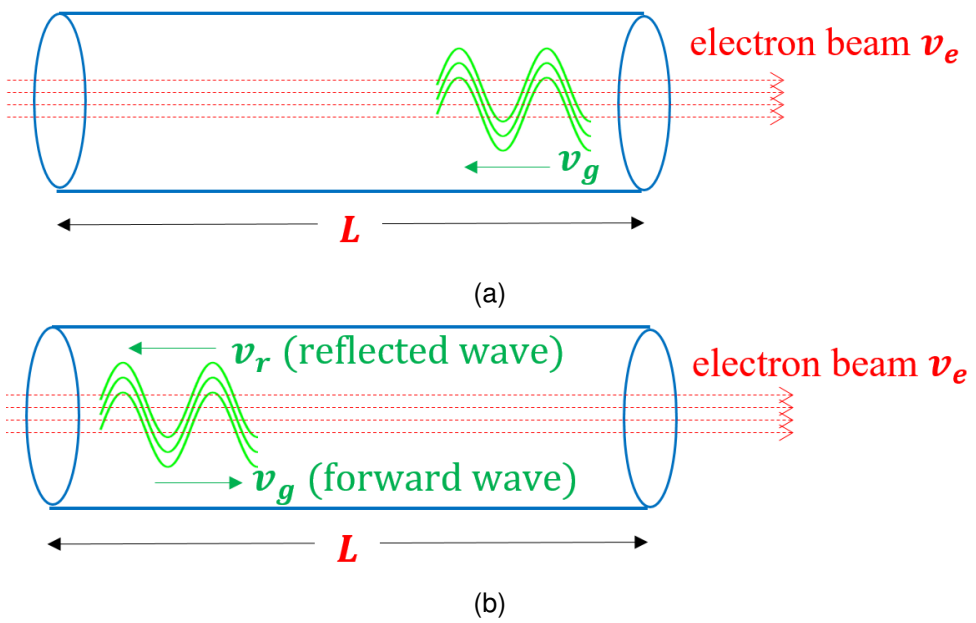

Figure 32: Contour plot of the electric field patterns of (a) the HE_{11} and (b) the HE_{12} modes.

duration of 15 ns, the equivalent magnetic field strength B_{ub} was about 0.3 T, and the undulator period λ_u was 4.95 mm which results in an undulator parameter K value of 0.14.

4.3 Laser-wave undulators

The development of high power laser technology and the availability of high brightness electron beams allows FEL operation with undulator fields provided by electromagnetic waves produced by the laser [200–202].

The following arguments are based on the possibility [203–205] to have a stimulated coherent emission by means of nonlinear Thomson electrons scattering off a high power CO_2 or Ti:Sa laser. In this process, relativistic electrons colliding head-on with laser photons having energy $\hbar\omega_L \ll m_e c^2$ are scattered emitting photons undergone through a double Doppler shift of the initial laser fundamental wavelength λ_L:

$$\lambda_R = \frac{1-\beta}{1+\beta}\lambda_L \tag{21}$$

where β is the normalized velocity of the electron beam. The electromagnetic laser pulse acts as an undulator, replacing the alternate static fields used in a conventional FEL facility: a net transverse momentum is imparted to the electron beam by a magnetic field, in either case. Within this picture, the strength parameter associated with a laser wave undulator of intensity I_L is given by the dimensionless laser field a_0, associated to the electric field amplitude E_0:

$$a_0 = \frac{eE_0}{m_e\omega_L c}, \quad K = a_0 \simeq 0.85\times 10^{-5}\lambda_L[m]\sqrt{I_L[W/m^2]} \tag{22}$$

At low power intensity, $a_0 \ll 1$, an electron acquires a small amplitude transverse oscillation at the laser wavelength λ_L. As the intensity increases to a few tenths, this oscillation wavelength starts deviating from λ_L. As the normalized amplitude increases as $a_0 \sim 1$, the Lorentz force associated with the laser magnetic field becomes significant, and the electron acquires an oscillation along the direction of laser propagation, in addition to the transverse oscillation. If the laser pulse is long enough, collective effects are dominant in the radiation emitted by electrons in the Thomson scattering. and the system behaves like a conventional FEL, with an equivalent resonant wavelength λ_R defined as:

$$\lambda_R = \frac{\lambda_L}{4\gamma^2}\left(1+\frac{a_0^2}{2}\right) \tag{23}$$

Table 19: Estimates of the FEL performance in a laser wave undulator.

	CO_2	Ti:Sa
laser wavelength (μm)	10	0.8
laser peak power (TW)	0.1	1
laser spot radius (μm)	40	5
a_0 parameter	0.3	0.5
resonant wavelength (nm)	0.54	0.048
Pierce ρ (10^{-4})	1.46	1.25
gain length L_g (cm)	0.41	0.52
saturation power P_{sat} (MW)	9	7

An FEL facility exploiting such a concept achieves a twofold improvement:

- electron beams with energy of the order of a few hundreds MeV can be used to cover the hard X-ray region;
- construction, operation and maintenance of long undulator sections are avoided resulting in a size effective facility.

On the other hand, this concept requires extremely high quality electron beams, in order to support a significant SASE growth of the FEL peak power. An estimate of the FEL performance is given considering the equivalent Pierce ρ parameter of the associated planar undulator line:

$$\rho = \frac{8.36 \times 10^{-3}}{\gamma} \sqrt[3]{j \left[\frac{A}{m^2}\right] (\lambda_L[m] a_0 f_b(a_0))^2} \tag{24}$$

where

$$f_b(a_0) = J_0(\xi) - J_1(\xi), \quad \xi = \frac{a_0^2}{2} \frac{1}{2 + a_0^2}$$

described in terms of the Bessel $J_{0,1}(\xi)$ functions.

The FEL performance is therefore described in terms of the gain length L_g and the saturation power P_{sat}, as in the following definitions:

$$L_g = \chi\left(\rho, \frac{\sigma_E}{E}\right) \frac{\lambda_u}{4\pi\rho\sqrt{3}}, \quad P_{sat} = \Phi\left(\rho, \frac{\sigma_E}{E}\right) \sqrt{2}\rho P_E \tag{25}$$

where χ and Φ are correction functions accounting for energy spread deteriorating effects and P_E is the power associated to the electron beam.

Table 19 shows the FEL performance assuming an electron beam with energy 50 MeV, peak current 1 kA, energy spread $\sigma_E/E = 10^{-4}$, normalized emittance 0.2 $mm \times mrad$, together with the specified CO_2 and Ti:Sa lasers characteristics. These results have to be considered as preliminary as a full 3D simulation is needed in order to assess any interplay between transverse and longitudinal dynamics in this FEL mechanism.

A more recent and specific proposal [206] aims at exploiting the same dynamics in an FEL device consisting of a low energy linear accelerator and a ring cavity to confine and recirculate the laser wave, for multiple interactions with the electron beam. Figure 33 shows the optical scheme of this proposal.

The cavity length is adjusted on the distance separating two successive electron bunches. The FEL interaction occurs in the first section confined within two parabolic mirrors. The laser radiation is recirculated by means of two plane mirrors, two parabolic mirrors, two pairs of short focal length positive lenses aligned with respect to a central focusing lens, in order to get two waists of the laser beam along the same straight line.

While the electron beam interacts at the first laser waist section, with the micro-bunching mechanism taking place, the region of the second waist provides radiation, and the FEL coherent emission and growth occurs. After the first waist, the bunched electron beam passes through a magnetic chicane and the laser pulse is synchronized to interact at the second waist. Assuming an electron beam of 20 MeV energy, 3 kA current peak, provided by a high repetition rate electron injector of order 100 Hz, and integrated with a CO_2 laser device of peak power 130 GW, this scheme is able to provide a FEL peak power of about 1 MW.

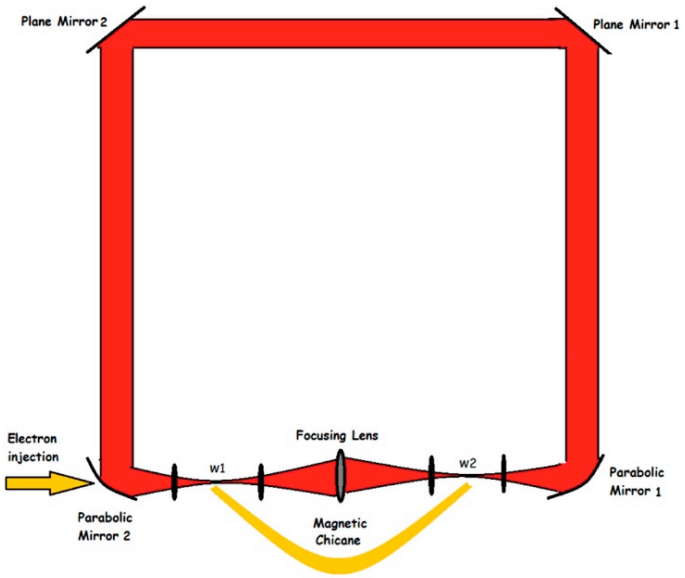

Figure 33: Optical scheme of the undulator system consisting of laser device, ring cavity and electron beam. Figure adapted from reference [206].

In conclusion, the development of the technologies – for high peak power lasers, high brightness electron beams and high repetition rate electron injectors – relevant to implement a very compact X-rays FEL facility based on laser wave undulator devices is approaching the necessary readiness level. However, this undulator scheme is not mature enough to be fully compared to the other technologies and is addressed here for completeness sake.

5 Comparison of technologies

5.1 Introduction

In this section the undulator technologies described in the preceding sections are compared. In section 5.2 the constraints arising from the photon science requirements are considered. In section 5.3 a quantitative comparison is made between the performance of the various technologies, which shows how the choice of undulator technology defines the required electron beam energy. Cost considerations are taken into account in section 5.4.

5.2 Constraints from the photon science requirements

5.2.1 Overview of user requirements and their impact on the undulator choice

This section considers constraints on the undulator choice arising from the FEL radiation characteristics specified for XLS-CompactLight [2], as summarised in Table 1:

- Perhaps the most obvious connection between the user requirements and undulator technology is photon energy (wavelength), which depends on undulator parameters and electron beam energy as given in Eq. 2. This dependence is assessed in detail in section 5.3.
- A further requirement (not listed in Table 1) is that tuning across photon energies will primarily be achieved by undulator scanning rather then electron energy scanning, in order to maximize efficient operation of the facility [2]. Given that both soft x-ray and hard x-ray regimes require a factor of 8 photon energy scaling to be covered with only 'a few discrete electron beam energies', the undulator should provide a factor of $\sim$2 wavelength tuning. All undulator technologies are expected to provide this.
- Another important relationship between the user requirements and undulator technology is the requirement for variable, selectable, polarization. This has significant implications for the undulator choice, and is considered in detail in Section 5.2.2.
- The requirement for two-colour operation does not have obvious consequences for the choice of undulator technology. Two-colour operation can be achieved either by passing two electron bunches along a single undulator line, or by using separate undulators. In the latter case, the required wavelength tuning of 10-20% is within the factor of 2 already specified above.
- The requirement for pulse duration down to 100 as could constrain the undulator choice in certain cases. To deliver pulse duration down to 100 as at the longest wavelength of the soft x-ray range requires FEL pulses of only a few cycles. This would most likely require novel FEL techniques involving very short undulator modules, consisting of only one or a few periods, or undulators with a strongly chirped undulator period. However, this is beyond the scope of this document. For most of the pulse duration range the undulator choice has little impact.
- Other parameters in Table 1 are expected to have little impact upon the undulator choice. Repetition rate up to 1 kHz should be achievable for all technologies, while the requirement for <10 fs synchronization is also unlikely to affect the undulator choice, though perhaps it should be considered in more detail for some of the more exotic technologies.

5.2.2 Variable polarisation and design choices

Overview of the main approaches for variable polarisation. The main approaches for generating FEL light with variable polarization are as follows:

1. The first option is to use an undulator technology providing variable polarization for the full undulator line. This method delivers excellent performance and is conceptually straightforward but it is not foreseen to be achievable for some technologies (SCU, cryogenic). This option would therefore exclude some of the undulator types with most potential to be compact and reduce the facility's electron beam energy (see Section 5.3).

2. Another approach is to entirely use undulators with a fixed polarization state. Variable polarization can be achieved using the crossed-undulator technique, in which the final undulator module is set to an orthogonal polarization state to the rest of the undulator. The polarization can be varied using an electron delay chicane to set the relative phase between radiation emitted in the main line and the final module. The benefit of this approach is that any undulator technology can be used - thereby allowing both the most compact undulator and the lowest electron beam energy for the facility, however the degree of polarization is relatively low.

3. Alternatively a combination of the two methods above can be used. In this case an undulator with fixed polarization is used for the main part of the line, and a variable polarization undulator is used for the final section (the afterburner). This has the advantage of allowing any undulator technology for the main line - so the most compact can be chosen. However the afterburner then sets the shortest wavelength achievable - either limiting the wavelength reach for variable polarization or requiring the maximum electron beam energy of the facility to be dictated by the afterburner, thereby lessening the advantage gained.

Study of feasibility of an after-burner for polarisation control Following what was discussed above in terms of generating variable polarisation, options 1 and 3 (setting a helical undulator as the main undulator) are compared in simulations to determine whether the latter option will allow a more compact FEL section, and, if so, how the performance compares. In the case studied, the helical undulator was assumed to be an SCU, and the variably polarising undulator was assumed to be a delta undulator set to planar mode.

The electron beam properties are given in Table 20 and the undulators resonant at 16keV have parameters shown in Table 21. The normal FEL saturation length and saturation power for the SCU and Delta undulators (in standalone mode) are given in Table 22—the saturation length for the delta is $L_{sat} = 29.13$m with saturation pulse energy 41.19 μJ.

Simulations of the SCU + delta planar afterburner configuration were done in Genesis1.3 [207]. Given that the normal saturation length for the SCU is 15.91m and the saturation length for the delta undulator is 29.13m, the SCU + afterburner solution is more compact as long as the length of the afterburner is less than 13m.

The ratios of pulse energies obtained at the end of the afterburner and the pulse energy at saturation for the delta planar undulator, for different layouts of SCU and delta planar afterburners, are shown in Figure 34. It is shown that the maximum pulse energy obtained at the

Table 20: Electron beam parameters.

Electron beam parameter	Value
Beam Energy	5.5 GeV
Peak Current	5 kA
Normalised $\varepsilon_{x,y}$	0.2 mm-mrad
RMS slice energy spread	0.01%
Maximum Photon Energy	16 keV
Average β function	9 meters

Table 21: Undulator parameters.

Undulator type	a_w	λ_u (mm)	Length of undulator section (m)
SCU	0.907	9.85	2.27
Delta planar afterburner	0.546	13.83	2.28

end of the afterburner (green dotted line in Figure 34) ranges from 17% up to 68.4% of the saturation pulse energy of the delta planar undulator. Table 23 shows the length reduction for the SCU + afterburner solution is up to 10.9 meters. It can be seen then that a compromise between compactness and FEL performance must be made. A shorter undulator line gives linearly polarized radiation but at the cost of reduced pulse energy.

It should be noted that the SCU + afterburner option assumes the radiation from the SCU is blocked before the afterburner. In consequence, the degree of polarisation is 100%. The way to achieve this in practice involves aligning the afterburner at a small angle to the SCU (beam diverted scheme) or installing an inverse taper on the SCU to suppress the background power coming from the main undulator but allowing the electron beam to bunch. [208]. The experimental results obtained by the inverse taper scheme demonstrated polarisation control successfully between a planar undulator and a helical afterburner [209].

Table 22: FEL figures of merits for both SCU and delta planar undulator, from steady state (SS) and time dependent (TD) simulations in Genesis1.3.

Undulator type	$L_{saturation}$ (m)		$P_{saturation}$ (GW)		$E_{pulse\ saturation}(\mu J)$	
	SS	**TD**	**SS**	**TD**	**SS**	**TD**
SCU	21.85	15.61	15.37	9.53	N/A	52.11
Delta planar undulator	36.24	29.13	3.52	7.53	N/A	41.19

Table 23: Reduction in length of the SCU + afterburner option compared to the delta planar undulator option.

Afterburner length (meters)	$L_{\text{undulator line}} - L_{\text{saturation Delta planar undulator}}$ **(meters)**
2.28	10.9
4.56	8.7
6.84	6.4
9.13	4.1
11.4	1.8

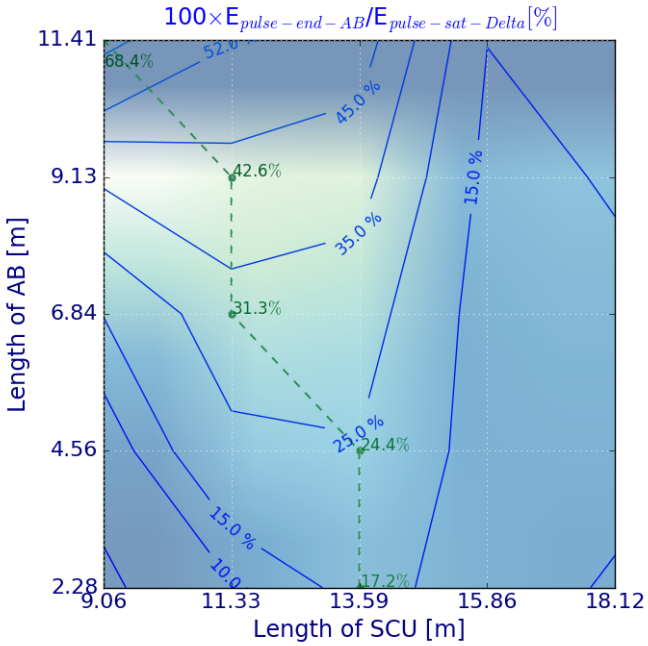

Figure 34: Ratio of the pulse energy for the SCU + afterburner option to the saturation pulse energy from the delta undulator, as a function of the lengths of the SCU and afterburner. Green dotted line represents the maximum ratio for each afterburner length.

5.3 Considerations on undulator technologies based on quantitative figures of merit

In this section a quantitative comparison is made the different undulator technologies, using the parameterisations of the estimated field, as a function of undulator period and gap, reported in the relevant earlier sections. Two approaches are combined . First, the semi-analytical model of Ming Xie [210] is used. The model extends the one-dimensional FEL theory, which applies in the limit of a 1D monoenergetic beam, to the case where degradation of performance due to finite emittance and energy spread is included. This model reliably predicts the FEL saturation power P_{sat}, and saturation length L_{sat} via the FEL ρ-parameter using corrections based on a parameterisation of a set of 3D numerical simulations. The results from the Xie analysis are combined with the analytical theory of Saldin [211] which allows the FEL longitudinal and transverse coherence to be calculated. Hence the FEL spectral brilliance can be determined.

This is a key parameter of interest to users because it tells them how many photons per second within a given bandwidth they can focus onto a sample of given transverse dimensions - i.e. it tells them how *useful* the light is.

One figure of merit chosen for the quantitative comparison is the ratio between the FEL peak brilliance and the saturation length as this is a convenient measure of performance vs compactness. The second figure of merit chosen is the FEL peak brilliance itself (i.e. not normalised to the saturation length) because there is a specific user requirement for a minimum brilliance. The analysis of both figures of merit is conducted as a function of electron beam energy to illustrate the advantage obtained by using the undulator technologies with the strongest fields and to determine the required electron beam energy that would be required so that the peak brilliance exceeds the user requirement. This allows us to set an upper limit on the electron beam energy for CompactLight that allows us to satisfy the following criteria:

- The electron beam energy is lower than any other X-ray FEL facility
- The photon energy reach is higher than that of SwissFEL which has a beam energy higher than CompactLight
- There are a number of viable options for undulator technology which can be assessed further in the next stages of the project.

The figure of merit calculations are shown in Fig 35 where the top plot is for beam energy 4.5 GeV, the middle plot is for 5.5 GeV and the bottom plot is for 6.5 GeV. The electron beam parameters used in the calculations are peak current $I = 5$kA, normalised emittance $\varepsilon_n = 0.2$ mm-mrad, relative RMS energy spread $\sigma_\gamma/\gamma_0 = 10^{-4}$ and average β-function $\bar{\beta} = 9$m. In each plot the horizontal axis is the undulator period λ_u and the vertical axis is the undulator K_{rms}. Each line shows the dependence of K_{rms} vs λ_u for a different undulator technology, as represented in the legend. For some technologies a full parameterisation over the space is not available—these technologies (for example the Microwave undulators) are represented by single points on the plot. The coloured region represents the $[K_{rms}, \lambda_u]$ parameter space in which the undulator resonant wavelength lies between $\lambda_r = 0.155$ nm (top edge) and $\lambda_r = 0.0775$ nm (bottom edge). The colour represents the value of the figure of merit B/L_{sat}.

The interpretation of these plots is as follows. The intersection of each undulator curve with the $\lambda_r = 0.155$nm line defines the period required for that undulator, at that beam energy, to be resonant at $\lambda_r = 0.155$nm. To tune to $\lambda_r = 0.0775$nm the undulator K strength is then reduced. For beam energy 4.5 GeV (top plot) it can be seen that for a number of technologies, for example APPLE-II, the merit function drops to zero at $\lambda_r = 0.0775$nm, indicating that these technologies are unviable at 4.5GeV—they provide insufficient field to cover the required tuning range. In fact, only those technologies for which the $[K_{rms}, \lambda_u]$ curve intersects the $\lambda_r = 0.155$ nm line at $\lambda_u < 12$mm provide any output at $\lambda_r = 0.0775$nm.

By increasing the beam energy to 5.5GeV (middle plot) all of the technologies are able to tune across the required range, but the merit function is low for those technologies with weaker field, indicating that a threshold could be defined in principle. Finally, at 6.5GeV, the trend continues of improving performance.

In general then, it is seen that

- the undulator technologies that provide the strongest K as a function of period, or the 'strongest' undulators, have the highest merit function,

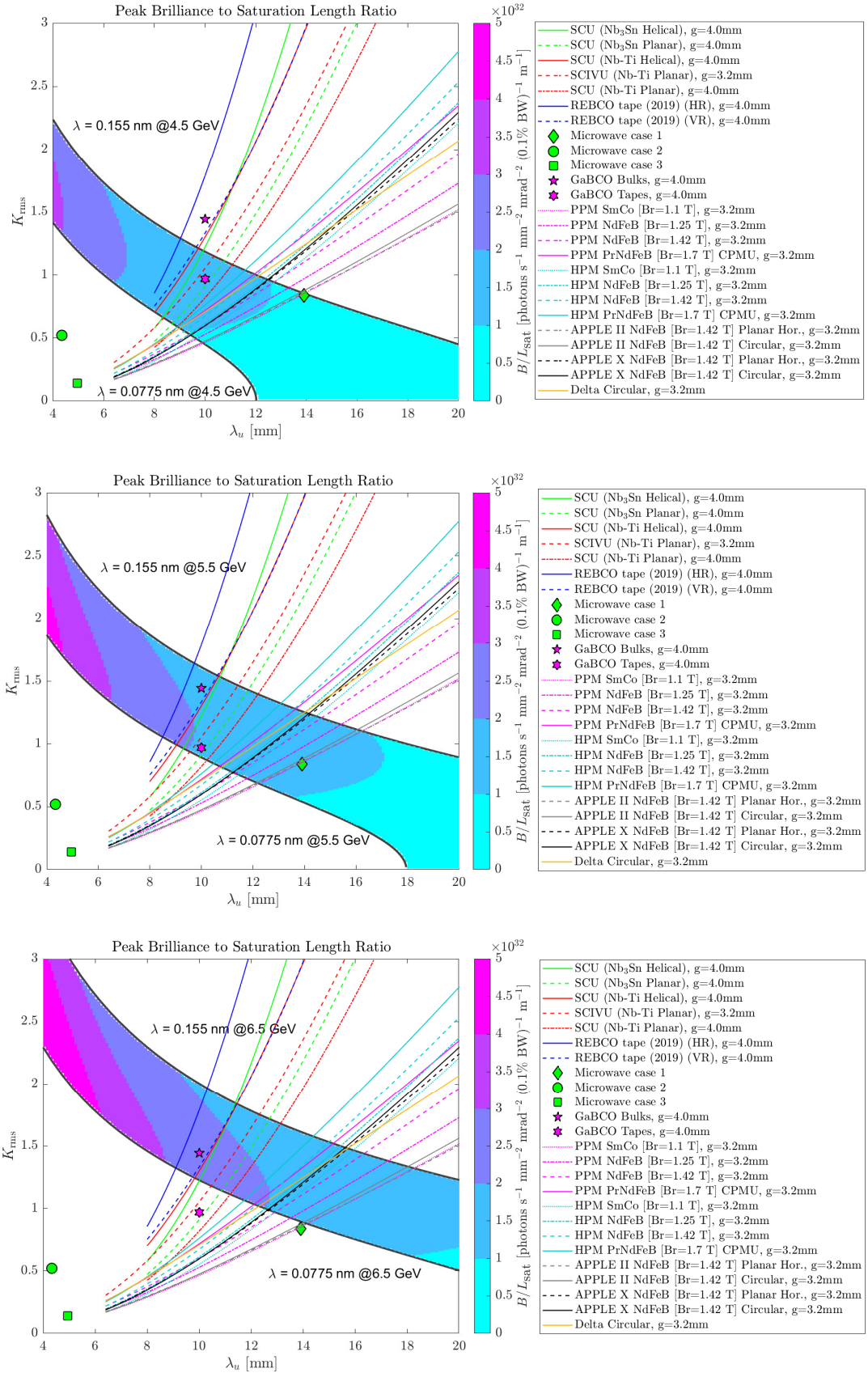

Figure 35: Figure of merit B/L_{sat} for electron beam energies 4.5GeV (top), 5.5GeV (middle) and 6.5GeV (bottom)

- at low beam energies only the strongest undulator can give any photon output across the whole tuning range
- as the beam energy is increased more technologies become viable and the merit function increases for all technologies.

Therefore the beam energy must be chosen appropriately—it must be as low as possible to enable a compact facility but high enough to provide the required FEL output. Also the decision is made that at this stage of the project, the beam energy choice must allow a number of undulator technologies to remain viable choices for further assessment of their potential performance, in combination with assessment of their relative costs and risks.

To further assess the required beam energy the peak brilliance is calculated for the different technologies, at three different beam energies. The user epecification is that peak brilliance should satisfy $B > 1 \times 10^{33}$ph/s/mm^2/mrad^2/0.1% bw at all photon energies. It is noted that the calculations here are for an ideal case and that in reality there are effects that may degrade the performance—for example the bunch may have an energy chirp, or there may be bandwidth broadening or power reduction due to undulator wakefields. Therefore, a factor of two contingency is added to the required peak brilliance, i.e. we require the choice of undulator tecnology and beam energy to provide $B > 2 \times 10^{33}$ph/s/mm^2/mrad^2/0.1% bw at all photon energies. The calculations are shown in Fig 36, where the yellow region corresponds to the peak brilliance exceeding the threshold including contingency. Clearly at $E =$4.5 GeV, none of the technologies provide sufficient brilliance, whereas at $E \geq 5.5$GeV, all of the undulator technologies are satisfactory.

Based on the previous discussions, we propose a nominal CompactLight beam energy of 5.5 GeV. As has been shown, this is the minimum beam energy at which all undulator technologies considered will provide sufficient FEL brilliance, but this energy is also lower than that of SwissFEL at PSI which has a lower photon energy reach. In addition we reiterate that as clearly shown in Fig 35 and ensuing discussion, the merit function is always stronger for those undulator technologies which provide the highest field which will be a critical factor in determining the final choice of undulator technology, together with the analyses of the risks and costs of each technology presented elsewhere.

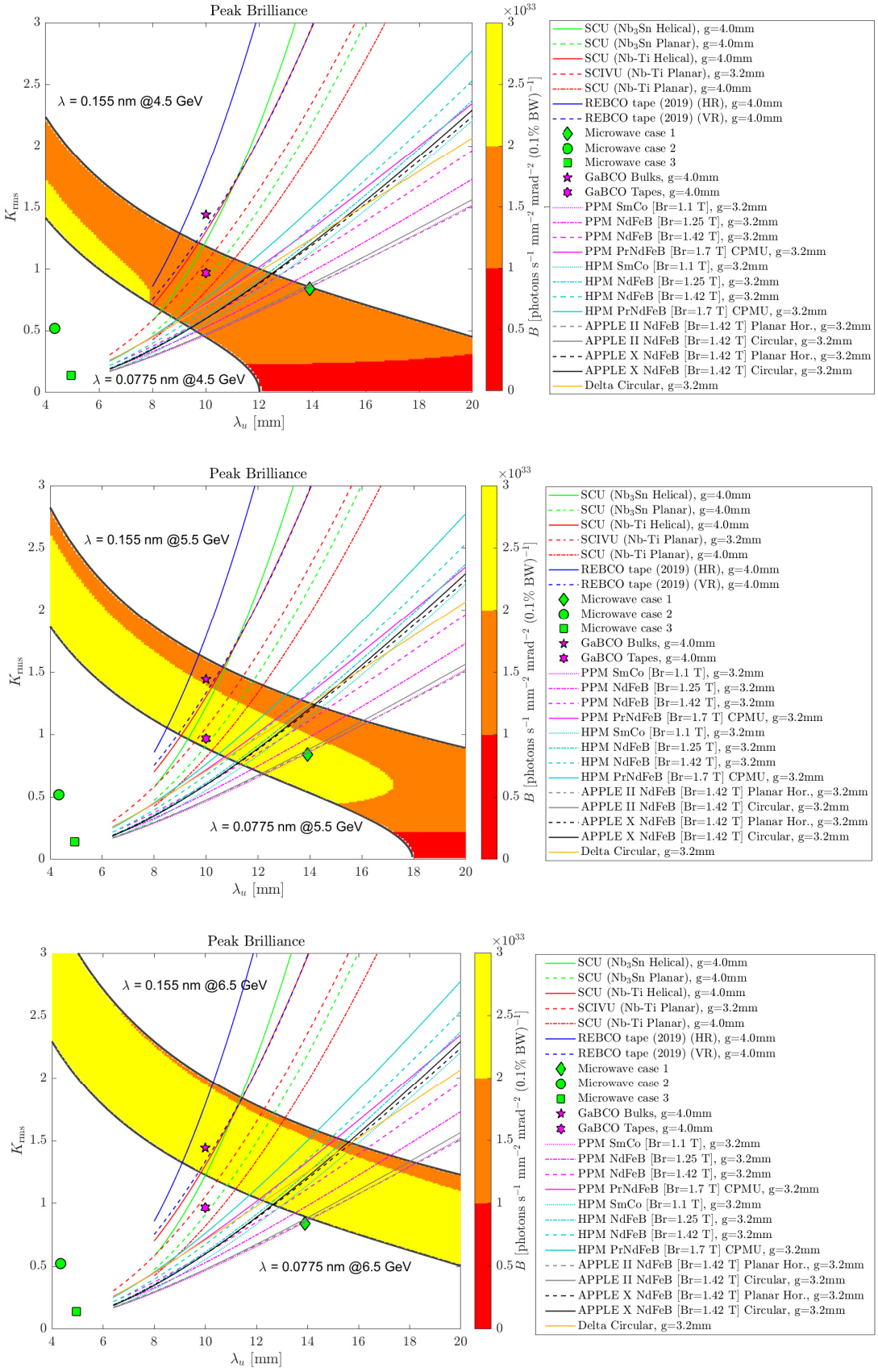

Figure 36: Peak brilliance for electron beam energies 4.5GeV (top), 5.5GeV (middle) and 6.5GeV (bottom)

5.4 Preliminary undulator cost matrix

5.4.1 Introduction

The price for the undulator(s) is not so easy to define because the total costs cover much more than the price for the hardware. The price for the undulators itself depend on the technology, planar out of vacuum, in-vacuum or even cryogenic, APPLE type undulators or superconducting but also on the number of undulators of same type to be built in series and if the undulators are built by the institutes or by industry. In all scenarios industry is involved, but in different realization stages.

Undulator projects for synchrotrons have been realized mostly with single, individual undulators, because of different needs for the specific beamlines, technological improvements and also because of the long work-up phase due to financial and human resources limitations. ESRF could already work different because of the large number of undulators. Now with the FELs one undulator line consists of 15 to 30 identical undulators, to be realized at the same time, within a time frame of 1 - 2 years. This has opened the view to scaling laws for small series production which have of course a significant impact on the costs. In addition, only the scale of the projects made certain developments possible like the automatiziation of the magnetic field tuning for the SwissFEL undulators at PSI. Nevertheless, the first costly part is the design respectively specification phase. Software tools like RADIA and SRW from ESRF, SPECTRA from SPring-8 are available for undulator design and heavily used by the community including companies working with all kinds of permanant magnet based undulators as well as electromagnetic undulators. This does not hold for superconducting undulator projects where costly commercial software is required (COMSOL, ANSYS), especially when industry licences have to be paid which is also the case for some research institutes. A handful companies in Europe and Japan can provide the entire chain from design based on the specifications, the production and magnetic optimization. But also the personnel and infrastucture is required at the facilities for quality control on site, maintenance and eventually repair of the systems. This is especially true for the FELs where an orchestra of the n undulators plus n-1 phase matchers needs to work together harmonically.

Investments are also required in the magnetic measurement laboratories. For FEL projects reasonable space is required to handle several undulators of up to 5m length in parallel and generally a good climatization with $\pm 0.1^{\circ}$ is required because the significant temperature coefficients of $-0.1\%/K$ for NdFeB magnets and -0.03-$-0.05\%/K$ for SmCo magnets. Because of the weight either a crane is required or in case of floor transportation either with air-cushions or by wheel-based solutions the floor space required is much larger than the footprint of the undulators itself.

The measurement infrastructure has changed in recent years. The granit bench based Hall probe systems have been replaced by more flexible laser based systems which have been originally developed for the in-situ magnetic measurements of cryogenic in-vacuum undulators. This systems are scaleable in length and reduce the investment by more than a factor of 2 to about 200 k€ per bench. For FELs it is best to orient the measurement benches in the same direction as the undulator line to avoid conflicts with the transverse component of the earth's magnetic field, which should be taken into account already in the design phase of the building infrastructure.

5.4.2 Cost optimisation strategies

For the production of undulators for FEL lines the design of the undulators should take into account the scaling laws for small series production. For the frame of the support structure cast materials are more efficient compared to welding structures because the price for the casting moulds can be distributed over several units.

Closed structures might result in more compact designs compared to C-structures with increased stability againts load changes. A general strategy might be to try to make designs as compact as possible while considering the needs for magnetic optimization.

The keepers which carry the magnets are better not to be costly single keeper but block keepers which can be even made from extrusions and host several periods. High machining precision is today easily up to $30--50\,\mathrm{cm}$. This allows also the individual magnets to be mounted by the magnet supplier so that in the lab only the keeper units need to be handled.

For planar undulators out of vacuum solutions should be compared to in-vacuum or crogenic in-vacuum undulator technology. The latest magnet technology allows pretty strong permanent magnets even at room temperature. A remanence of $B_r = 1.37\,\mathrm{T}$ with Tb diffused magnets and a coercivity of $Hc_j \geq 2400\,\mathrm{kA/m}$ is a significant improvement compared to the magnetic material which was available for the SwissFEL U15 production with a remanence of $B_r = 1.37\,\mathrm{T}$. The stronger magnets can be combined with very thin vacuum chambers made either of seamless drawn Cu tubes or Cu tubes made by a galvanic process both with wall thickness of about $0.2\,\mathrm{mm}$. This needs to be compared with the $0.1\,\mathrm{mm}$ foil needed to cover the magnets in in-vacuum undulators. So the diffence in gap between magnetic gap and vacuum stay-clear aperture is only $0.2\,\mathrm{mm}$ plus the required alignment tolerances. Such thin vacuum chambers are feasible at low rep rate FELs because of the very low heat load so that no cooling of the vacuum pipe is required. In-vacuum undulator technology is of course more flexible, i.e. it is easier to vary the minimum gap according to the impact of the wake fields or beam loss rates, but the price to pay is high. For the SwissFEL Athos undulator line with APPLE X undulators a round vacuum chamber with $0.2\,\mathrm{mm}$ wall thickness is used with a $5\,\mathrm{mm}$ inner diameter. For planar undulators an aspect ratio of 2:1 for the horizontal to vertical dimension of the chamber is possible.

In case of in-vacuum with less stringent vacuum requirements by the FELs a reduced design results in some space and costs savings because of reduced components. So a bakeout is not required so that the rail system to allow the lengthening of the heated inner I-beam with respect to the outer I-beam can be avoided and no special care has to be taken with magnets and Al keepers. Second, because of the low repetition rate the flexible taper which is absolutely mandatory for storage ring devices is not needed for FELs because the bunch to bunch interaction via electrical fields generated at steps in the vacuum chamber can be neglected at $100\,\mathrm{Hz}$.

A reduced number of columns mounted in a staggered array helps to reduce the number of components, the work and the risk of vacuum failures. For the SwissFEL U15 the number of columns could be reduced from 64 in conventional design to 20. In this staggered design is in first order there is no gap variation beetween the supporting columns, because the top I-beam follows a sine variation and the bottom I-beam a cosine variation. The exponential gap vari-

ation is replaced by a virtual change of position in the gap which follows a cosh function and is therefore less harmful. For cryogenic undulators an additional benefit of this configuration is less heat transfer through the columns.

Costs can also be reduced by an appropriate choice of the motor control system. A very high sophisticated controller is not needed. As the undulators are operated with very low frequencies the standard PLC based motion control systems are adequate and are successfully used in several laboratories. An alternative to a classical (servo-) motor, spindel, optionally gear box or wedge system is a hydraulic system with high precision valves recently brought on the market by Bosch-Rexroth, which combines the strenght of a hydraulic system with a precision which was so far only available with motor based systems and high speed. This is very interesting for fast helicity switching in APPLE undulators.

A time consuming and therefore costly procedure is the field optimization for trajectory and phase. For this at PSI a robot based automated magnet tuning has been realized. The block keeper provides a flexor system which allows a wedge based height adjustment of the individual magnet. The flexor works also a spring which is preloaded by $60\,\mu m$ when the magnet is assmebled. At the optimzation the magnet can be adjusted by $\pm 30\,\mu m$ with sub μm resolution. A screw robot shares the linear stage with the Hall-probe sensor. So within about 1 hour all magnets can be adjusted very precisely. In practice a few iterations are required, but the full optimization was done in one or two days. For the U19 production the field optimization happened without a vacuum chamber. After installation into the chamber a second measurement system was needed to correct the errors resulting from the reassembling and to do the field maps used for operation. The field error could be perfectly reproduced by adjusting the columns only. To avoid this two step process with two measurement systems, without vacuum chamber and inside the chamber but without vacuum, the robot system has been downsized. This allows i.e. an eventually reshimming of an U15 because of radiation damage without disassembling the magnet structure. This considerably speeds-up the optimization time and the investment in the measurement infrastructure for benches and floor space. In future this will be further developed to be vacuum compatible to scope for cryogenic undulators.

For soft x-ray beamlines the undulators need to provide variable polarization. There can be all undulators of APPLE type with polarization control or alternatively only the last few undulator modules having the majority with cheaper planar undulators. With the trick of inverse tapering the linear horizontal polarized light out of the planar undulators can be switched off while the bunching of the electrons remains, so that a few so called afterburner undulators with variable polarization are sufficient but of course with less flexibility.

Of course, these are only few flash lights on effective cost saving strategies and the list can and has to be prolongated.

5.4.3 Cost Matrix for different types of undulators and fabrication

Beside the rf-system the undulators are a major part of the costs in an FEL project. As already discussed earlier, the cost are determined by various aspects where the costs will depend on. But data from recent realized projects can give a good orientation and start for an cost estimate. The costs discussed below are based on WTO conform procurements for single

Table 24: Cost matrix for undulators for FELs and single devices. Turn key no means Design and optimzation by the institute, yes means undulators delivered ready to use according specifications.

type	period [mm]	L [m]	N_{per}	price k€	N_{modules}	L_{tot} [m]	price k€	turn key
hard x-ray:								
planar out-vac	40	5	125	400	33	165	13.2	no
planar in-vac	15	4	265	800	13	52	10.4	no
planar in-vac	15	3	200	1300	1			yes
soft x-ray:								
planar out-vac	65	5	75	400	33	165	13	no
APPLE	38	2	50	550	16	32	8,8	no
APPLE	70	2	28	600	1			yes
planar out-vac	80	2	25	500	1			yes

units at storage rings (in-vacuum) and series productions for out-of-vacuum and in-vacuum room temperature planar undulators and out-of vacuum APPLE undulators. A first in-vacuum APPLE undulator is under construction at HZB for BESSY II. Superconducting undulators have been only realized in a collaboration of KIT/Noell (2 individual devices) and at ANL for the APS (3 devices). But all these had prototype status. Series production for FELs might be at the midterm horizon for high rep rate machines like LCLS II and EUXFEL.

The prices are given per undulator module, which however depend on the technology and also on the period length. The price for the magnets cover normally between $10-20\%$ of the total costs, so this is not the driving factor. But longer periods means also more undulator modules to reach saturation. SwissFEL, U15, 13 modules of 4m length with 265 periods each, EUXFEL, U40, 33 modules of 5m with 125 periods. The number of periods to reach saturation at hard x-ray are similar about 3500 for SwissFEL to 4000 at EUXFEL. For soft x-ray these number are lower: SwissFEL UE38, 16 modules of 2m each with 50 periods compared to U65 with again 33 modules and 75 periods. EUXFEL uses planar U65 undulators and only 4 UE90 afterburner to provide the variable polarization. The series price tag for planar out of vacuum undulators is at about 400 k€ per module. Half of the price is needed for the magnet array, the other for the support structure including drive system. Vacuum chamber and phase matchers are not included. The series price tag for in-vacuum undulators is 800 k€ per module. The specific price for APPLE undulators is higher, also in series production it is about 550 k€. In these numbers, design and magnetic optimization is done by the laboratories. Industry produces the components and assembles i.e. the support structure and magnets into keeper etc.. Another price can be given for a single in-vacuum undulator built turn-key ready by industry after specifications by a laboratory. The price for such a devices is at about 1.3 M€ for a 3m long device.

In table 24 these numbers are summarized for a better overview. The numbers are given in price per unit, the number of periods in each undulator and price to reach saturation for out of vacuum, in-vacuum and APPLE and add the prices for single device built by industry. It is interesting to see that the costs for different approaches are in the end similar. The EUXFEL

has a total length of 165 m, SwissFEL only 52 m but the overall costs are with 13.2 and 20.4 k€ very similar. Second interesting approach is that soft x-ray undulator beamlines could be cheaper if concepts like Optical Klystron configurations with enlarged phase advance in the intersections between the undulator modules are taken into account.

6 Concluding remarks

A comprehensive and detailed survey of undulator technologies is presented, addressing the readiness level, the limits and the opportunities associated to each technology, and also providing some perspectives, especially for the most recent and innovative concepts.

Furthermore, a systematic technology comparison in terms of undulator period and strength is performed, driven by potential XLS-CompactLight users' requests on the peak brilliance and on the target resonant wavelength, and constrained by the current studies on electron beam energy and quality.

In principle, a full and integrated design of the XLS-CompactLight undulator will also take account of the electron beam distribution under study within the present project, also including wakefield effects as well as other sources deteriorating the electron beam quality inside the undulator line. In this view, a more and more realistic and accurate description of the FEL dynamics associated to the specific undulator system will be considered.

As an additional guideline, this report also presents a preliminary estimate of the undulator system cost. These results will be complemented by also drawing an appropriate risk model associated to the undulator technologies selected for the final design.

References

[1] B. D. Patterson et al., *Science Opportunities at the SwissFEL X-ray Laser*, CHIMIA International Journal for Chemistry **68** (2014) 73, ISSN: 0009-4293, DOI: 10.2533/chimia.2014.73, URL: http://www.ingentaconnect.com/content/10.2533/chimia.2014.73.

[2] A. Mak et al., *FEL Science Requirements and Facility Design, XLS-CompactLight Deliverable D2.1*, tech. rep., 2018, URL: https://www.compactlight.eu/uploads/Main/D2.1_XLS_Specification.pdf.

[3] H. Motz, W. Thon, R. N. Whitehurst, *Experiments on radiation by fast electron beams*, Journal of Applied Physics **24** (1953) 826, ISSN: 00218979, DOI: 10.1063/1.1721389.

[4] K. Halbach, *Physical and optical properties of rare earth cobalt magnets*, Nuclear Instruments and Methods **187** (1981) 109, ISSN: 0029554X, DOI: 10.1016/0029-554X(81)90477-8.

[5] K. Halbach, *Permanent magnet undulators*, Le Journal de Physique Colloques **44** (1983) 1, ISSN: 0449-1947, DOI: 10.1051/jphyscol:1983120.

[6] S. Sasaki, *Analyses for a planar variably-polarizing undulator*, Nuclear Inst. and Methods in Physics Research, A (1994), ISSN: 01689002, DOI: 10.1016/0168-9002(94)91859-7.

[7] S. Sasaki et al., *Design of a new type of planar undulator for generating variably polarized radiation*, Nuclear Inst. and Methods in Physics Research, A (1993), ISSN: 01689002, DOI: 10.1016/0168-9002(93)90153-9.

[8] T. Schmidt et al., *A fixed gap APPLE II undulator for SLS*, AIP Conference Proceedings, vol. 879, 2007, p. 400, ISBN: 0735403732, DOI: 10.1063/1.2436084.

[9] A. B. Temnykh, *Delta undulator for Cornell energy recovery linac*, Physical Review Special Topics - Accelerators and Beams **11** (2008) 120702, DOI: 10.1103/PhysRevSTAB.11.120702.

[10] T. Schmidt, M. Calvi, *APPLE X Undulator for the SwissFEL Soft X-ray Beamline Athos*, Synchrotron Radiation News **31** (2018) 35, DOI: 10.1080/08940886.2018.1460174.

[11] M. Calvi et al., *Transverse gradient in Apple-type undulators*, Journal of Synchrotron Radiation **24** (2017) 600, DOI: 10.1107/s1600577517004726.

[12] J. Bahrdt et al., *Undulators for the BESSY soft-X-ray FEL*, Proceedings of FEL2004, JACoW, Trieste, Italy, 2004, p. 610, URL: http://www.jacow.org.

[13] H. Nuhn et al., *Commissioning of the Delta polarizing undulator at LCLS*, Proceedings of FEL2015, JACoW, Daejeon, Korea, 2015, WED01, ISBN: 9783954501342.

[14] J. Chavanne, P. Elleaume, *Technology of insertion devices*, Undulators, wigglers and their applications, ed. by H. Onuki, P. Elleaume, Taylor & Francis, London, 2003, DOI: 10.1201/9780203218235.

[15] J. Bahrdt, *Pushing the limits of short period permanent magnet undulators*, Proceedings of FEL2011, JACoW, Shanghai, China, 2011, THOAI1, ISBN: 9783954501175.

[16] T. Schmidt et al., *Magnetic design of an APPLE III undulator for SwissFEL*, Proceedings of FEL2014, JACoW, Basel, Switzerland, 2014, MOP043, ISBN: 9783954501335, URL: http://accelconf.web.cern.ch/AccelConf/FEL2014/papers/mop043.pdf.

[17] K. Park, K. Hiraga, M. Sagawa, *Effect of Metal-Coating and consecutive heat treatment on coercivity of thin Nd-Fe-B sintered magnets*, Proceedings 16th International Workshop on Rare-Earth magnets and their applications, Sendai, 2000, p. 257.

[18] P. Van Vaerenbergh, J. Chavanne, P. Elleaume, *Ageing of permanent magnet devices at the ESRF*, Proceedings of RADECS 99, IEEE, Fontevraud, France, 1999, p. 246, ISBN: 0780357264, DOI: 10.1109/radecs.1999.858589.

[19] T. Ikeda, S. Okuda, *Magnetic flux loss of the permanent magnets used for the wigglers of FELs by the irradiation with high-energy electrons or X-rays*, Nuclear Instruments and Methods in Physics Research, Section A: Accelerators, Spectrometers, Detectors and Associated Equipment **407** (1998) 439, ISSN: 01689002, DOI: 10.1016/S0168-9002(98)00065-5.

[20] T. Bizen et al., *Demagnetization of undulator magnets irradiated high energy electrons*, Nuclear Instruments and Methods in Physics Research, Section A: Accelerators, Spectrometers, Detectors and Associated Equipment **467-468** (2001) 185, ISSN: 01689002, DOI: 10.1016/S0168-9002(01)00270-4.

[21] T. Bizen et al., *Radiation Damage in Magnets for Undulators at Low Temperature*, Proceedings of EPAC2004, JaCoW, Lucerne, Switzerland, 2004, p. 2092.

[22] T. Hara et al., *Cryogenic permanent magnet undulators*, Physical Review Special Topics - Accelerators and Beams2 **7** (2004) 050702, DOI: 10.1103/PhysRevSTAB.7.050702.

[23] L. M. García et al., *Orbital magnetic moment instability at the spin reorientation transition of Nd2Fe14B*, Physical Review Letters **85** (2000) 429, ISSN: 00319007, DOI: 10.1103/PhysRevLett.85.429.

[24] C. Benabderrahmane et al., *Nd2Fe14B and Pr2Fe14B magnets characterisation and modelling for cryogenic permanent magnet undulator applications*, Nuclear Instruments and Methods in Physics Research, Section A: Accelerators, Spectrometers, Detectors and Associated Equipment **669** (2012) 1, DOI: 10.1016/j.nima.2011.12.015.

[25] K. Uestuener et al., *Sintered (Pr,Nd)-Fe-B permanent magnets with (BH)max of 520 kJ/m3 at 85K for cryogenic applications*,
20th Rare Earth Permanent Magnets Conference, Crete, Greece, 2008, p. 397,
URL: https://www.researchgate.net/publication/228994765.

[26] T. Tanabe, *Measurements of High Coercitivity PrFeB magnets at the Louis Neel*,
tech. rep., Brookhaven National Laboratory U.S., 2018, p. 209393,
URL: https://www.osti.gov/servlets/purl/1480943.

[27] E. R. Moog, R. J. Dejus, S. Sasaki, *Comparison of Achievable Magnetic Fields with Superconducting and Cryogenic Permanent Magnet Undulators - A Comprehensive Study of Computed and Measured Values* (2017), DOI: 10.2172/1372292,
URL: http://energy.gov/downloads/doe-public-access-plan.%20http://www.osti.gov/servlets/purl/1372292/.

[28] *VACODYM 131 TP / VACODYM 131 DTP for low temperature applications*, tech. rep.,
Vacuumshmelze, URL: https://www.vacuumschmelze.com/fileadmin/Medienbiliothek_2010/Downloads/DM/Vacodym_131_en.pdf.

[29] E. Trakhtenberg et al.,
Undulator for the LCLS project - From the prototype to the full-scale manufacturing,
Nuclear Instruments and Methods in Physics Research, Section A: Accelerators, Spectrometers, Detectors and Associated Equipment **543** (2005) 42,
DOI: 10.1016/j.nima.2005.01.110.

[30] H. Nuhn et al., *RnD towards a Delta-type undulator for the LCLS*,
Proceedings of FEL2013, JACoW, New York, USA, 2013, TUPSO52.

[31] J. N. Galayda, *The LCLS-II: a high power upgrade to the LCLS*,
Proceedings of IPAC2018, JACoW, Vancouver, Canada, 2018, MOYGB2,
ISBN: 9783954501847, DOI: 10.18429/JACoW-IPAC2018-MOYGB2.

[32] K. Tian, H. Nuhn, *Numerical study of the DELTA II polarizing undulator for LCLS II*,
Proceedings of IPAC2019 (2019) TUPRB102,
DOI: 10.18429/JACoW-IPAC2019-TUPRB102,
URL: http://jacow.org/IPAC2018/papers/frzplm2.pdf.

[33] A. Schops et al., *Recent undulator developments at DESY*,
Journal of Physics: Conference Series, vol. 425, Institute of Physics Publishing, 2013, p. 032002, DOI: 10.1088/1742-6596/425/3/032002.

[34] J. Pflueger et al.,
Status of the undulator systems for the European X-Ray Free Electron Laser,
Proceedings of FEL2013, JACoW, New York, USA, 2013, TUPSO60,
ISBN: 9783954501267.

[35] P. Li et al., *Magnetic design of an Apple-X afterburner for the SASE3 undulator of the European XFEL*, Nuclear Instruments and Methods in Physics Research, Section A: Accelerators, Spectrometers, Detectors and Associated Equipment **870** (2017) 103,
DOI: 10.1016/j.nima.2017.07.023.

[36] M. Kokole et al., *Magnetic characterization of the FEL-1 undulators for the FERMI at ELETTRA Free-Electron Laser*, Proceedings of FEL2010,
JACoW, Malmö, Sweden, 2010, THPC08.

[37] M. Kokole et al., *Magnetic characterization of the FEL-2 undulators for the FERMI at ELETTRA Free-Electron Laser*, Proceedings of IPAC2011, JACoW, San Sebastián, Spain, 2011, THPC170.

[38] D. E. Kim et al., *Undulator commissioning experience at PAL-XFEL*, Proceedings of IPAC2017, JACoW, Copenhagen, Denmark, 2017, TUPAB087, ISBN: 9783954501823.

[39] F. Wolff-Fabris et al., *Status of radiation damage on the European XFEL undulator systems*, Proceedings of IPAC2018, ed. by JACoW, Vancouver, Canada, 2018, WEYGBD2, ISBN: 9783954501847, DOI: 10.18429/JACoW-IPAC2018-WEYGBD2.

[40] H. Tarawneh et al., *Compact APPLE X for future SXL FEL and 3 GeV ring at MAX IV laboratory*, Proceedings of IPAC2019 (2019) TUPRB072, DOI: 10.18429/JACoW-IPAC2019-TUPRB072, URL: http://jacow.org/IPAC2018/papers/frzplm2.pdf.

[41] N. Strelnikov et al., *Vertically polarizing undulator with the dynamic compensation of magnetic forces for the next generation of light sources*, Review of Scientific Instruments **85** (2014) 113303, ISSN: 10897623, DOI: 10.1063/1.4900544.

[42] N. Strelnikov et al., *Performance of the 3.4 meter long vertical polarizing undulator prototype for LCLS-II*, Proceedings of NAPAC2016, JACoW, Chicago, USA, 2016, WEPOB23, ISBN: 9783954501809.

[43] F. Ciocci et al., *Segmented undulator operation at the SPARC-FEL test facility*, Proceedings of SPIE **9512** (2015) 951203, DOI: 10.1117/12.2185099.

[44] D. Alesini, *EuPRAXIA at SPARC_LAB Conceptual Design Report*, tech. rep., 2018, LNF, URL: http://www.lnf.infn.it/sis/preprint/pdf/getfile.php?filename=INFN-18-03-LNF.pdf.

[45] W. Gudat et al., *An undulator/multipole wiggler for the BESSY Storage Ring*, Nuclear Instruments and Methods in Physics Research Section A: Accelerators, Spectrometers, Detectors and Associated Equipment **246** (1986) 50, DOI: 10.1016/0168-9002(86)90043-4.

[46] S. Yamamoto et al., *Construction of an in-vacuum type undulator for production of undulator x rays in the 5-25 keV region*, Review of Scientific Instruments **63** (1992) 400, ISSN: 00346748, DOI: 10.1063/1.1142768.

[47] T. Tanaka et al., *In-vacuum undulators*, Proceedings of FEL2005, Stanford, California, USA, 2005, p. 370.

[48] T. Bizen et al., *Baking effect for NdFeB magnets against demagnetization induced by high-energy electrons*, Nuclear Instruments and Methods in Physics Research Section A: Accelerators, Spectrometers, Detectors and Associated Equipment **515** (2003) 850, ISSN: 01689002, DOI: 10.1016/j.nima.2003.07.030.

[49] T. Tanaka et al., *In-situ undulator field measurement with the SAFALI system*, Proceedings of FEL2007, JACoW, Novosibirsk, Russia, 2007, WHPPH052.

[50] T. Tanaka, T. Seike, H. Kitamura, *Measurement of SPring-8 XFEL undulator prototype with the SAFALI system*, Proceedings of FEL20082, JACoW, Gyeongju, Korea, 2008, TUPPH053.

[51] M. Calvi et al., *Magnetic assessment and modelling of the Aramis undulator beamline*, Journal of Synchrotron Radiation **25** (2018) 686, DOI: 10.1107/s1600577518002205.

[52] J. Campmany et al., *A New Bench Concept for Measuring Magnetic Fields of Big Closed Structure*, Physics Procedia **75** (2015) 1222, ISSN: 18753892, DOI: 10.1016/j.phpro.2015.12.124.

[53] T. Tanaka et al., *Undulator commissioning by characterization of radiation in x-ray free electron lasers*, Physical Review Special Topics - Accelerators and Beams **15** (2012) 110701, DOI: 10.1103/PhysRevSTAB.15.110701.

[54] T. Schmidt et al., *SwissFEL U15 prototype design and first results*, Proceedings of FEL2012, JACoW, Nara, Japan, 2012, THPD64, ISBN: 9783954501236.

[55] C. Yu et al., *First results of the IVU16 prototype undulator measurements*, Proceedings of IPAC2019, JACoW, Melbourne, Australia, 2019, TUPRB055, DOI: 10.18429/JACoW-IPAC2019-TUPRB055.

[56] T. Bizen et al., *Radiation-induced magnetization reversal causing a large flux loss in undulator permanent magnets*, Scientific Reports **6** (2016) 37937, DOI: 10.1038/srep37937.

[57] M. Calvi et al., *Swissfel U15 magnet assembly: first experimental results*, Proceedings of FEL2012, May, JACoW, Nara, Japan, 2012, THPD63, ISBN: 9783954501236.

[58] M. Dalli et al., *Development of a new magnetic measurement bench for in-vacuum undulators*, SN Applied Sciences **1** (2019) 704, ISSN: 2523-3963, DOI: 10.1007/s42452-019-0725-8, URL: http://link.springer.com/10.1007/s42452-019-0725-8.

[59] R. Kinjo et al., *Development of a magnet system to cancel the attractive force toward structual reform of undulators*, Proceedings of FEL2014, JACoW, Basel, Switzerland, 2014, MOP023, ISBN: 9783954501335.

[60] R. Kinjo et al., *Lightweight-compact variable-gap undulator with force cancellation system based on multipole monolithic magnets*, Review of Scientific Instruments **88** (2017), ISSN: 10897623, DOI: 10.1063/1.4991652.

[61] J. Bahrdt et al., *In-Vacuum APPLE II Undulator*, Proceedings of IPAC2018, JACoW Publishing, Vancouver, Canada, 2018, p. 4114, ISBN: 9783954501847, DOI: 10.18429/JACoW-IPAC2018-THPMF031, URL: https://accelconf.web.cern.ch/AccelConf/ipac2018/papers/thpmf031.pdf.

[62] J. Bahrdt, S. Grimmer, *In-vacuum APPLE II undulator with force compensation*, AIP Conference Proceedings **2054** (2019) 030031, ISSN: 15517616, DOI: 10.1063/1.5084594.

[63] M. E. Couprie, *Insertion device development for a broad range of radiation properties*, Journal of Physics: Conference Series **425** (2013) 032012, DOI: 10.1088/1742-6596/425/3/032012.

[64] M. Valleau et al., *Development of cryogenic permanent magnet undulators at SOLEIL*, Synchrotron Radiation News **31** (2018) 42, DOI: 10.1080/08940886.2018.1460175.

[65] C. Benabderrahmane et al., *Development of Pr2Fe14B cryogenic undulator CPMU at SOLEIL*, Proceedings of IPAC2011, JACoW, San Sebastián, Spain, 2011, THPC149.

[66] E. Longhi et al., *A new cooling system for cryocooled permanent magnet undulators at Diamond Light Source*, Proceedings of IPAC2014, JACoW, Dresden, Germany, 2014, WEPRO047, ISBN: 9783954501328, DOI: 10.18429/JACoW-IPAC2014-WEPRO047.

[67] J. Bahrdt, E. Gluskin, *Cryogenic permanent magnet and superconducting undulators*, Nuclear Instruments and Methods in Physics Research, Section A: Accelerators, Spectrometers, Detectors and Associated Equipment, Advances in Instrumentation and Experimental Methods (Special Issue in Honour of Kai Siegbahn) **907** (2018) 149, ISSN: 0168-9002, DOI: 10.1016/j.nima.2018.03.069.

[68] R. Kinjo, T. Bizen, T. Tanaka, *Undulator development for SPring-8-II*, Synchrotron Radiation News **28** (2015) 45.

[69] J.-C. Huang et al., *Development of a Cryogenic Permanent Magnet Undulator for the TPS*, Proceedings of IPAC2017, JACoW, Copenhagen, Denmark, 2017, TUPAB106, ISBN: 9783954501823.

[70] J. Chavanne et al., *Construction of a cryogenic permanent magnet undulator at the ESRF*, Proceedings of EPAC2008, JACoW, Genoa, Italy, 2008, WEPC105.

[71] J. Chavanne et al., *First operational experience with a cryogenic permanent magnet undulator at the ESRF*, Proceedings of PAC09, Vancouver, Canada, 2009, WE5RFP067.

[72] T. Tanaka et al., *In situ correction of field errors induced by temperature gradient in cryogenic undulators*, Physical Review Special Topics - Accelerators and Beams **12** (2009) 120702, DOI: 10.1103/physrevstab.12.120702.

[73] T. Tanaka et al., *In-situ magnetic correction for cryogenic undulators*, Proceedings of IPAC2010, JACoW, Kyoto, Japan, 2010, WEPD026.

[74] J. Schouten, E. Rial, *Electron beam heating and operation of the cryogenic undulator and superconducting wigglers at Diamond*, Proceedings of IPAC2011, JACoW, 2011, THPC179.

[75] C. Benabderrahmane et al., *Development and operation of a Pr2Fe14B based cryogenic permanent magnet undulator for a high spatial resolution x-ray beam line*, Physical Review Accelerators and Beams **20** (2017) 033201, DOI: 10.1103/PhysRevAccelBeams.20.033201.

[76] T. Tanaka et al., *Magnetic characterization for cryogenic permanent-magnet undulators: A first result*, Journal of Synchrotron Radiation **14** (2007) 416, ISSN: 09090495, DOI: 10.1107/S0909049507026507.

[77] G. Le Bec, *Overview of magnetic measurement activities at the ESRF*, presented at IMMW20, Didcot, UK, 2017, URL: http://www.diamond.ac.uk/Conference/dms/Conference/IMMW20/Presentations/G-LeBec/G%20LeBec.pdf.

[78] M. Valléau et al., *Construction and optimization of cryogenic undulators at SOLEIL*, Proceedings of FLS2018, JACoW, Shanghai, China, 2018, THP2WD01, ISBN: 9783954502066, DOI: 10.18429/JACoW-FLS2018-THP2WD01.

[79] C. Kuhn et al., *Hall-probe bench for cryogenic in-vacuum-undulators*, Proceedings of IPAC2013, JACoW, Shanghai, China, 2013, WEPWA003, ISBN: 9783954501229.

[80] C. W. Ostenfeld, M. Pedersen, *Cryogenic in-vacuum undulator at Danfysik*, Proceedings of IPAC 2010, JACoW, Kyoto, Japan, 2010, WEPD006, ISBN: 9789290833529.

[81] J. Chavanne et al., *Recent developments in Insertion Devices at the ESRF: working toward diffraction-limited Storage Rings*, Synchrotron Radiation News **28** (2015) 15.

[82] Y. He et al., *Cryogenic permanent magnet undulator of SSRF*, Proceedings of IPAC2018, JACoW, Vancouver, Canada, 2018, THPMK066, ISBN: 9783954501847, DOI: 10.18429/JACoW-IPAC2018-THPMK066.

[83] J. Bahrdt et al., *Status of the cryogenic undulator CPMU-17 for EMILAT BESSY II/HZB*, Proceedings of IPAC2017, JACoW, Copenhagen, Denmark, 2017, TUPAB026, ISBN: 9783954501823.

[84] Z. Patel et al., *Insertion Devices at Diamond Light Source: a retrospective plus future developments*, Proceedings of IPAC2017, JACoW, Copenhagen, Denmark, 2017, TUPAB116, ISBN: 9783954501823.

[85] C. Kuhn et al., *Development of advanced magnet structures for cryogenic in vacuum permanent magnet undulators*, Proceedings of IPAC2014, JACoW, Dresden, Germany, 2014, WEPRO029, ISBN: 9783954501328, DOI: 10.18429/JACoW-IPAC2014-WEPRO029.

[86] J. Bahrdt, C. Kuhn, *Cryogenic Permanent Magnet Undulator Development at HZB/BESSY II*, Synchrotron Radiation News **28** (2015) 9, DOI: 10.1080/08940886.2015.1037673.

[87] F. O'Shea et al., *Development of a short period cryogenic undulator at RadiaBeam*, Proceedings of NAPAC2016, JACoW, Chicago, USA, 2016, WEPOB47, ISBN: 9783954501809.

[88] P. Elleaume, O. Chubar, J. Chavanne, *Computing 3D magnetic fields from insertion devices*, Proceedings of PAC97, Vancouver, Canada, 1997, p. 3509, ISBN: 078034376X, DOI: 10.1109/pac.1997.753258.

[89] O. Chubar, P. Elleaume, J. Chavanne, *A three-dimensional magnetostatics computer code for insertion devices*, Journal of Synchrotron Radiation **5** (1998) 481, ISSN: 0909-0495, DOI: 10.1107/s0909049597013502.

[90] P. Elleaume, J. Chavanne, B. Faatz, *Design considerations for a 1 angstrom SASE undulator*, Nuclear Instruments and Methods in Physics Research, Section A: Accelerators, Spectrometers, Detectors and Associated Equipment **455** (2000) 503, ISSN: 01689002, DOI: 10.1016/S0168-9002(00)00544-1.

[91] C. Bocchetta, A. Abrami, E. Allaria, *Fermi at Elettra, Conceptual Design Report*, tech. rep., 2007, URL: https://www.elettra.trieste.it/it/lightsources/fermi/fermi-machine/fermicdr.html.

[92] J. A. Clarke, *The Science and Technology of Undulators and Wigglers*, Oxford University Press, 2004, DOI: 10.1093/acprof:oso/9780198508557.001.0001.

[93] R. Dejus, M. Jaski, S. Kim, *On-Axis Brilliance and Power of In-Vacuum Undulators for the Advanced Photon Source*, tech. rep., 2009.

[94] L. R. Elias et al., *Observation of Stimulated Emission of Radiation by Relativistic Electrons in a Spatially Periodic Transverse Magnetic Field*, Physical Review Letters **36** (1976) 717, ISSN: 0031-9007, DOI: 10.1103/PhysRevLett.36.717, URL: https://link.aps.org/doi/10.1103/PhysRevLett.36.717.

[95] L. R. Elias, J. M. Madey, *Superconducting Helically Wound Magnet for the Free-electron Laser*, Review of Scientific Instruments **50** (1979) 1335, ISSN: 0034-6748, DOI: 10.1063/1.1135721.

[96] M. Bazin et al., *Design of an Undulator for A.C.O. and Its Possible Use as Free Electron La Ser*, Nuclear Instruments and Methods **172** (1980) 61, ISSN: 0029-554X, DOI: 10.1016/0029-554X(80)90608-4.

[97] C. Bazin et al., *First Results of a Superconducting Undulator on the ACO Storage Ring*, en, Journal de Physique Lettres **41** (1980) 547, ISSN: 0302-072X, DOI: 10.1051/jphyslet:01980004102305470O.

[98] L. M. Barkov et al., *A Proposal to Install a Superconducting Wiggler Magnet on the Storage Ring VEPP-3 for Generation of the Synchrotron Radiation*, Nuclear Instruments and Methods **152** (1978) 23.

[99] A. S. Artamonov et al., *The First Experiments with an Optical Klystron Installed on the VEPP-3 Storage Ring*, Nuclear Instruments and Methods **177** (1980) 247, ISSN: 0029-554X, DOI: 10.1016/0029-554X(80)90557-1.

[100] N. A. Mezentsev, E. A. Perevedentsev, *Survey of Superconducting Insertion Devices for Light Sources*, Proceedings of the 2005 Particle Accelerator Conference, 2005, p. 256, DOI: 10.1109/PAC.2005.1590409.

[101] N. Mezentsev, E. Wallen, *Superconducting Wigglers*, Synchrotron Radiation News **24** (2011) 3, ISSN: 0894-0886, DOI: 10.1080/08940886.2011.583883.

[102] Y. Ivanyushenkov et al., *Development and operating experience of a short-period superconducting undulator at the Advanced Photon Source*, Physical Review Special Topics - Accelerators and Beams **18** (2015) 1, ISSN: 10984402, DOI: 10.1103/PhysRevSTAB.18.040703.

[103] Y. Ivanyushenkov et al., *Development and operating experience of a 1.1m long superconducting undulator at the Advanced Photon Source*, Phys. Rev. Accel. Beams **20** (2017) 100701, DOI: 10.1103/PhysRevAccelBeams.20.100701.

[104] S. Casalbuoni et al., *Performance of a Full Scale Superconducting Undulator with 20 mm Period Length at the KIT Synchrotron*, Proceedings, 9th International Particle Accelerator Conference (IPAC 2018): Vancouver, BC Canada, 2018, THPMF066, DOI: 10.18429/JACoW-IPAC2018-THPMF066.

[105] S. Casalbuoni et al., *Characterization and long term operation of a novel superconducting undulator with 15 mm period length in a synchrotron light source*, Phys. Rev. Accel. Beams **19** (2016) 110702, DOI: 10.1103/PhysRevAccelBeams.19.110702.

[106] P. Emma et al., *A plan for the development of superconducting Undulator prototypes for LCLS-II and future FELs*, en, Proceedings of the 36th International Free Electron Laser Conference, FEL 2014 (2014) 649.

[107] A. V. Bragin et al., *Test Results of the CLIC Damping Wiggler Prototype*, IEEE Transactions on Applied Superconductivity **26** (2016), ISSN: 10518223, DOI: 10.1109/TASC.2016.2516341.

[108] D. Potratz et al., *A helium thermosiphon cooling loop for the APS superconducting undulator*, AIP Conference Proceedings, American Institute of Physics, 2012, p. 1991, DOI: 10.1063/1.4707139, URL: http://aip.scitation.org/doi/abs/10.1063/1.4707139.

[109] J. Fuerst et al.,
A second-generation superconducting undulator cryostat for the APS, en,
IOP Conference Series: Materials Science and Engineering, vol. 278, 1, 2017,
p. 12176, DOI: 10.1088/1757-899X/278/1/012176,
URL: http://stacks.iop.org/1757-899X/278/i=1/a=012176?key=crossref.4933205765a9fd53aaa62eeed3203cf3.

[110] E. A. Bekhtenev et al., *A multipole superconducting wiggler for Canadian light source*,
Physics of Particles and Nuclei Letters **3** (2006) S16, ISSN: 1531-8567,
DOI: 10.1134/S1547477106070041,
URL: https://doi.org/10.1134/S1547477106070041.

[111] C. Boffo et al., *Development of the Next Generation Superconductive Undulators for Synchrotron Light Sources*,
IEEE Transactions on Applied Superconductivity **19** (2009) 1324, ISSN: 1051-8223,
DOI: 10.1109/TASC.2009.2018515.

[112] C. Boffo et al., *Performance of SCU15: The New Conduction-Cooled Superconducting Undulator for ANKA*, IEEE Transactions on Applied Superconductivity **26** (2016) 1,
ISSN: 10518223, DOI: 10.1109/TASC.2016.2535861,
URL: http://ieeexplore.ieee.org/document/7422030/.

[113] Y. Ivanyushenkov et al.,
A design concept for a planar superconducting undulator for the APS,
IEEE Transactions on Applied Superconductivity **21** (2011) 1717, ISSN: 10518223,
DOI: 10.1109/TASC.2010.2086412,
URL: http://ieeexplore.ieee.org/document/5643144/.

[114] J. D. Fuerst et al.,
Review of New Developments in Superconducting Undulator Technology at the APS,
Proc. 60th ICFA Advanced Beam Dynamics Workshop (FLS'18), Shanghai, China,
JACoW Publishing, Geneva, Switzerland, 2018,
DOI: https://doi.org/10.18429/JACoW-FLS2018-MOA2PL03,
URL: http://jacow.org/fls2018/papers/moa2pl03.pdf.

[115] A. Bernhard et al., *A CLIC damping wiggler prototype at anka: Commissioning and preparations for a beam dynamics experimental program*,
IPAC 2016 - Proceedings of the 7th International Particle Accelerator Conference,
2016, WEPMW002, ISBN: 9783954501472,
DOI: 10.18429/JACOW-IPAC2016-WEPMW002,
URL: http://inspirehep.net/record/1470215/?ln=de.

[116] S. Casalbuoni et al.,
Superconducting Undulators: From Development towards a Commercial Product,
Synchrotron Radiation News **31** (2018) 24, ISSN: 0894-0886,
DOI: 10.1080/08940886.2018.1460171.

[117] Y. Ivanyushenkov et al., *Status of the Development of Superconducting Undulators at the Advanced Photon Source*, Synchrotron Radiation News **31** (2018) 29,
ISSN: 0894-0886, DOI: 10.1080/08940886.2018.1460172.

[118] J. A. Clarke, *Optimisation of Superconducting Undulators for X-Ray FELs*, English,
Geneva, Switzerland, 2018.

[119] D. Schoerling, *Superconducting wiggler magnets for beam-emittance damping rings* (2012), URL: http://cds.cern.ch/record/1435176.

[120] S. V. Khrushchev et al., *The Research of the Superconducting Undulator Prototype with Neutral Poles and Features of the Magnetic Field Distribution in It*, Physics Procedia, Proceedings of the International Conference "Synchrotron and Free Electron Laser Radiation: Generation and Application" (SFR-2016), July 4 - 7, 2016, Novosibirsk, Russia **84** (2016) 62, ISSN: 1875-3892, DOI: 10.1016/j.phpro.2016.11.011.

[121] N. A. Vinokurov, *Insertion Device Development at Novosibirsk*, Nuclear Instruments and Methods in Physics Research Section A: Accelerators, Spectrometers, Detectors and Associated Equipment **246** (1986) 105, ISSN: 0168-9002, DOI: 10.1016/0168-9002(86)90055-0.

[122] D. J. Scott et al., *Demonstration of a High-Field Short-Period Superconducting Helical Undulator Suitable for Future TeV-Scale Linear Collider Positron Sources*, Physical Review Letters **107** (2011) 174803, ISSN: 0031-9007, DOI: 10.1103/PhysRevLett.107.174803, URL: https://link.aps.org/doi/10.1103/PhysRevLett.107.174803.

[123] Y. Ivanyushenkov et al., *Status of the Development of Superconducting Undulators for Storage Rings and Free Electron Lasers at the Advanced Photon Source*, Proceedings, 2nd North American Particle Accelerator Conference (NAPAC2016): Chicago, Illinois, USA, October 9-14, 2016, 2017, THA1CO06, DOI: 10.18429/JACoW-NAPAC2016-THA1CO06.

[124] M. Kasa et al., *Design, Construction, and Magnetic Field Measurements of a Helical Superconducting Undulator for the Advanced Photon Source*, Proc. 9th International Particle Accelerator Conference (IPAC'18), Vancouver, BC, Canada, April 29-May 4, 2018, International Particle Accelerator Conference 9, JACoW Publishing, Geneva, Switzerland, 2018, p. 1263, ISBN: 978-3-95450-184-7, DOI: doi:10.18429/JACoW-IPAC2018-TUPMF008, URL: http://jacow.org/ipac2018/papers/tupmf008.pdf.

[125] Y. Ivanyushenkov et al., *Status of the Development of Superconducting Undulators at the Advanced Photon Source*, Proceedings, 8th International Particle Accelerator Conference (IPAC 2017): Copenhagen, Denmark, May 14-19, 2017, 2017, WEOCA3, DOI: 10.18429/JACoW-IPAC2017-WEOCA3.

[126] A. Bernhard et al., *Spectral Characterisation of the ANKA-SCU Radiation*, Particle accelerator. Proceedings, 23rd Conference, PAC'09, Vancouver, Canada, May 4-8, 2009, 2010, WE5RFP084, URL: http://accelconf.web.cern.ch/AccelConf/PAC2009/papers/we5rfp084.pdf.

[127] J. Bahrdt, Y. Ivanyushenkov, *Short Period Undulators for Storage Rings and Free Electron Lasers*, Journal of Physics: Conference Series **425** (2013) 032001, ISSN: 1742-6588, DOI: 10.1088/1742-6596/425/3/032001, URL: http://stacks.iop.org/1742-6596/425/i=3/a=032001?key=crossref.f795b55a4ac7a612e20098d8ae11d11e.

[128] K. Batchelor et al.,
Status of the visible free-electron laser at the Brookhaven accelerator test facility,
Nuclear Instruments and Methods in Physics Research Section A: Accelerators, Spectrometers, Detectors and Associated Equipment **318** (1992) 159,
ISSN: 0168-9002,
DOI: https://doi.org/10.1016/0168-9002(92)91043-9,
URL: http://www.sciencedirect.com/science/article/pii/0168900292910439.

[129] Bilfinger Noell GmbH, *Superconducting Undulator Wiggler SCUW*, 2019,
URL: https://www.noell.bilfinger.com/en/business-segments/magnet-technologies/insertion-devices-undulators-and-wigglers/superconducting-undulator-wiggler-scuw/.

[130] S. Casalbuoni et al., *Magnetic Field Measurements of Full-Scale Conduction-Cooled Superconducting-Undulator-Coils*,
IEEE Transactions on Applied Superconductivity **28** (2018) 1, ISSN: 1051-8223,
DOI: 10.1109/TASC.2018.2791953.

[131] A. V. Zlobin et al.,
Advantages and Challenges of Nb3Sn Superconducting Undulators,
Proc. 9th International Particle Accelerator Conference (IPAC'18), Vancouver, BC, Canada, April 29-May 4, 2018, International Particle Accelerator Conference 9, JACoW Publishing, Geneva, Switzerland, 2018, p. 2734, ISBN: 978-3-95450-184-7,
DOI: doi:10.18429/JACoW-IPAC2018-WEPML025,
URL: http://jacow.org/ipac2018/papers/wepml025.pdf.

[132] S. O. Prestemon et al.,
Design, fabrication, and test results of undulators using Nb3Sn superconductor,
IEEE Transactions on Applied Superconductivity **15** (2005) 1236, ISSN: 1051-8223,
DOI: 10.1109/TASC.2005.849540.

[133] L. Garcia Fajardo et al., *Design of Nb3Sn Wiggler Magnets for the Compact Linear Collider and Manufacturing of a Five-Coil Prototype*,
IEEE Transactions on Applied Superconductivity **26** (2016), ISSN: 10518223,
DOI: 10.1109/TASC.2016.2517938.

[134] I. Kesgin et al.,
Development of short-period Nb3Sn superconducting planar undulators,
IEEE Transactions on Applied Superconductivity **29** (2019) 1, ISSN: 15582515,
DOI: 10.1109/TASC.2019.2897645.

[135] Y. Ivanyushenkov et al., *Development Status of a Magnetic Measurement System for the APS Superconducting Undulator*, en,
Proceedings of 2011 Particle Accelerator Conference, New York, NY, USA, 2011, p. 3.

[136] S. Casalbuoni, *A Review of Magnetic Field Measurements of Full Scale Conduction Cooled Superconducting Undulator Coils*, en,
Superconductor Science and Technology **32** (2018) 23001, ISSN: 0953-2048,
DOI: 10.1088/1361-6668/aaf27f.

[137] X. Xu, *A review and prospects for Nb3Sn superconductor development*, Superconductor Science and Technology **30** (2017) 093001, ISSN: 0953-2048, DOI: 10.1088/1361-6668/aa7976, URL: http://stacks.iop.org/0953-2048/30/i=9/a=093001?key=crossref.8f6a543a56839943e603c55cf6eb105c.

[138] T. Boutboul et al., *Heat Treatment Optimization Studies on PIT Nb3Sn Strand for the NED Project*, IEEE Transactions on Applied Superconductivity **19** (2009) 2564, ISSN: 1051-8223, DOI: 10.1109/TASC.2009.2019017.

[139] C. V. Renaud, T. Wong, L. R. Motowidlo, *ITT Nb3Sn processing and properties*, IEEE Transactions on Applied Superconductivity **15** (2005) 3418, ISSN: 1051-8223, DOI: 10.1109/TASC.2005.848951.

[140] P. Emma et al., *Electron Beam Collimation for the Next Generation Light Source*, Conf. Proc. **C1205201** (2012) 1695.

[141] R. Flükiger, *IRRADIATION EFFECTS IN LOW T C SUPERCONDUCTORS*, tech. rep., 2009, DOI: 10.5170/CERN-2009-001.55, URL: http://cds.cern.ch/record/1163716%20http://cds.cern.ch/record/1163716/files/p55.pdf.

[142] E. Rochepault et al., *Error analysis and field correction methods in superconducting undulators*, IEEE Transactions on Applied Superconductivity **24** (2014) 1, ISSN: 10518223, DOI: 10.1109/TASC.2013.2285095.

[143] D. Arbelaez et al., *Magnetic Field Correction Methods for Hybrid Permanent Magnet and Superconducting Undulators*, Synchrotron Radiation News **31** (2018) 9, ISSN: 0894-0886, DOI: 10.1080/08940886.2018.1460168.

[144] M. Duda et al., *Power test of the Second-Generation Compact Linear Collider (CLIC) Nb 3 Sn damping wiggler short model*, IEEE Transactions on Applied Superconductivity (2019), ISSN: 15582515, DOI: 10.1109/TASC.2019.2896774.

[145] D. Schoerling et al., *Design and system integration of the superconducting wiggler magnets for the Compact Linear Collider damping rings*, Physical Review Special Topics - Accelerators and Beams (2012), ISSN: 10984402, DOI: 10.1103/PhysRevSTAB.15.042401.

[146] S. H. Kim, *A scaling law for the magnetic fields of superconducting undulators*, Nuclear Instruments and Methods in Physics Research, Section A: Accelerators, Spectrometers, Detectors and Associated Equipment **546** (2005) 604, ISSN: 01689002, DOI: 10.1016/j.nima.2005.03.150.

[147] Cobham Technical Services, *Opera (2d/3d) Vector Fields Software*, Oxford, UK, 2018.

[148] A. Mak et al., *Undulator Considerations in the Baseline Design of the MAX IV Soft X-Ray Laser*, tech. rep., DEPARTMENT OF PHYSICS and ASTRONOMY UPPSALA UNIVERSITY, 2018, URL: http://uu.diva-portal.org.

[149] M. K. Wu et al., *Superconductivity at 93 K in a new mixed-phase Y-Ba-Cu-O compound system at ambient pressure*, Physical Review Letters **58** (1987) 908, ISSN: 0031-9007, DOI: 10.1103/PhysRevLett.58.908, URL: https://link.aps.org/doi/10.1103/PhysRevLett.58.908.

[150] D. C. Larbalestier et al., *Isotropic round-wire multifilament cuprate superconductor for generation of magnetic fields above 30 T*, Nature Materials **13** (2014) 375, ISSN: 1476-1122, DOI: 10.1038/nmat3887, URL: http://www.nature.com/articles/nmat3887.

[151] J. van Nugteren, *High temperature superconductor accelerator magnets*, PhD thesis, 2016, ISBN: 981-02-3361-2, URL: http://cds.cern.ch/record/2228249.

[152] A. Golovashkin et al., *Low temperature direct measurements of Hc2 in HTSC using megagauss magnetic fields*, Physica C: Superconductivity **185-189** (1991) 1859, ISSN: 09214534, DOI: 10.1016/0921-4534(91)91055-9, URL: https://linkinghub.elsevier.com/retrieve/pii/0921453491910559.

[153] H. W. Weijers et al., *High Field Magnets With HTS Conductors*, IEEE Transactions on Applied Superconductivity **20** (2010) 576, ISSN: 1051-8223, DOI: 10.1109/TASC.2010.2043080, URL: http://ieeexplore.ieee.org/document/5433303/.

[154] J. van Nugteren et al., *Powering of an HTS dipole insert-magnet operated standalone in helium gas between 5 and 85 K*, Superconductor Science and Technology (2018), ISSN: 0953-2048, DOI: 10.1088/1361-6668/aab887, URL: https://doi.org/10.1088/1361-6668/aab887%0Ahttp://iopscience.iop.org/article/10.1088/1361-6668/aab887.

[155] P. Ferracin et al., *Development of the EuCARD Nb3Sn Dipole Magnet FRESCA2*, IEEE Transactions on Applied Superconductivity **23** (2013) 4002005, ISSN: 1051-8223, DOI: 10.1109/TASC.2013.2243799, URL: http://ieeexplore.ieee.org/document/6423253/.

[156] G. Willering et al., *Cold Powering Tests and Protection Studies of the FRESCA2 100 mm Bore Nb3Sn Block-Coil Magnet*, IEEE Transactions on Applied Superconductivity **28** (2018) 1, ISSN: 1051-8223, DOI: 10.1109/TASC.2018.2797907, URL: http://ieeexplore.ieee.org/document/8269388/.

[157] S. H. Kim et al., *Feasibility of a short-period superconducting undulator using 2G HTS tapes*, IEEE Transactions on Applied Superconductivity **21** (2011) 1709, ISSN: 10518223, DOI: 10.1109/TASC.2010.2089030.

[158] S. Prestemon et al., *Development and Analysis of HTS-Undulator Components for FEL Applications*, IEEE Transactions on Applied Superconductivity **21** (2011) 1880, ISSN: 1051-8223, DOI: 10.1109/TASC.2010.2098014, URL: http://ieeexplore.ieee.org/document/5682365/.

[159] T. Holubek et al., *A novel concept of high temperature superconducting undulator*, Superconductor Science and Technology **30** (2017) 115002, ISSN: 0953-2048, DOI: 10.1088/1361-6668/aa87f1, URL: http://stacks.iop.org/0953-2048/30/i=11/a=115002?key=crossref.a88369c98b5ecb4a1540b9a529e20776.

[160] I. Kesgin et al., *Feasibility and electromagnetic analysis of a REBCO superconducting undulator*, Superconductor Science and Technology **29** (2016) 055001, ISSN: 0953-2048, DOI: 10.1088/0953-2048/29/5/055001, URL: http://stacks.iop.org/0953-2048/29/i=5/a=055001?key=crossref.2643db3ea8bbb282588a3481ca6db109.

[161] I. Kesgin et al., *High-temperature superconducting undulator magnets*, Superconductor Science and Technology **30** (2017) 1, ISSN: 13616668, DOI: 10.1088/1361-6668/aa5d48, URL: http://dx.doi.org/10.1088/1361-6668/aa5d48.

[162] Y. H. Choi et al., *Partial insulation of GdBCO single pancake coils for protection-free HTS power applications*, Superconductor Science and Technology **24** (2011) 125013, ISSN: 0953-2048, DOI: 10.1088/0953-2048/24/12/125013, URL: http://stacks.iop.org/0953-2048/24/i=12/a=125013?key=crossref.4d8c3a9b7d093aa457e464ebe154ef8f.

[163] S. Hahn et al., *HTS Pancake Coils Without Turn-to-Turn Insulation*, IEEE Transactions on Applied Superconductivity **21** (2011) 1592, ISSN: 1051-8223, DOI: 10.1109/TASC.2010.2093492, URL: http://ieeexplore.ieee.org/document/5675711/.

[164] G. Brittles, R. Bateman, *Stability and quench - dynamic behaviour of Tokamak Energy REBCO QA coils*, Talks at WAMHTS, Budapest, Budapest, 2019, URL: https://indico.cern.ch/event/775529/contributions/3334053/attachments/1829923/3003215/20190412_GB_Stability_and_quench_dynamic_behaviour_of_Tokamak_Energy_REBCO_QA_coils_Indico.pdf.

[165] S. Otten et al., *Bending properties of different REBCO coated conductor tapes and Roebel cables at T = 77 K*, Superconductor Science and Technology **29** (2016), ISSN: 13616668, DOI: 10.1088/0953-2048/29/12/125003.

[166] J. Fleiter, A. Ballarino, *In-Field Electrical Resistance at 4.2 K of REBCO Splices*, IEEE Transactions on Applied Superconductivity **27** (2017) 1, ISSN: 10518223, DOI: 10.1109/TASC.2017.2659618.

[167] G. Majkic et al., *Over 15 MA/cm2 of critical current density in 4.8 um thick, Zr-doped (Gd,Y)Ba2Cu3Ox superconductor at 30 K, 3T*, Scientific Reports **8** (2018) 6982, ISSN: 2045-2322, DOI: 10.1038/s41598-018-25499-1, URL: http://www.nature.com/articles/s41598-018-25499-1.

[168] K. Matsumoto et al., *Flux Pinning Characteristics of Artificial Pinning Centers With Different Dimension*, IEEE Transactions on Applied Superconductivity **19** (2009) 3248, ISSN: 1051-8223, DOI: 10.1109/TASC.2009.2018186, URL: http://ieeexplore.ieee.org/document/5153240/.

[169] V. Selvamanickam et al.,
High critical currents in heavily doped (Gd,Y)Ba2Cu3Ox superconductor tapes,
Applied Physics Letters **106** (2015) 032601, ISSN: 0003-6951,
DOI: 10.1063/1.4906205,
URL: http://aip.scitation.org/doi/10.1063/1.4906205.

[170] A. Sundaram et al., *2G HTS wires made on 30 µm thick Hastelloy substrate*,
Superconductor Science and Technology **29** (2016), ISSN: 13616668,
DOI: 10.1088/0953-2048/29/10/104007.

[171] F. Trillaud et al.,
Normal zone propagation experiments on HTS composite conductors,
Cryogenics **43** (2003) 271, ISSN: 00112275,
DOI: 10.1016/S0011-2275(03)00044-4, URL: https://linkinghub.elsevier.com/retrieve/pii/S0011227503000444.

[172] W. K. Chan, G. Flanagan, J. Schwartz,
Spatial and temporal resolution requirements for quench detection in (RE)Ba 2 Cu 3 O x magnets using Rayleigh-scattering-based fiber optic distributed sensing,
Superconductor Science and Technology **26** (2013) 105015, ISSN: 0953-2048,
DOI: 10.1088/0953-2048/26/10/105015,
URL: http://stacks.iop.org/0953-2048/26/i=10/a=105015?key=crossref.d81dfb54ccb0f42ca222f8c1991027da.

[173] M. Marchevsky et al.,
Acoustic emission during quench training of superconducting accelerator magnets,
Cryogenics **69** (2015) 50, ISSN: 00112275,
DOI: 10.1016/j.cryogenics.2015.03.005, URL: https://linkinghub.elsevier.com/retrieve/pii/S0011227515000399.

[174] M. Marchevsky, S. A. Gourlay, *Acoustic thermometry for detecting quenches in superconducting coils and conductor stacks*,
Applied Physics Letters **110** (2017) 012601, ISSN: 0003-6951,
DOI: 10.1063/1.4973466,
URL: http://aip.scitation.org/doi/10.1063/1.4973466.

[175] P. D. Noyes et al., *Protection Heater Development for REBCO Coils*,
IEEE Transactions on Applied Superconductivity **22** (2012) 4704204,
ISSN: 1051-8223, DOI: 10.1109/TASC.2012.2188370,
URL: http://ieeexplore.ieee.org/document/6153351/.

[176] D. Zola et al., *A study of coupling loss on bi-columnar BSCCO/Ag tapes through ac susceptibility measurements*,
Superconductor Science and Technology **17** (2004) 501, ISSN: 0953-2048,
DOI: 10.1088/0953-2048/17/3/033,
URL: http://stacks.iop.org/0953-2048/17/i=3/a=033?key=crossref.50bc89b6a9eb46c1ce5477ae322fa898.

[177] Y. C. Huang et al., *Compact far-IR FEL design*,
Nuclear Inst. and Methods in Physics Research, A (1992), ISSN: 01689002,
DOI: 10.1016/0168-9002(92)91155-3.

[178] R. Kinjo et al., *Demonstration of a High-Field Short-Period Undulator Using Bulk High-Temperature Superconductor*, Applied Physics Express **6** (2013) 042701, ISSN: 1882-0778, DOI: 10.7567/APEX.6.042701, URL: http://stacks.iop.org/1882-0786/6/i=4/a=042701?key=crossref.20dd9f4814c0b9436e9da1aca46b2adc.

[179] J. H. Durrell et al., *A trapped field of 17.6 T in melt-processed, bulk Gd-Ba-Cu-O reinforced with shrink-fit steel*, Superconductor Science and Technology **27** (2014) 082001, ISSN: 0953-2048, DOI: 10.1088/0953-2048/27/8/082001, URL: http://stacks.iop.org/0953-2048/27/i=8/a=082001?key=crossref.7a914bde4498f1b1db54d83680d3c2e3.

[180] J. H. Durrell et al., *Bulk superconductors: a roadmap to applications*, Superconductor Science and Technology **31** (2018) 103501, ISSN: 0953-2048, DOI: 10.1088/1361-6668/aad7ce, URL: http://stacks.iop.org/0953-2048/31/i=10/a=103501?key=crossref.d1e9903b49b59a09b9ddeb229b8884df.

[181] Y. Acremann et al., *Time-resolved imaging of spin transfer switching: Beyond the macrospin concept*, Physical Review Letters (2006), ISSN: 00319007, DOI: 10.1103/PhysRevLett.96.217202.

[182] T. Shintake et al., *Microwave undulator*, Japanese Journal of Applied Physics (1982), ISSN: 13474065, DOI: 10.1143/JJAP.21.L601.

[183] T. Shintake et al., *Development of Microwave Undulator*, Japanese Journal of Applied Physics **22** (1983) 844, ISSN: 0021-4922, DOI: 10.1143/JJAP.22.844, URL: http://stacks.iop.org/1347-4065/22/844.

[184] S. Tantawi et al., *Experimental demonstration of a tunable microwave undulator*, Physical Review Letters (2014), ISSN: 10797114, DOI: 10.1103/PhysRevLett.112.164802.

[185] C. Pellegrini, *X-band microwave undulators for short wavelength free-electron lasers*, AIP Conference Proceedings **807** (2006) 30, ISSN: 0094243X, DOI: 10.1063/1.2158757.

[186] R. A. Alvarez, *Some properties of microwave resonant cavities relevant to pulse-compression power amplification*, Review of Scientific Instruments **57** (1986) 2481, ISSN: 00346748, DOI: 10.1063/1.1139097.

[187] C. Chang et al., *Electron dynamics and transverse-kick elimination in a high-field short-period helical microwave undulator*, Applied Physics Letters **101** (2012), ISSN: 00036951, DOI: 10.1063/1.4759002.

[188] G. B. Bowden et al., *Application of the Balanced Hybrid Mode in Overmoded Corrugated Waveguides to Short Wavelength Dynamic Undulators*, Particle accelerator. Proceedings, 2nd International Conference, IPAC 2011, San Sebastian, Spain, 2011, p. 3328.

[189] F. Toufexis, S. G. Tantawi, M. Park, *A 1.75 mm PERIOD RF-DRIVEN UNDULATOR* () 1.

[190] J. M. Neilson et al., *Determination of the Resonant Frequencies in a Complex Cavity Using the Scattering Matrix Formulation*, IEEE Transactions on Microwave Theory and Techniques **37** (1989) 1165, ISSN: 15579670, DOI: 10.1109/22.31074.

[191] L. Zhang et al., *Bandwidth Study of the Microwave Reflectors with Rectangular Corrugations*, Journal of Infrared, Millimeter, and Terahertz Waves **37** (2016), ISSN: 18666906, DOI: 10.1007/s10762-016-0280-y.

[192] J. P. Crenn, C. Charollais, *Propagation and radiation characteristics of the circular electric, circular magnetic and hybrid waveguide modes*, International Journal of Infrared and Millimeter Waves (1996), ISSN: 01959271, DOI: 10.1007/BF02088503.

[193] P. J. Clarricoats, A. D. Olver, *Corrugated Horns for Microwave Antennas*, IET, The Institution of Engineering and Technology, Michael Faraday House, Six Hills Way, Stevenage SG1 2AY, UK, 1984, ISBN: 9780863410031, DOI: 10.1049/PBEW018E, URL: https://digital-library.theiet.org/content/books/ew/pbew018e.

[194] L. Zhang et al., *Systematic study of a corrugated waveguide as a microwave undulator*, Journal of Synchrotron Radiation **26** (2019) 11, DOI: 10.1107/s1600577518014297.

[195] A. M. Gaponenko et al., *LENGTHENING OF MICROWAVE PULSE IN A 3-GW RELATIVISTIC BW01*, 2000 13th International Conference on High-Power Particle Beams (2000) 730.

[196] V. V. Rostov et al., *Superradiant Ka-band Cherenkov oscillator with 2-GW peak power*, Physics of Plasmas **23** (2016), ISSN: 10897674, DOI: 10.1063/1.4962189.

[197] N. S. Ginzburg et al., *Generation of Electromagnetic Fields of Extremely High Intensity by Coherent Summation of Cherenkov Superradiance Pulses*, Physical Review Letters **115** (2015) 1, ISSN: 10797114, DOI: 10.1103/PhysRevLett.115.114802.

[198] S. V. Kuzikov et al., *Configurations for short period rf undulators*, Physical Review Special Topics - Accelerators and Beams **16** (2013) 1, ISSN: 10984402, DOI: 10.1103/PhysRevSTAB.16.070701.

[199] L. Zhang et al., *Microwave Undulator Using a Helically Corrugated Waveguide*, IEEE Transactions on Electron Devices **65** (2018) 5499, ISSN: 00189383, DOI: 10.1109/TED.2018.2873726.

[200] P. Dobiasch, P. Meystre, M. O. Scully, *Optical Wiggler Free-Electron X-Ray Laser in the 5A Region*, IEEE Journal of Quantum Electronics (1983), ISSN: 15581713, DOI: 10.1109/JQE.1983.1071798.

[201] F. Ciocci, G. Dattoli, J. E. Walsh, *A short note on the wave-undulator FEL operation*, Nuclear Inst. and Methods in Physics Research, A (1985), ISSN: 01689002, DOI: 10.1016/0168-9002(85)90378-X.

[202] J. Gea-Banacloche et al., *Soft X-Ray Free-Electron Laser with a Laser Undulator*, IEEE Journal of Quantum Electronics (1987), ISSN: 15581713, DOI: 10.1109/JQE.1987.1073559.

[203] Y. Y. Lau et al., *Nonlinear Thomson scattering: A tutorial*, Physics of Plasmas (2003), ISSN: 1070-664X, DOI: 10.1063/1.1565115.

[204] A. Bacci et al., *Transverse effects in the production of x rays with a free-electron laser based on an optical undulator*, Physical Review Special Topics - Accelerators and Beams (2006), ISSN: 10984402, DOI: 10.1103/PhysRevSTAB.9.060704.

[205] G. Dattoli, V. Petrillo, J. V. Rau, *FEL SASE and wave undulators*, Optics Communications **285** (2012) 5341, ISSN: 00304018, DOI: 10.1016/j.optcom.2012.07.128.

[206] A. Curcio et al., *An optical cavity design for a compact wave-undulator based-FEL*, Optics Communications **405** (2017), ISSN: 00304018, DOI: 10.1016/j.optcom.2017.08.029.

[207] S. Reiche, *GENESIS 1.3: a fully 3D time-dependent FEL simulation code*, Nuclear Instruments and Methods in Physics Research Section A: Accelerators, Spectrometers, Detectors and Associated Equipment **429** (1999) 243, ISSN: 0168-9002, DOI: 10.1016/S0168-9002(99)00114-X, URL: https://www.sciencedirect.com/science/article/pii/S016890029900114X?via%3Dihub.

[208] E. A. Schneidmiller, M. V. Yurkov, *Obtaining high degree of circular polarization at x-ray free electron lasers via a reverse undulator taper*, Physical Review Special Topics - Accelerators and Beams **16** (2013) 110702, ISSN: 1098-4402, DOI: 10.1103/PhysRevSTAB.16.110702, URL: https://link.aps.org/doi/10.1103/PhysRevSTAB.16.110702.

[209] A. A. Lutman, J. P. MacArthur, M. Ilchen, *Polarization control in an X-ray free-electron laser*, Nature Photonics **10** (2016) 468, ISSN: 1749-4885, DOI: 10.1038/nphoton.2016.79, URL: http://www.nature.com/articles/nphoton.2016.79.

[210] Ming Xie, *Design optimization for an X-ray free electron laser driven by SLAC linac*, Procedures of IEEE Particle Acceleration Conference, Dallas, TX, USA, 1995, p. 183, DOI: 10.1109/pac.1995.504603.

[211] E. L. Saldin, E. A. Schneidmiller, M. V. Yurkov, *Statistical and coherence properties of radiation from x-ray free-electron lasers*, New Journal of Physics **12** (2010) 035010, ISSN: 1367-2630, DOI: 10.1088/1367-2630/12/3/035010, URL: http://stacks.iop.org/1367-2630/12/i=3/a=035010?key=crossref.1d6a11bf3834ba2332f40daa9164e0a6.